Wnt signaling in right ventricular remodeling

Inaugural Dissertation

submitted to the

Faculty of Medicine

in partial fulfillment of the requirements

for the PhD-Degree

of the Faculties of Veterinary Medicine and Medicine

of the Justus Liebig University Giessen

by

Tretyn, Aleksandra Karolina

of

Torun, Poland

Gießen 2012

From the Department of Medicine

Director / Chairman: Prof. Dr. med. Werner Seeger

of the Faculty of Medicine of the Justus Liebig University Giessen

First Supervisor and Committee Member: Prof. Dr. rer. nat. Ralph Theo Schermuly

Second Supervisor and Committee Member: Prof. Dr. Dr. habil. Hans-Christian Siebert

Committee Members: Prof. Dr. Dr. Thomas Braun, Prof. Dr. Dr. habil. Gerald Reiner

Date of Doctoral Defense: 29th May 2013

Table of Contents

List of Figures

List of Tables

List of Abbreviations

ACE	Angiotensin converting enzyme
αCAA	α-cardiac actin
αSKA	α-skeletal actin
αSMA	α-smooth muscle actin
Ang II	Angiotensin II
ANP	Atrial natriuretic peptide
APC	Adenomatous polyposis coli
BNP	Brain natriuretic peptide
CFs	Cardiac fibroblasts
CK1	Casein kinase 1
Ct	Cycle threshold
Dkk	Dickkopf
Dvl	Dishevelled
ECM	Extracellular matrix
ERK 1/2	Extracellular signal-regulated kinases 1/2
ET-1	Endothelin-1
FHF	First heart field
Fz receptors	Frizzled receptors
GSK3	Glycogen synthase kinase 3
HIF1α	Hypoxia inducible factor-1α
HPV	Hypoxic pulmonary vasoconstriction
FAK	Focal adhesion kinase
LEF	Lymphoid enhancer-binding factor
LRP	Low density lipoprotein receptor-related protein
LV	Left ventricle
MCT	Monocrotaline
MHC	Myosin heavy chain

MI	Myocardial infarction
MMPs	Matrix metalloproteinases
NFAT	Nuclear factor of activated T cells
PAB	Pulmonary artery banding
PAH	Pulmonary arterial hypertension
PAP	Pulmonary arterial pressure
PCP	Planar Cell Polarity
PDE-5	Phosphodiesterase-5
PH	Pulmonary hypertension
PI3K	Phosphatidylinositol 3-kinase
PVR	Pulmonary vascular resistance
RV	Right ventricle
sFRP	Soluble Frizzled Related Protein
SHF	Second heart field
TAC	Transverse aortic constriction
TCF	T-cell factor
WISP-1	Wnt1-induced secreted protein
WGA	Wheat Germ Agglutinin

1. Introduction

Right ventricular hypertrophy and dysfunction are connected to several conditions including pulmonary hypertension (PH), congenital heart disease or valvular disease. However, in the past, the importance of right ventricle (RV) function in health and disease has been often underestimated. In fact, for many years the emphasis in the literature was placed on the left ventricular physiology. Only recently, in 2006, the National Heart, Lung and Blood Institute recognized the physiology of right ventricle as priority in cardiovascular research [1]. Nevertheless, a lot of insight has been achieved in the pathophysiology of LV function and one could assume most of the mechanisms should be common for both ventricles. Still one should keep in mind the developmental and structural differences of both. During development, the heart is formed from two distinct populations of cardiac progenitors. First heart field (FHF) progenitor cells exclusively contribute to the development of left ventricular myocardium while second heart field (SHF) cells contribute to development of outflow tract and right ventricular myocardium [2]. Additionally, right ventricle has different shape than the left ventricle. Whereas LV has ellipsoidal shape, the RV appears triangular (side view) and crescent shaped (cross section view). Right ventricle is also thinner than the left ventricle, which reflects the low hydraulic impedance characteristics of pulmonary vascular bed. Due to low pulmonary vasculature resistance right ventricle pumps the same effective stroke volume as the left ventricle but with approximately one fifth of the stroke work. Finally, compared with the LV, the RV demonstrates an elevated sensitivity to afterload change [3, 4]. Pulmonary hypertension is one of the essential causes of right ventricular remodeling. In fact right ventricle function is one of the major determinants of PH patients' survival [5].

1.1 Pulmonary hypertension

Pulmonary hypertension is a condition characterized by vascular narrowing leading to a progressive increase in pulmonary vascular resistance, increase in the afterload and right heart hypertrophy and dysfunction. It is clinically defined as mean pulmonary arterial

pressure (PAP) of more than 25 mm Hg at rest or 30 mm Hg during exercise, while normal PAP at rest comes to around 15 mm Hg [6, 7]. The causes of PH were classified according to the clinical diagnosis into 5 major groups: i) pulmonary arterial hypertension (PAH, with idiopathic and familial PAH), ii) PH owing to left heart disease, iii) PH owing to lung diseases and/or hypoxia, iv) chronic thromboembolic pulmonary hypertension and v) PH with unclear multifactorial mechanisms [8]. According to a broad study in France the prevalence of PAH is 15 cases per million, with an average age of 50 ± 15 years at the time of diagnosis, a female predisposition of 2:1 and an average mean PA pressure of 55 mmHg [9]. Most patients with PAH present exertional dyspnea, indicating an inability to increase cardiac output. Other reported symptoms include: fatigue or weakness, syncope and angina pectoris which are indicative of right heart dysfunction [10]. Exertional intolerance is determined based on the classification of the World Health Organization (WHO) (see Table 1). The estimated median survival of patients remains within a range of 2.8-4 years post diagnosis [5, 11].

Class	Description
I	Patients with pulmonary hypertension in whom there is no limitation of usual physical activity; ordinary physical activity does not cause increased dyspnea, fatigue, chest pain, or presyncope.
II	Patients with pulmonary hypertension who have mild limitation of physical activity. There is no discomfort at rest, but normal physical activity causes increased dyspnea, fatigue, chest pain, or presyncope.
III	Patients with pulmonary hypertension who have a marked limitation of physical activity. There is no discomfort at rest, but less than ordinary activity causes increased dyspnea, fatigue, chest pain, or presyncope.
IV	Patients with pulmonary hypertension who are unable to perform any physical activity at rest and who may have signs of right ventricular failure. Dyspnea and/or fatigue may be present at rest and symptoms are increased by almost any physical activity.

Table 1: World Health Organization classification of functional status of patients with pulmonary hypertension

1.1.1 Pathogenesis of PAH

A number of abnormalities underlie the pathogenesis of PAH including: i) formation of plexiform lesions and neointima ii) muscularization of distal precapillary arteries iii) medial thickening of large pulmonary muscular arteries [12], iv) adventitial thickening [13] and v) sustained vasoconstriction [14].

Intimal changes are largely responsible for narrowing of small pulmonary arteries and have potentially large impact on the pulmonary vascular resistance. Those changes may encompass eccentric, concentric and plexiform lesions. Eccentric proliferation or fibrosis in the intima usually occurs at any level of pulmonary vessels and causes only mild luminal obstruction. Concentric intimal proliferation on the other hand is mostly limited to small muscular arteries and arterioles and is typically associated with nearly complete luminal occlusion [15]. Plexiform lesions are complex, glomeruloid-like vascular structures, usually found distal to branch points of small- to medium-sized pulmonary arteries. They are composed of vascular channels lined up by endothelial cells and a core of myofibroblasts or less well-differentiated cells. These lesions are considered to be a hallmark of obstructive remodeling associated with severe PAH [16, 17]

Arterial muscle layer typically comes up to around 10-15% of total vessel diameter in healthy individuals, while in PAH this value can be increased up to 60% [18]. However, structural changes within medial wall vary along longitudinal axis of pulmonary vessels. This is caused by differences in cellular composition along this axis. The main alterations include medial thickening of elastic and muscular proximal vessels as well as muscularization of small, previously non-muscularized vessels. In proximal vessels, medial hypertrophy occurs probably due to the proliferation of a distinct population of smooth muscle-like cells, which exist in relatively undifferentiated state [19, 20]. Hypertrophy of the media in the distal vessels, considered a characteristic feature of PAH, is most probably occurring due to cellular hypertrophy and hyperplasia and contribution of other cells [21]. An interesting alteration in the course of pulmonary hypertension is muscularization of small alveolar wall vessels. Several mechanisms were proposed to underlie this process

including recruitment of interstitial fibroblasts or extravasation of inflammatory and mesenchymal precursor cells [14, 22].

Pulmonary hypertension is also characterized by significant fibroproliferative changes in the adventitial layer of both, large and small pulmonary arteries. Thickening of adventitia occurs as a result of excessive production and deposition of extracellular matrix (ECM) proteins (e.g., collagens), adventitial fibroblast proliferation and accumulation of myofibroblasts [14, 23]. Additionally adventitial thickening can also result from proliferation of resident and circulating progenitor cells. It has been shown that circulating mesenchymal precursors of a monocyte/macrophage lineage, including fibrocytes, can also contribute to pulmonary vascular remodeling [24].

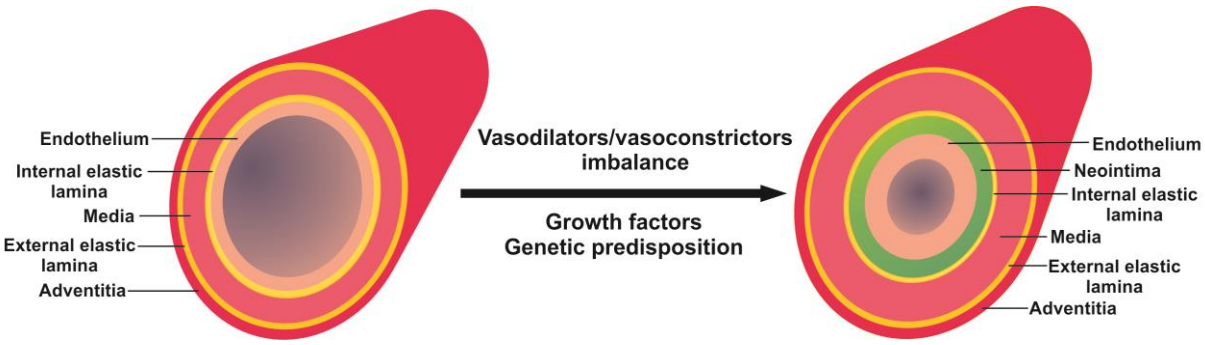

Fig.1 Schematic representation of pulmonary artery structure and vascular remodeling observed in the progression of PAH: Presented on the left is the normal structure of pulmonary arteries consisting of tunica adventitia, external elastic lamina, tunica media, internal elastic lamina and endothelial layer. Several growth factors as well as the imbalance between vasodilators and vasoconstrictors may lead to the narrowing of pulmonary arteries lumen during vascular remodeling, presented on the right. This process includes: formation of neointima, hypertrophy of the muscular layer and thickening adventitial layer (Based on: Barst, RJ 2005)[25]

Another mechanism contributing to the development of PAH is sustained vasoconstriction of pulmonary vessels in response to hypoxia. Hypoxic pulmonary vasoconstriction (HPV) is an adaptive response to alveolar hypoxia allowing optimizing the matching between ventilation and perfusion and thus improving gas exchange. In normal conditions vasoconstriction occurs within seconds after exposure to moderate hypoxia and reverses quickly under normoxic conditions. However, in people exposed to chronic hypoxia

(e.g. high-altitude residents) global vasoconstriction throughout the pulmonary circulation is observed leading to increased PVR [26]. Chronic hypoxia can further lead to structural changes in pulmonary vasculature and to the development of PH [27]. One of the underlying mechanisms observed in both, chronic hypoxic PH as well as PAH is activation of hypoxia-inducible factor 1α (HIF1α) and nuclear factor of activated T cells (NFAT) transcription factors, decreasing Kv1.5 expression [28].

1.2 Cardiac remodeling

Cardiac remodeling refers to changes in size, shape and function of the heart triggered by cardiac injury. It is a progressive disorder which may be connected to myocardial infarction (MI), pressure overload (hypertension), inflammatory heart muscle disease (myocarditis), idiopathic dilated cardiomyopathy or volume overload (valvular regurgitation). As the heart remodels, changes in its geometry, ventricular mass, composition and volume occur [29]. This process involves cellular changes including myocyte hypertrophy, increased collagen synthesis, fibroblast proliferation and cardiomyocyte apoptosis [30-33]. Irrespective of the underlying causes of cardiac remodeling, this condition progresses and is highly correlated with mortality from cardiovascular disease [34].

1.2.1 Cardiac hypertrophy

The preservation of normal hemodynamics in patients suffering from heart failure and PAH depends on stable function of the heart. Sustained demands on the heart can result in development of cardiac hypertrophy. Meerson described three stages of cardiac hypertrophy caused by aorta stenosis: “transient breakdown stage” occurring directly after stenosis with left ventricular insufficiency and pulmonary congestion, “protracted stage” of relatively stable “hyperfunction” and the third stage of progressing cardiosclerosis (with fibrotic changes and cardiac insufficiency) [35]. Cardiac hypertrophy can occur in response

to different stimuli. It can be triggered by chronic exercise (physiological hypertrophy) and diverse disease conditions (pathological hypertrophy). Intensive training for instance, can lead to the development of left ventricular hypertrophy. Changes observed in athletes include increase in left ventricular chamber size, wall thickness and mass and their advancement and general properties may depend on the type of exercise (endurance versus strength exercise). Nevertheless, physiological hypertrophy is associated with preserved function of the heart [36]. Pathological hypertrophy, on the other hand, is accompanied by various molecular changes leading to cardiac dysfunction. It is now known that distinct signaling cascades can be activated in those conditions (e.g. IGF-PI3K vs. ANGII, ET-1/Calcineurin, NFAT) [37].

Thus, the right ventricle may initially adapt to increased afterload [38]. During the initial escalation in afterload, the increase in right ventricular end diastolic volume helps to preserve cardiac output, in accordance with Frank-Starling mechanism. To reduce the wall stress and allow maintaining an appropriate stroke volume, the right ventricle undergoes hypertrophy. [39]. Following the Laplace's law, where an increase in ntraluminal pressure of a thin-walled chamber results in an increase in wall stress (Fig.2).

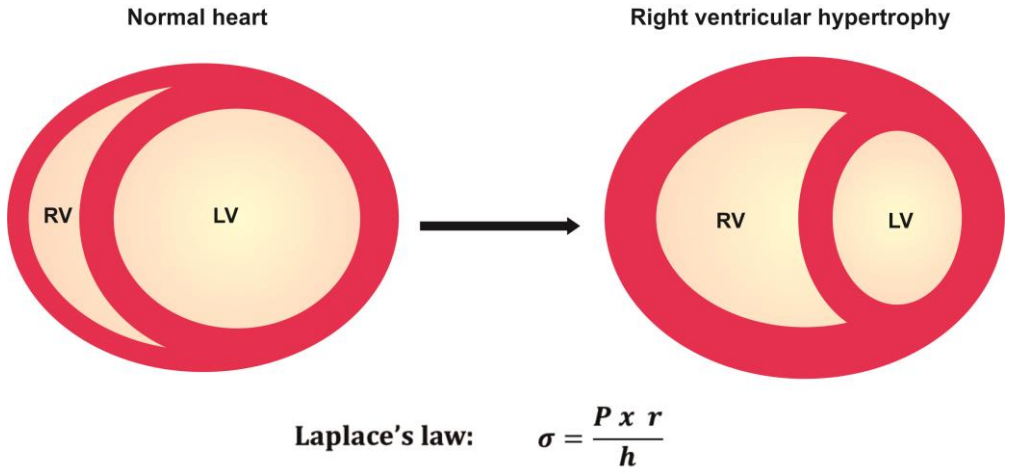

Fig.2 Right ventricular structure in normal conditions and in right ventricular hypertrophy: According to Laplace's law, increased RV wall stress (σ) due to an elevated intraluminal pressure (P) and increased chamber radius (r) may be attenuated by increasing the right ventricular wall thickness (h)(Based on: Bogaard, HJ *et al.*, 2009)[40]

This wall stress can be reduced by either an increase in the wall thickness or by reducing internal radius of the chamber.

Myocardial hypertrophy induced by the increase in afterload occurs mainly by increasing the size of the cells, the addition of sarcomeres and protein synthesis [41-43]. Apart from mechanical stress, right ventricular adaptation to the pressure load is a complex process and may also depend on several other factors, e.g. myocardial fibrosis [44]. Although cardiac hypertrophy is thought to be beneficial, sustained long-term pressure overload is eventually leading to right ventricular dilatation. This process is characterized by contractility dysfunction of the right heart, unbalanced ratio of oxygen supply to the demand and structural changes within the myocardium (e.g. fibrosis, cardiomyocyte apoptosis). Increased ventricular volume may further lead to tricuspid regurgitation resulting in right ventricular volume overload and further influencing the right ventricle remodeling [45]. A dilated right ventricle can shift the interventricular septum resulting in an impaired left ventricular filling [46]. These processes, together with right ventricular dysfunction are the components contributing to the development of heart failure.

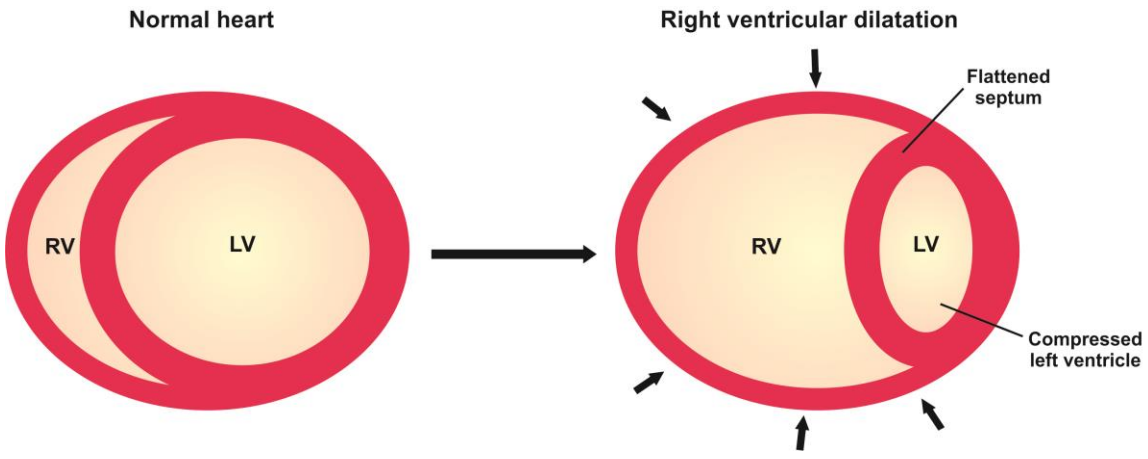

Fig.3 Interventricular septum shift during right ventricular dilatation: Dilated right ventricle shifts interventricular septum towards left contributing to the change of left ventricular geometry and its underfilling. This leads to decrease in cardiac output in patients with severe PAH. (Based on: Haddad, F *et al.* 2008)[47].

1.2.2 Cardiac fibroblasts and myocardial fibrosis

The non-myocyte cell populations of the heart are increasingly appreciated to contribute to the function of the normal and failing heart. In fact, the normal adult human heart comprises of only 30% cardiomyocytes and 70% non-myocyte cells [48]. Cardiac fibroblasts (CFs) have been described as the major component of non-myocyte cell fraction of the heart. They are arranged in a 3D network that surrounds myocytes and other cell types. A network of fibrillar collagen provides scaffolding for cardiomyocytes and other cells. Individual muscle fibers are surrounded by endomysial collagen, which is interspersed with single cardiac fibroblasts. The endomysium serves also as scaffolding for blood vessels. Perimysial strands further surround the muscle fibers and finally the entire muscle is strengthened and wrapped by a coarse epimysium [49, 50](Figure 4, left).

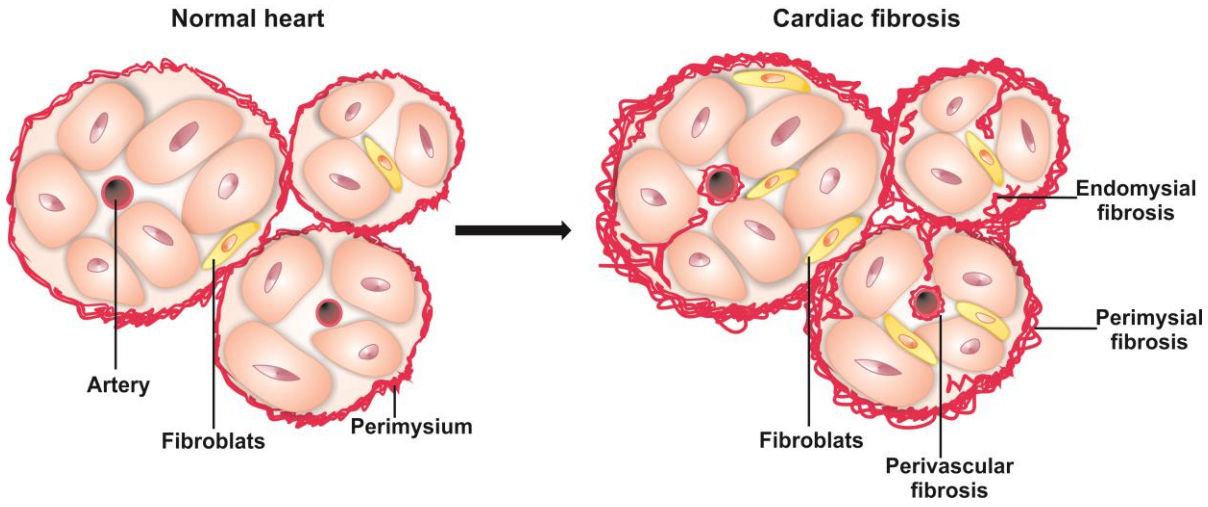

Fig. 4 Schematic representation of changes in the collagen network due to hypertension: In the normal heart, muscle fibers are surrounded by thin layers of endo- and perimysium with single interspersed fibroblasts (left). In cardiac hypertrophy, an excessive deposition of ECM proteins as well as fibroblast proliferation occurs, leading to perivascular fibrosis and fibrosis of the endomysium and perimysium (right)(Based on: Berk, B.C. 2007)[51].

Cardiac fibroblasts play an important role in preserving the structure of cardiac tissue. They are responsible for (i) synthesis and deposition of ECM components, (ii) ECM degradation and turnover through synthesis and release of matrix metalloproteinases (MMPs), and (iii)

the generation of mechanical stress on epimysial collagen network [32]. Cardiac ECM is composed mainly of three types of collagen, namely types I, III and V, which constitute almost 90% of the entire portion of collagen.

Collagen type I and III are major components of the network of collagen fibers. Their relative proportion is thought to influence the physical properties of the heart. Type I collagen forms mainly thick fibers and is associated with tensile strength. Type III collagen, in turn, forms a fine network of fibers and is associated with tissue elasticity. Other collagens found in the heart are type IV, V and VI which are found in basement membranes, interstitium and vessels [52].

During the initial phase of pressure overload, the synthesis of collagen increases in proportion to the increase in heart weight. The existing collagen matrix becomes thicker and denser. This process allows the heart muscle to become a more efficient power generator. Another important feature is the accumulation of thick collagen fibers around small coronary arteries (Figure 5, right). In established hypertrophy thin collagen fibers increase in the intermuscular space. Thick collagen fibers become entwined in the thin filaments (later only thick filaments are visible). This particular remodeling of collagen matrix has a great effect on myocardial stiffness. Muscle fibers are not easily stretched in diastole, this limits the length dependent force generation. Such a pattern of myocardial fibrosis may therefore be responsible for the conversion of compensated to decompensated heart function and for manifestation of pathological hypertrophy in long-term pressure overload. Another pattern of myocardial fibrosis is observed in the late phase of established hypertrophy. It is clearly initiated in response to cell death. The presence of fibrosis has a reparative role and leads to replacement scarring. Systolic and diastolic stiffness are increasing [49].

The excess of collagen in the myocardium observed in the right ventricular hypertrophy (RVH) is a result of both, increased collagen synthesis and decreased collagen degradation [30]. Extracellular matrix remodeling also includes an increased expression of specific matrix metalloproteinases (MMPs) and their inhibitors in the myocardium that are associated with

the progression to heart failure [53]. This process is associated with reduced collagen cross-linking caused by the activity of MMPs [54]. Fibroblast proliferation, collagen synthesis as well as expression and activation of MMPs can be induced by several molecules that are elevated in pulmonary hypertension, including the renin-angiotensin system and cytokines [32]. Since fibroblasts can respond to a wide range of humoral factors, they may become a new target for development of new therapeutic approaches against heart failure.

1.3 Mechanical stress and signaling in hypertrophic response

1.3.1 Integrins

Changes in afterload are sensed by integrins, the heterodimeric transmembrane receptors interacting with ECM components and cytoskeleton proteins. Integrins have several functions in the cell that include: regulation of cellular phenotype, adhesion, migration and most interestingly they serve as mechanotransducers and thus serve an important role in hypertrophic response. The onset of pressure overload seems to be accompanied by coordinated changes in expression profile and localization of integrins and ECM [55]. Integrins shedding into extracellular space has been observed during transition from cardiac hypertrophy to dilatation, which seems to be important process allowing cardiac cells to change their size and shape [56]. Furthermore, mechanical stress sensing by integrins results in intracellular signaling. It has been shown that the pressure overload triggers integrin activation and focal assembly of signaling proteins, including focal adhesion kinase (FAK) and Src in pulmonary artery banded (PAB) cat model. Also signaling through extracellular signal-regulated kinases (ERK1/2) and phosphatidylinositol 3-kinases (PI3Ks) has been reported in hypertrophied myocardium [57, 58].

1.3.2 Renin-Angiotensin system

One of important factors influencing cardiac hypertrophy is the renin-angiotensin system (with its primary effector molecule – angiotensin II; Ang II). Angiotensin II primarily regulates salt/water homeostasis and vasoconstriction thus regulating blood pressure, however long-term exposure to Ang II plays an essential role in cardiac hypertrophy and remodeling. In response to reduced perfusion, juxtaglomerular cells in the kidney secret renin that cleaves angiotensinogen to angiotensin I (Ang I). Subsequently Ang I is converted to Ang II by angiotensin converting enzyme (ACE) [59]. Angiotensin II has been shown to have direct growth effect on left ventricle in response to pressure overload [60]. This effect is mediated by angiotensin type 1 receptor (AT_1R) as administration of its antagonist diminishes Ang-II-induced cardiac hypertrophy [61]. In the right ventricular hypertrophy an increased density of AT_1R along with reduced contractility was observed in response to Ang II. Treatment with ACE inhibitor, ramipril has been shown to have cardioprotective effect supporting the idea that increased local levels of Ang II may cause receptor desensitization [62].

1.3.3 Endothelin-1

Endothelins belong to a family of peptides which includes endothelin-1, endothelin-2 and endothelin-3 (ET-1, ET-2 and ET-3, respectively). Endothelin-1 is the main isoform expressed in the vasculature where it acts as a potent vasoconstrictor. The main function of ET-1 is the regulation of blood pressure and vascular tone. The main sources of ET-1 generation are the endothelial cells, but ET-1 (as well as ET-2) can also be produced by the myocardium. Endothelin is mainly considered as a locally acting paracrine factor. Nonetheless, venous plasma concentration of ET-1 can be used as a marker for peptide synthesis by the vascular endothelium [63]. Endothelin-1 exerts its biological effects through two isoforms of G protein-coupled receptors, namely, endothelin receptor A (ET_A) and endothelin receptor B (ET_B). Both are expressed within the pulmonary vasculature and in cardiac muscle [64, 65].

ET-1 may contribute to the pathophysiology of PH and heart failure, particularly through its vasopressor properties. Furthermore, it may interact with other neuroendocrine effectors such as angiotensin II and catecholamines [66]. In addition to its vascular effect, endothelin-1 may also exert direct effects on the heart. It is well known that ET-1 has a positive inotropic effect on the human myocardium. In studies on neonatal cardiomyocytes it has been shown that ET-1 can be locally produced by the heart in response to angiotensin II and contribute to cardiac hypertrophy [67]. This effect may be due to stimulation of contractile protein production by cardiomyocytes [68] as well as the proliferation of cardiac fibroblasts [69]. In humans, increased levels of ET-1 were observed in a failing myocardium [70].

1.3.4 Calcineurin and NFAT signaling

Variety of humoral factors triggering hypertrophic response (e.g. Ang II, ET-1) is signaling through elevation of intracellular Ca^{2+} levels. This signal is sensed by calmodulin-dependent phosphatase – calcineurin. Calcineurin is a dimeric protein that is activated by binding to calmodulin when it is saturated with Ca^{2+}. It directly binds to and dephosphorylates NFAT transcription factors. This in turn allows their nuclear translocation and triggering of hypertrophic response genes. In fact activated NFAT3 transcription factor has been shown to be necessary and sufficient to evoke cardiac hypertrophy [71]. Additionally, calcineurin-NFAT signaling can be modulated by cross talk with other signaling pathways. For example it has been described that glycogen synthase kinase 3β (GSK3β) can induce phosphorylation of NFAT in cardiac fibroblasts [72].

1.4 Gene expression changes in cardiac hypertrophy

Cardiac hypertrophy is not simply an increase in diameter of myocytes and fibrosis, but it also promotes changes in gene expression profile in the myocardium. These changes can be

both qualitative and quantitative. Interestingly, it is believed that in the pressure-overloaded hearts a re-expression of neonatal genes is triggered [73].

One of the hallmarks of maladaptive cardiac hypertrophy is the isoform switching of myosin heavy chain (MHC) proteins. Cardiac sarcomeric thick filaments may be composed of two different MHC isoforms, namely αMHC and βMHC. Myosin isoforms comprised from αMHC or βMHC demonstrate marked mechanical and enzymatic differences. The βMHC isoform has lower adenosine triphosphate activity and contraction velocity [74]. In adult human heart the amount of αMHC and βMHC comes to approximately 23% and 77%, respectively. In heart failure due to PAH, this ratio is disturbed and αMHC drops to about 5.6% and an increased percentage of βMHC observed. Given the differences in shortening velocity of both isoforms, such decrease in αMHC can contribute to lowering of cardiac systolic function observed in PAH [75]. Sustained pressure overload can also trigger changes in expression of genes encoding thin filament proteins. Two α-actin isoforms are expressed in adult hearts: α-skeletal muscle actin (αSKA) and α-cardiac actin (αCAA). In hypertrophied myocardium due to pressure overload an increase in the expression of αSKA and α-smooth muscle actin (αSMA) was reported, both in human and in animal models [76-78].

The changes in gene expression profile in response to increased afterload are not only limited to components of the contractile apparatus. In the disease progression of PH, natriuretic peptides were shown to play an essential role. The family of cardiac natriuretic peptides consists of atrial (ANP), brain (BNP) and C-Type natriuretic peptides, of which ANP and BNP are synthesized and secreted into circulation by the heart. The cardiac natriuretic peptides are synthesized as high molecular weight precursors and therefore have to undergo multiple steps involving proteolytic cleavage before yielding the biologically active molecules. Upon binding to their receptors (NPR-A and NPR-C) the particulate guanylate cyclase, produces cyclic guanosine monophosphate, which further acts as the intracellular messenger. ANP is mainly released from atria, whereas BNP produced in ventricular cardiomyocytes. Their expression and release is triggered by increased ventricular stretch, but this response is modulated by many other factors, such as ATII, ET-1 or circulating

catecholamines [79]. Indeed, an upregulation of ANP and BNP expression in the right ventricle has been reported in pulmonary artery banding model [31]. Moreover plasma levels of both natriuretic peptides were elevated in patients suffering from PAH showing a strong positive correlation with total pulmonary resistance and RV end-diastolic pressure. Interestingly, in patients receiving prostacyclin therapy follow-up BNP plasma level was an independent predictor of mortality in PAH. Thus, plasma BNP levels may serve as a noninvasive prognostic indicator of PAH [80].

Many other signaling pathways and deregulation of gene expression underlies maladaptive cardiac growth, which do not fall within the scope of this dissertation. For other pathways the reader is referred to some excellent reviews [40, 72, 73]. The summary of key changes in the right ventricular hypertrophy is represented in Figure 5.

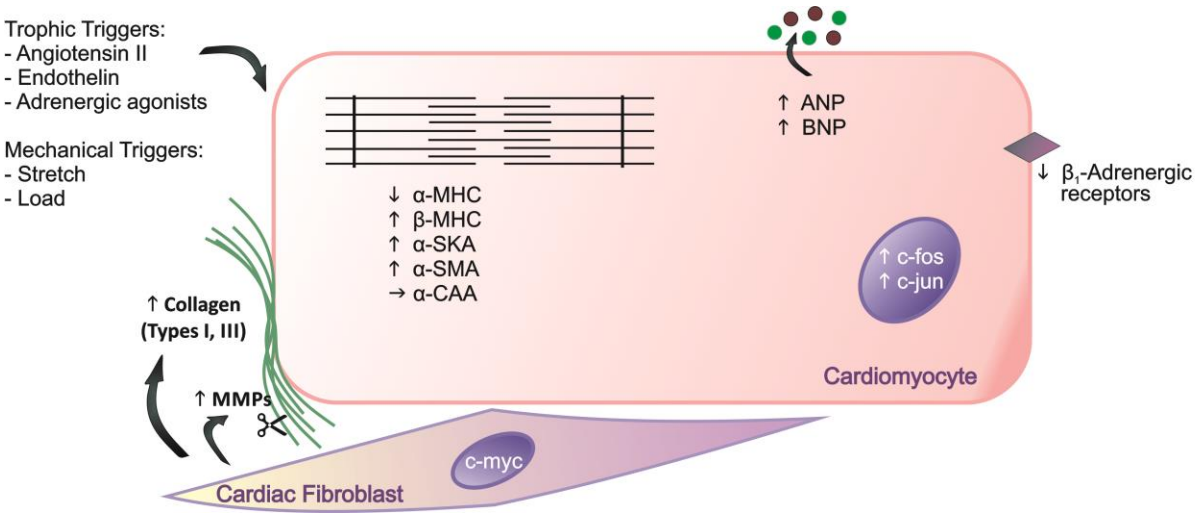

Fig. 5 Gene expression changes during pressure-induced cardiac hypertrophy: A summary of essential molecular changes during progression of right ventricular hypertrophy is depicted; α-CAA – α-cardiac actin, α-MHC – α-myosin heavy chain, α-SKA – α-skeletal actin, α-SMA – α-smooth muscle actin, ANP – atrial natriuretic peptide, β-MHC – β-myosin heavy chain, BNP – brain natriuretic peptide, MMPs – matrix metalloproteinases (Based on: Boheler and Schwartz 1992)[73]

1.5 Current strategies in treatment of PAH and right heart failure

Despite the successful introduction of several new pulmonary-selective vasodilatory therapies in the last decade, the prognosis of PAH patients still remains poor. It is important to note that it is the failing right ventricle itself (not the load *per se*) that leads to death. The treatment strategy for PAH should definitely consider the origin of RV failure. The aims of therapy include optimization of preload, afterload, and contractility [47].

Aside from the therapy, some general lifestyle modifications are advisable for PAH patients including low-sodium diet. Fluid retention can be further minimized by application of diuretics. Patients should be encouraged to low-grade exercises within symptom limits. One of utilized therapies in PAH is prostacyclin administration, as dysregulation of the prostacyclin metabolic pathways has been shown in patients with PAH. Besides continuous intravenous epoprostenol infusions, prostacyclin analogs were developed including subcutaneous treprostinil, oral beraprost and inhaled iloprost. Since endothelin is an important factor influencing PAH (see 1.3.3), also targeted therapies against this molecule have been developed. Bosentan, an orally available dual ET_A and ET_B receptor antagonist, has been evaluated in PAH in five randomized clinical trials that have shown improvement in exercise capacity, functional class, hemodynamics, and time to clinical worsening [81]. Also phosphodiesterase-5 (PDE-5) inhibitors have been approved for the treatment of pulmonary hypertension, as PDE5 is induced in the remodeled pulmonary arteries. Inhibition of the cGMP-degrading PDE-5 results in local vasodilatation through the activation of nitric oxide/cGMP pathway at sites expressing this enzyme. Interestingly, PDE5 inhibitors have also been shown to target specifically the right ventricle. While the expression of PDE5 is minimal in the normal RV, its expression is markedly induced in the hypertrophied right ventricles of rats and humans. In addition to the positive effect of PDE-5 inhibitors on afterload by dilating and reversing the remodeled pulmonary arteries, they were also found to have positive inotropic effect on the hypertrophied RV [82]. Inhibition of the angiotensin system and β-blockers may be considered in selected patients, although their benefit remains unclear and controversial [82]. Lung transplantation remains as a

mainstay for individuals that do not respond to available therapies. Additionally, numerous compounds are currently undergoing phase II and III clinical trials, namely stimulators and activators of cGMP, tyrosine kinase inhibitors and serotonin antagonists [81]. Despite the progress in the development of therapeutic strategies against PAH, the survival of patients remains unsatisfactory. Hence, there is a need to develop additional therapeutic options targeting specifically the heart in order to improve symptoms and further prognosis.

1.6 Wnt signaling pathway

Wnt (Wingless and INT-1) signaling pathway is essential for animal development and has been associated with several diseases, most likely by influencing cell proliferation, survival, fate and behavior [83]. Wnts are cysteine-rich proteins that undergo glycosylation and lipid modifications prior to its secretion. Nineteen Wnt genes have been identified in humans, whose orthologs have highly conserved sequences among different species of vertebrates [84, 85]. Wnt molecules are thought to activate a number of different signaling pathways. These molecules have been historically divided into two classes – canonical Wnts (activating β-catenin-dependent pathway, including Wnt1 or Wnt3A) and non-canonical Wnts (activating β-catenin-independent pathway, including Wnt5A or Wnt11). However, in light of present knowledge, it seems that it's not the Wnt molecules who decide about the activation of canonical versus non-canonical pathways but the repertoire of their different receptors [86]. Indeed, Wnt proteins have been reported to interact with several classes of receptors [87].

First and probably best known class of Wnt receptors are members of the Frizzled (Fz) family. Frizzleds are seven transmembrane-spanning receptors that belong phylogenetically to the family of G protein-coupled receptors. Ten Fz family members have been described to date in mammals. Frizzled receptors mediate activation of three major signaling pathways: the canonical Wnt pathway, calcium (Ca^{2+})-dependent pathway, and PCP (planar cell polarity) pathway (Figure 6).

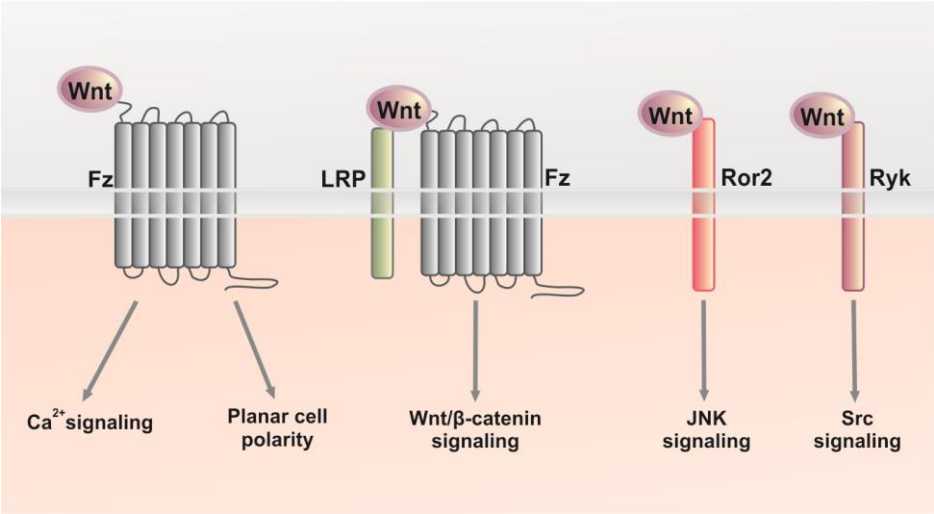

Fig. 6 The current sensing model of Wnt signaling via different receptors: Frizzled receptors mediate activation of three major signaling pathways: the β-catenin-dependent pathway (with the involvement of Lrp co-receptors), (Ca^{2+})-dependent pathway, and planar cell polarity (PCP) pathway. Also signaling through tyrosine kinase receptors from Ryk and Ror family has been described. (based on: van Amerongen *et al.* 2008)[86]

In addition, a number of secreted proteins antagonizing Wnt signaling are observed in the extracellular matrix. They can be divided into two functional classes, soluble frizzled related proteins (sFRP) class and the Dickkopf (Dkk) class. Members of the first class bind directly to the Wnts, thereby altering their ability to bind to their receptor. These particles are considered to antagonize both, Wnt canonical and non-canonical signaling. The family members of Dkk, inhibit Wnt signaling by binding to LRP5/6 component of the Wnt receptor complex, which mainly antagonizes the canonical pathways [88].

1.6.1 Wnt canonical signaling

Canonical (or Wnt/β-catenin) signaling pathway is probably the best understood among all types of Wnt signal transduction. The hallmark of this pathway is the accumulation and nuclear translocation of β-catenin [89]. There are two pools of β-catenin existing in the

cells. A membrane-bound pool represents stable β-catenin and is located in cellular adherens junctions where it binds to E-cadherin and α-catenin. A soluble pool represents highly unstable cytoplasmic β-catenin involved in Wnt signal transduction [90]. The stability of cytoplasmic β-catenin levels is regulated by degradation complex comprised of glycogen synthase kinase 3 (GSK3), casein kinase 1 (CK1), Axin and adenomatous polyposis coli (APC). In this complex Axin seems to be a key scaffolding molecule promoting its rapid assembly and disassembly whereas APC is required for efficient loading of β-catenin onto the complex. Both facilitate the sequential phosphorylation of β-catenin by CK1 and GSK3 at highly conserved serine/threonine residues. This leads to its ubiquitylation by β-TrCP containing E3 ligase and subsequent proteasomal degradation (Figure 7) [91].

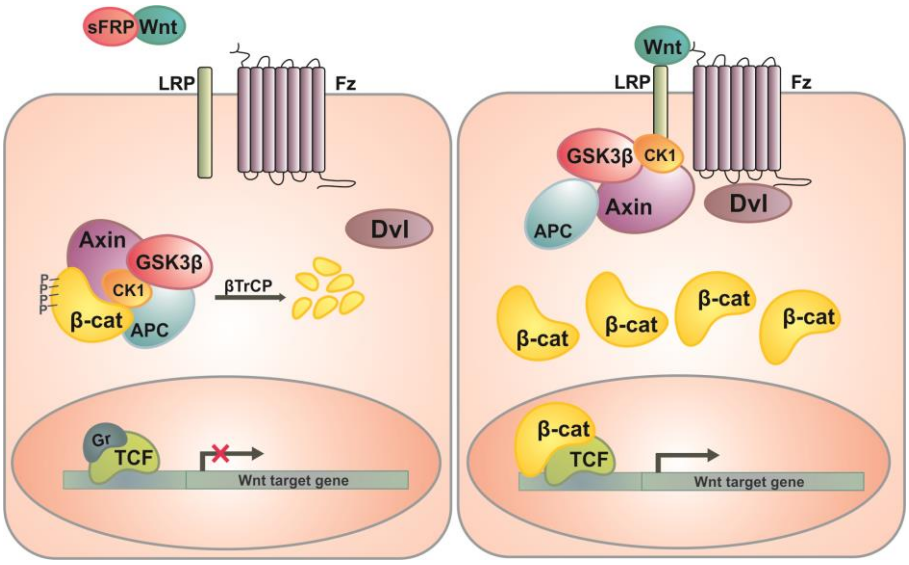

Fig. 7 Canonical Wnt Signaling: In the absence of Wnt ligands (left panel) β-catenin is phosphorylated by CK1 and GSK3α/β leading to its subsequent ubiquitylation and proteasomal degradation. Prospective Wnt target genes remain in a repressed state. During activation of Wnt signaling (right panel), Dvl proteins undergo phosphorylation and are translocated to the cell membrane to interact with Fz receptors. LRP 5/6 co-receptors are also phosphorylated by GSK3β and CK1γ, thus regulating the docking of Axin. The recruitment of Axin away from the degradation complex leads to the accumulation of β-catenin in the cytoplasm and its subsequent nuclear translocation. In the nucleus, β-catenin binds to T-cell factor (TCF) and lymphoid binding protein (LEF)-family transcription factors and activates transcription of target genes. (based on: Clevers, H. 2006)[91]

The binding of Wnt molecules to their Fz/LRP5/6 receptor complex recruits Axin, the key negative regulator of signaling, to the cell membrane where it interacts with LRP co-receptors. The translocation of Axin to the cell membrane is enabled by GSK3β- and CK1γ- mediated phosphorylation of LRP5/6. Since Axin is present in cells at low levels, its sequestration to the membrane might compete with its function in the degradation complex, thereby allowing stabilization of β-catenin. It is noteworthy that in the presence of Wnt, GSK3ß can also fulfill a positive function in Wnt signal transduction. In the presence of Wnt signaling Dishevelled is recruited to the plasma membrane, precisely to the Fz receptors.

Dvl is phosphorylated by number of kinases (including CK1) and most probably its phosphorylation status is regulating its subcellular localization. It has been shown that activation of Dvl facilitates the inactivation of degradation complex but the underlying mechanism remains elusive. This may likely occur through association of Dvl with Axin [87]. In fact it has been proposed that upon Wnt signaling and recruitment of Dvl to Frizzled receptors this protein forms polymers. These polymers provide a dynamic scaffold for recruitment and inactivation of Axin [92]. Stabilized β-catenin accumulates in the cytoplasm and translocate into the nucleus (although β-catenin itself has no nuclear localization sequence). Here, it binds to T-cell factor (TCF) and lymphoid binding protein (LEF)-family proteins to co-activate the transcription of Wnt target genes, e.g. c-Myc or Cyclin D1 [91]. Interestingly, TCFs alone are incapable of modulating transcription. Instead, they recruit a number of auxiliary proteins to the regulatory regions of target genes. In the absence of Wnt signaling, TCF/LEF proteins function as transcriptional co-repressors by binding of the Groucho family proteins and recruiting histone deacetylases [93]. Activation of Wnt target genes occurs through direct competition of ß-catenin and Groucho for binding to TCF/LEF proteins [94]. After binding of TCF/LEF proteins, β-catenin engages the assistance of CBP/p300 and Brg1-containing complexes in the transcriptional activation of target genes (e.g. Cyclin D1, c-Myc) [93].

1.6.2 Wnt non-canonical pathways

The least understood aspect of Wnt signaling is β-catenin independent pathways termed as non-canonical signaling. It has been suggested that vertebrate non-canonical Wnt signaling might be involved in various processes as cochlear hair cell morphology, cardiac development, dorsoventral patterning, neuronal migration, and cancer. Wnt non-canonical pathways are mediated by binding of certain Wnts to Frizzled receptors independently of LRP5/6 co-receptors. This leads to the activation of Disheveled and further signal transduction via two distinct signaling pathways: Planar Cell Polarity pathway (PCP) and Wnt/Ca^{2+} pathway. [95].

Planar cell polarity pathway controls the orientation of hairs, bristles, and in vertebrates, stereocilia in the sensory epithelium of the inner ear, by regulating the actin cytoskeleton. In this pathway Dvl is activating two parallel signaling cascades via small GTPases Rho and Rac. This in turn activates JNK or rho-associated protein kinase. Wnt/Ca^{2+} signaling leads to release of Ca^{2+} from intracellular stores and activates calcium-sensitive proteins including protein kinase C, Calcineurin and Calcium- and Calmodulin-dependent kinase II. These kinases control independently other proteins and transcription factors (e.g. NFAT), thus regulating many cellular processes including cytoskeletal organization, cell polarity and motility [89].

1.7 Wnt signaling in cardiac hypertrophy

Several intracellular pathways have been implicated in the development of cardiac hypertrophy (see chapter 1.3). Recently, the importance of Wnt signaling in this pathological process has received considerable interest. This signaling pathway is crucial for the development and has been implicated in several diseases [83]. Depletion of β-catenin results in embryonic lethality [96]. Mice lacking GSK3β (but not GSK3α) die during embryonic development due to heart defects [97]. Moreover Wnt canonical signaling has

been shown to have a fundamental role in the development of SHF and promotes right ventricular and interventricular myocardial expansion [98]. To date, the literature on the role of the Wnt pathway is derived exclusively from studies on left ventricular hypertrophy. It has been demonstrated that in rats subjected to aortic banding and in porcine model of chronic heart failure, Dvl1 protein levels are increased. Overexpression of Dvl1 led to the development of maladaptive cardiac hypertrophy via both, canonical and non-canonical Wnt pathways [99]. On the other hand in mice lacking Dvl-1, the hypertrophic response induced by aortic constriction was attenuated as shown by decreased left ventricular wall thickness and decreased expression of ANP and BNP. In those mice an increased activity of GSK3β and decreased β-catenin levels were observed [100].

1.7.1 The role of GSK3β

Glycogen synthase kinase 3β (GSK3β) has been described to be a potent anti-hypertrophic agent and its role in cardiac hypertrophy has been extensively investigated. As previously mentioned GSK3β plays a fundamental role in normal heart development. Deletion of GSK3β leads to hyperproliferation of cardiomyocytes and death of mice caused by heart malformations whereas mice lacking GSK3α are born without obvious cardiac developmental defects. It has been postulated that this effect is most likely β-catenin independent [97]. Concerning cardiac hypertrophy, a decreased kinase activity of GSK3β has been detected in response to hypertrophic stimuli both *in vitro* and *in vivo*. This inhibition seemed to be important for the enhanced protein accumulation and ANP expression by cardiomyocytes [101]. On the other hand, when GSK3β is overexpressed, the development of concentric hypertrophy is attenuated. This results in impaired contractile function of the heart and may progress to the heart failure [102]. Interestingly, in human hearts, inhibition of GSK3β was seen in the end-stage of heart failure, but was not observed in chronic hypertrophy. The authors speculate that GSK3β downregulation could protect cells from apoptosis and allow NFAT to enter the nucleus to activate hypertrophic response genes [103].

1.7.2 The role of β-catenin

Although β-catenin has been recognized as an important factor of maladaptive cardiac growth, its exact role in this process remains controversial. β-catenin is stabilized upon hypertrophic stimuli, which involves the inhibition of GSK3β kinase activity. β-catenin alone was sufficient to induce hypertrophic growth when expressed in cardiomyocytes *in vitro* and *in vivo* [104]. In addition, it has been found that targeted depletion of β-catenin in the heart leads to a blunted hypertrophic in response to transaortic constriction. The authors speculated this effect is attributable to β-catenin transcriptional co-activation properties as expression of a dominant inhibitory mutant of Lef-1 caused dramatic reduction in cardiomyocyte growth [105]. However, an opposite role of β-catenin in cardiac hypertrophy was also reported. Baurand *et al.* found that in the absence of hypertrophic stimuli, mice lacking β-catenin develop adaptive hypertrophy whereas stabilization of β-catenin results in slightly decreased cardiomyocyte cross-sectional area. Two weeks of AngII infusion did not affect further the hypertrophy in β-catenin-depleted mice, whereas mice with stabilized β-catenin displayed impaired hypertrophic response [106]. Overall, these observations lead to the conclusion that β-catenin has the potential to regulate cardiac hypertrophy, which may (at least in the experimental approach) depend on the type of hypertrophic stimulus. Future studies need to address the precise role of β-catenin in this pathological process.

In conclusion, Wnt signaling pathway plays an important role in left ventricular remodeling in response to hypertrophic stimuli. While all of the available literature describes the impact of this signaling cascade in maladaptive growth of the left ventricle, its role in the right heart hypertrophy is thus far unknown.

2. Aims of the study

Considering the role of Wnt signaling in left ventricular remodeling, we hypothesized that it plays a crucial role in the development of right heart hypertrophy. As this pathway is essential for the development of right ventricle we speculated its contribution to RVH could be more prominent. The main aims of this study focused on:

a) To define Wnt molecules expression on mRNA and protein levels in two animal models: rat monocrotaline (MCT) pulmonary hypertension model and pulmonary artery banding (PAB) model of right ventricular hypertrophy
b) To determine mRNA expression of key molecules of Wnt canonical pathway, β-catenin and GSK3β in cardiac fibroblasts
c) To characterize cardiac fibroblasts derived from right and left ventricles PAB and Sham operated rats
d) To elucidate the influence of Wnt3a stimulation on β-catenin localization
e) To determine if Wnt3a stimulation or β-catenin siRNA-mediated knockdown can influence cardiac fibroblast proliferation and collagen expression
f) To investigate Wnt pathway activation *in vivo* in BAT-Gal reporter mice

3. Materials and Methods

3.1 Materials

3.1.1 Equipment

Name	Company
Analytical balance	Sartorius, Germany
Biological safety cabinet, Cellgard	NuAire, USA
Cell culture Incubator, Hera Cell	Thermo Scientific, USA
Cell culture pump	Integra Biosciences, Switzerland
Cell culture waterbath	Memmert, Germany
Centrifuge – Heracell S Fresco 21	Thermo Scientific, USA
Centrifuge, Heraeus Multifuge	Thermo Scientific, USA
CFX96 Real Time System	BioRad, USA
Confocal Microscope, LSM 710	Carl Zeiss, Germany
Cryotome Leica CM3050S	Leica, Germany
DNA electrophoresis unit, Compact M	Biometra, Germany
Freezer (+4°C, -20°C)	Bosh, Germany
Freezer (-80°C)	New Brunswick Scientific, USA
FujiFilm LAS-4000	FujiFilm, Japan
Gel iX Imager	Intas, Germany
Infinite 200 PRO multiplate reader	Tecan, Switzerland
Ligth microscope	Hund, Germany
Magnetic stirrer	Heidolph, Germany
PCR Thermocycler	Eppendorf, Germany
pH meter	Shott Instruments, Germany
Pipetboy and Pipettes	Eppendorf, Germany
Polyacrylamide gel electrophoresis unit	Biorad, USA

Power supply – PowerPac Basic	Biorad, USA
Precellys homogenizer	Peqlab, Germany
Precision balance EK-300i	A&D, Japan
Protein blotting chamber	Biorad, USA
Shaker, unimax 2010	Heidolph, Germany
Thermoblock	Bioer, China
Vortex	Scientific Industries, USA

3.1.2 Plasticware and other materials

Name	**Company**
Amicon Ultra centrifugal filter units	Millipore, USA
Disposable base molds	Thermo Scientific, USA
Cell culture chamber slides	BD Biosciences, USA
Cell culture flasks (25cm^2, 75cm^2)	Greiner Bio-One, Austria
Cell culture plates (6-, 48-, and 96-well)	Greiner Bio-One, Austria
Cell culture plates (60mm, 100mm)	Greiner Bio-One, Austria
Cell scrapers	BD Biosciences, USA
Cover slides	Carl Roth, Germany
Falcons (15, 50ml)	Greiner Bio-One, Austria
Glassware	Duran, Germany
Hemocytometer	Marienfeld, Germany
Multiwell plate	Corning, USA
Nitrocellulose membrane	PALL, USA
PCR 96-well plate, low profile	Biorad, USA
Pipette tips, filter tips (10, 100, 1000µl)	Greiner Bio-One, Austria
Plastic pipettes (5, 10, 25, 50ml)	Greiner Bio-One, Austria
Polyacrylamide gel electrophoresis glass plates	Biorad, USA

Precellys ceramic kit (1,4; 2,8mm)	Peqlab, Germany
Reaction tubes (0,2ml)	Biozym, Germany
Reaction tubes (2; 1,5; 0,5ml)	Eppendorf, Germany
Superfrost plus slides	Thermo Scientific,USA

3.1.3 Animal experiments equipment and reagents

Name	**Company**
16-gauge needles	B Braun, Germany
Animal ventilator, SAR-830/P	Dwyer, USA
Buprenorphine hydrochloride	Essex Pharma, Germany
Bepanthen	Bayer Health Care, Germany
Domitor	Pfizer, USA
Hemostatic clips	Teleflex (Weck), USA
Isoflurane	Baxter, USA
Ketamine (10%)	Medistar, Germany
Monocrotaline	Sigma-Aldrich, USA
NaCl solution	B Braun, Germany
Rymadyl	Pfizer, USA
Surgical instruments	Aeskulap, Germany
Stiches (Vicryl Plus)	Ethicon, USA
Syringes	B Braun, Germany

3.1.4 Kits

Name	**Company**
BioRad DC Protein Assay	BioRad, USA
Sircol Collagen Assay	Biocolor, UK

RNeasy Fibrous Mini Kit	Qiagen, Germany
ImProm-II Reverse Transcription kit	Promega, USA
IQ™ Sybr Green Sypermix	BioRad, USA
Cell Proliferation ELISA, BrdU (colorimetric)	Roche, Switzerland
RNeasy Mini Kit	Qiagen, Germany
ProteoExtract Subcellular Proteome Extraction kit	Merck (Calbiochem), Germany

3.1.5 Chemicals

Name	**Company**
2-butanol	Carl Roth, Germany
Acetic acid (CH_3COOH)	Sigma-Aldrich, USA
Acrylamid 30% (w/v)	Sigma-Aldrich, USA
Agarose	Carl Roth, Germany
Ammonium persulfate (APS) $(NH_4)_2S_2O_8$ 10% (w/v)	Sigma-Aldrich, USA
Bovine serum albumin powder	Carl Roth, Germany
Bovine serum albumin solution (2 mg/ml)	BioRad, USA
Bromophenol blue	Merck, Germany
Collagenase II	Gibco, USA
Dimethyl sulfoxide (DMSO)	Sigma-Aldrich, USA
Disodium hydrogen phosphate (Na_2HPO_4)	Carl Roth, Germany
Dulbecco's Modified Eagle Medium (DMEM), 4,5g/l glucose	Sigma-Aldrich, USA
Ethanol, absolut	Carl Roth, Germany
Ethidium bromide	Carl Roth, Germany
Ethylenediaminetetraacetic acid (EDTA), 0.5M, pH 8.0	Carl Roth, Germany
Fetal calf serum (Gold)	PAA Laboratories, Austria
Fluorescent Mounting Medium	Dako, Denmark

Glucose	Carl Roth, Germany
Glycerol	Sigma-Aldrich, USA
Glycine	Sigma-Aldrich, USA
Hank's Balanced Salt Solution (HBSS)	Gibco, USA
HEPES	Sigma-Aldrich, USA
Hydrochloric acid (HCl) 37%	Carl Roth, Germany
L-glutamine	Lonza, Switzerland
Lithium Chloride (LiCl)	Sigma-Aldrich, USA
Loading dye for DNA electrophoresis (5x)	Fermentas, USA
Magnesium sulfate ($MgSO_4$)	Carl Roth, Germany
Methanol	Carl Roth, Germany
Opti-MEM Glutamax I cell culture medium	Gibco, USA
Penicillin-streptomycin	PAA Laboratories, Austria
Pepsin	Sigma-Aldrich, USA
Phosphatases and proteases inhibitor cocktail	Thermo Scientific, USA
Phosphate buffered saline (PBS)	PAA Laboratories, Austria
Potassium chloride (KCl)	Carl Roth, Germany
Potassium di-hydrogen phosphate (KH_2PO_4)	Carl Roth, Germany
Radioimmunoprecipitation assay (RIPA) buffer (1x)	Thermo Scientific, USA
Rainbow™ Molecular Weight Marker	GE healthcare, USA
Rat fibroblasts cell culture medium	Cell Applications, USA
Restore Western Blot Stripping Buffer	Thermo Scientific, USA
Skim milk powder	Carl Roth, Germany
Sodium chloride (NaCl)	Carl Roth, Germany
Sodium dihydrogen phosphate (NaH_2PO_4)	Carl Roth, Germany
Sodium dodecyl sulfate (SDS)	Sigma-Aldrich, USA
Sodium dodecyl sulfate (SDS) 20% (w/v)	Carl Roth, Germany
Sodium hydroxide (NaOH) 1M solution	Merck, Germany
Sodium hydroxide, pellets	Carl Roth, Germany

SuperSignal West Femto Chemiluminescent Substrate	Thermo Scientific, USA
Tetramethylethylenediamine (TEMED)	Sigma-Aldrich, USA
Tissue-Tek	Sakura, USA
Tris-HCl 0,5M, pH=6,8	Amresco, USA
Tris-HCl 1,5M, pH=8,9	Amresco, USA
Trizma-base	Sigma-Aldrich, USA
Trypsin/EDTA (10x)	Lonza, Switzerland
Water bath protection, Akasolv	Carl Roth, Germany
Wnt3a, recombinant	R&D systems, USA
Xtreme Gene transfection reagent	Roche, Switzerland
β-Mercaptoethanol	Sigma-Aldrich, USA

3.1.6 Oligonucleotides

Small interfering RNAs

Two different predesigned siRNAs against β-catenin as well as scrambled siRNA were purchased from Qiagen, Germany. (#1: SI02012003, #2: SI02012010). Cy3-labeled scrambled siRNA was purchased from Ambion (Life Technologies, USA).

siRNA	Strand	Sequence (5'-3')
β-catenin #1	Sense	GUU UGA UAC CGA CCU GUA ATT
	Antisense	UUA CAG GUC GGU AUC AAA CCA
β-catenin #2	Sense	GGG UGC GAU CCC ACG ACU ATT
	Antisense	UAG UCG UGG GAU CGC ACC CTG

qRT- PCR primers

All qRT-PCR primers were designed and purchased from Metabion (Germany). For primer sequences please see Appendix Table 1.

3.1.7 Antibodies and cellular dyes

For detailed list of primary and secondary antibodies used as well as cellular and nuclear dyes please see Appendix Tables 2-4.

3.2 Methods

3.2.1 Animal experiments

All pulmonary artery banding and monocrotaline experiments were performed on 250-300g weighting Sprague-Dawley (SD) rats purchased from Charles River (Sulzfeld, Germany). All experimental protocols involving animals were approved by Federal Authorities for Animal Research (Regierungspräsidium Darmstadt, Germany, AZ 17/2010, B2/191 and B2/285) and were performed by Dr med vet Wiebke Janssen, Julia Neuman and Uta Eule.

Pulmonary artery banding of rats

Rats were anesthetized with inhaled 1.5–2.0% Isoflurane, intubated and ventilated with oxygen. The thorax of animals was opened, a 16-guage needle was placed above the pulmonary artery and a suture was placed around both of them. Next, the needle was removed resulting in constriction of pulmonary artery to 1.7mm of diameter. Sham animals underwent the same operation excluding the banding procedure. All surgical procedures were performed under Isoflurane anesthesia (2.0% vol/vol) and an intraperitoneal administration of 0.06mg/kg buprenorphine hydrochloride. Two weeks after surgery, animals were sacrificed following organ harvest and/or cardiac fibroblasts isolation (see 3.2.2).

Monocrotaline-induced pulmonary hypertension model

Monocrotaline was dissolved in 0.5M HCl and the pH adjusted to 7.4 with 0.5M NaOH. For induction of pulmonary hypertension in SD rats a single subcutaneous injection of monocrotaline (60mg/kg, Sigma Aldrich) was administered. Control rats received an equal volume of isotonic saline instead. Organ harvest was performed at four, five and six weeks after saline/MCT injections.

BAT-Gal reporter mice

BAT-Gal reporter mice [107] were kindly provided by Dr. rer nat. Stefan Liebner (Johann Wolfgang Goethe-University, Frankfurt, Germany). BAT-Gal mice were anesthetized with inhaled 1.5–2.0% Isoflurane, intubated and ventilated with oxygen. After left sided upper thoracotomy pulmonary artery banding was applied using sterile hemostatic clips (Weck,

USA). Sham-operated animals underwent the same procedure excluding clipping of the pulmonary artery. Tissue harvest was performed 2 weeks after operation. Both procedures were performed on genotyped positive mice 12-18 week of age. Wild-type mice and negative littermates were used.

Right ventricular hypertrophy assessment

For assessment of right ventricular hypertrophy the hearts were removed, the chambers were opened, and any excess blood was removed. After removal of atria and large blood vessels right ventricle wall was separated from left ventricle and septum. A ratio was determined based on the weight ratio of RV to LV plus septum.

3.2.2 Cardiac fibroblast isolation

For cardiac fibroblasts isolation Sham or PAB rats were anesthetized with 5 % (vol/vol) Isoflurane followed by i.p. injection of ketamine (90mg/kg) and domitor (0.1mg/kg). Hearts were harvested and further processed in sterile conditions. Right and left ventricles were separated and minced in sterile petri plates in cold 10ml 1x Ads buffer.

5x Ads buffer (500 ml)	
NaCl	17g
HEPES	11.9g
NaH_2PO_4	0.3g
Glucose	2.5g
KCl	1g
$MgSO_4$	0.25g
dd H_2O	up to 500ml
pH adjusted to 7,35 with 1M NaOH	

Minced tissue was placed in upstanding 75cm^2 cell culture flasks and washed with 1x Ads buffer. Next, tissue was subjected to repeated (3x) collagenase II digestion (0.5mg/ml; 2% trypsin in 1x Ads) for 20 min. in 37°C. Each fraction was then neutralized with fetal calf serum, centrifuged (1800 rpm) and subsequently resuspended in FCS. Finally all fractions were suspended in culture media (DMEM, 4.5mg glucose, 20% FCS; 0.1%

penicillin/streptomycin) and seeded in 75 cm^2 culture flasks. Culture medium was changed 24h after isolation and replaced with 10% FCS containing medium upon cell attachment and/or cell migration (1-2 weeks after isolation). Further culture was performed according to standard cell culture protocol, as described below.

3.2.3 Cell Culture

Rat cardiac fibroblasts from whole hearts were purchased from Cell Aplications (San Diego, USA) and grown on Fibroblast Growth Medium supplied by the company (RCF GF medium). For serum starvation, basal medium supplemented with 0.1% FCS was used (for collagen assays, apart from assays after siRNA treatment, medium did not contain any FCS). All cells used were in passage three to five.

Right- and left-ventricular cardiac fibroblasts isolated from PAB- and Sham operated rats were maintained as decribed in 3.2.2 and characterized for fibroblast markers expression by qRT-PCR and IF staining techniques. All experiments were performed on cells in passage two to three. Cells were incubated in a humidified atmosphere of 5% CO_2 in air at 37°C.

3.2.4 siRNA-mediated β-catenin knockdown

ß-catenin knockdown in rat cardiac fibroblasts was carried out using two different purchased siRNAs (Qiagen, Germany) and Xtreme-Gene transfection reagent (Roche, Switzerland) according to manufacturer's instructions. Shortly, required amounts of siRNA and transfection reagent were diluted in Opti-MEM Glutamax I medium (Gibco, USA) and incubated together for 20 min with 1:5 ratio (µg siRNA: µl transfection solution). Cells were transfected with 1-2µg siRNA (final concentration: 40-80nM) in Opti-MEM/Rat fibroblast medium (1:1) for 6h. Next, medium was replaced to appropriate growth medium (containing FCS and antibiotics) and cells were cultured for the next 24-48 h followed by RNA and protein isolations. For each experiment blank (medium only), mock (transfection reagent only) and negative (scrambled siRNA) controls were included. Transfection

efficiency was monitored using Cy^3-labeled scrambled and anti-GAPDH siRNAs (Ambion, USA). For that reason cells seeded in chamber slides were exposed Cy^3-labeled siRNA (final concentration: 75-150nM, corresponding to 1-2µg siRNA per 6-well) according to the same protocol and incubated 24h. This was followed by cell fixation, slides mounting and visualization on confocal microscopy (general protocol described in 3.2.13.1).

3.2.5 RNA isolation and cDNA synthesis

Total RNA from heart tissues was isolated using RNeasy Fibrous Mini Kit (Qiagen, Germany) following manufacturer's protocol. The procedure included proteinase K digestion step for removing abundant proteins in fiber-rich PAB right ventricles. 30 mg of heart tissue was used for each sample. Tissue was homogenized prior to isolation in RLT buffer (provided by kit) using Precellys homogenizer (Peqlab, Germany). Total RNA from cells was isolated using RNeasy Mini Kit (Qiagen, Germany) following manufacturers protocol. RNA concentration and purity was determined using Infinite 200 PRO NanoQuant reader (Tecan, Switzerland).

cDNA was synthesized by two step system using ImProm-II Reverse Transcription kit (Promega, USA) according to the manufacturer's instructions. Briefly, 1µg of total RNA was incubated with 1µl oligo(dT) primers (total volume of 5µl) at 70°C for 5 min and next chilled on ice. Reverse transcription "master mix" was then prepared and added as follows:

Reaction component	Final concentration	Volume
ImProm-II. 5X Reaction Buffer	1x	4µl
25 mM $MgCl_2$	1.9 mM	1.5µl
10 mM dNTP mix	0.5 mM	1µl
RNasin® Ribonuclease Inhibitor (40U/µl)	20U	0.5µl
ImProm-II. Reverse Transcriptase (1U/µl)	0.5U	1µl
Nuclease free water	-	7µl

Samples were then subjected to cDNA synthesis by annealing step (25°C, 5min), synthesis step (42°C, 1h) and finally heat inactivation of reverse transcriptase (70°C, 15 min). cDNA

samples were then cooled on ice and their concentration and quality was determined using Infinite 200 PRO NanoQuant reader.

3.2.6 Quantitative real time-PCR (qRT-PCR)

700ng of newly synthesized cDNA (see 3.2.5) was then subjected to real-time polymerase chain reaction (qRT-PCR). Specific intron-spanning primers were designed by using Primer3 and Primer Blast programs and specificity of primers was once more cross-checked by blasting them against the whole genome (for primer details please see Appendix Table 1). The product size ranged between 150 and 200 bp. For qRT-PCR reactions IQ™ Sybr Green Sypermix (BioRad, USA) was used containing reaction buffer, hot-start iTaq DNA polymerase, 6mM MgCl2, Sybr Green and fluorescein as reference dye. The reactions were prepared as follows:

Reaction component	Final concentration	Volume
IQ™ Sybr Green Sypermix	1x	12.5 µl
Forward primer	200nM	0.5µl
Reverse primer	200nM	0.5µl
Nuclease free water	-	9.5µl
cDNA template	700ng	2µl

To monitor reaction specificity, no template control (NTC) was included for each primer pair and melting curve was generated for each sample. The PCR reactions were performed in BioRad CFX96 Real Time System in the following conditions:

Step	Temperature	Time	
Initial denaturation	95°C	3min	
Denaturation	95°C	10s	Repeat 39x
Annealing	See App. Table 1	20s	
Elongation	72°C	30s	
Melting curve	65 - 95°C	-	

Threshold cycle (Ct) was determined for each sample. For comparison of expression levels, Ct values of gene of interest (GOI) were normalized to reference gene - Porphobilinogen Deaminase (PBGD) and expressed as ΔCt ($Ct_{GOI} - Ct_{reference}$). Alternatively, differences were expressed as ΔΔCt ($\Delta Ct_{treated} - \Delta Ct_{control}$). Each sample was loaded as duplicate and each experiment was repeated.

3.2.7 Agarose gel electrophoresis of PCR products

For verification of primer specificity, qRT-PCR products were mixed with 5x loading dye (Fermentas, USA) and separated on 1.5% agarose gel containing 5µl ethidium bromide in tris-acetate-EDTA (TAE) buffer. The DNA bands were detected by Gel iX Imager (Intas, Germany).

TAE buffer component	Final concentration
Tris-HCl	40nM
Acetic acid	40nM
EDTA, 0.5M, pH 8.0	1mM

3.2.8 Protein isolation

For protein isolation from hearts, 100mg of tissue was homogenized in Precellys homogenizer (Peqlab, Germany) with 500µl RIPA buffer containing 1x protease and phosphatase inhibitor cocktail (Thermo Scientific, USA). Tissue homogenates were centrifuged 30 min at 14000 rpm and supernatants were transferred to new tubes.

For protein isolation from cells, cell media was discarded and cells were carefully washed with PBS. PBS was then discarded and cells were incubated with appropriate amount of RIPA buffer containing proteases and phosphatases inhibitor cocktail (approximately 7µl/cm^2) for 10min in 4°C. Next, lysed cells were scratched with cell scrapers and lysates

were transferred to 1.5ml tubes. Cell lysates were then centrifuged 30 min at 14.000 rpm and transferred to new tubes.

Protein concentration was measured using BioRad DC Protein Assay, which is based on Lowry's protein detection method. A series of bovine serum albumin (BSA) solution with concentrations ranging from 0.1 to 2 mg/ml served as standard. For measurement, tissue-derived proteins were diluted 40x and cell-derived proteins 3x prior to the measurement. Each sample was measured as duplicate using Infinite 200 PRO multiplate reader at λ=750nm.

3.2.9 Protein fractionation

For protein fractionation experiments rat cardiac fibroblasts were grown in 75cm^2 flasks, serum-starved for 24 hours and stimulated with Wnt3a (2,5ng/ml) for 1,3 and 6 hours. Control samples were further starved for 6 hours. Next, cell media was removed and the cells were tripsinized, peleted and snap frozen until further use. Cells derived from two culture flasks were pooled together making up to approximately 3 million cells per sample. Each group was represented by two samples. Protein fractionation was then performed with a use of ProteoExtract® Subcellular Proteome Extraction Kit (Calbiochem, Germany) according to manufacturer's instructions. Briefly frozen cell pellets were gently resuspended in ice-cold Extraction Buffer I and incubated for 10 min under agitation. The samples were centrifuged a 1000g for 10 min and supernatant was collected in a separate tube representing cytosolic fraction. The remaining pellet was resuspended in Extraction Buffer II and incubated for 30 min under gentle agitation. The samples were again centrifuged for 10 min at 6000g and supernatant (membrane/organelle fraction) was collected in a separate tube. Insoluble pellet was resuspended in Extraction Buffer III, incubated for 10min and centrifuged at 7000g (10min). The supernatant (nuclear fraction) was collected in a separate tube and remaining pellet was discarded. All extraction buffers were provided by kit and mixed prior to use with protease inhibitor cocktail.

Due to considerably high volumes of Extraction buffers it was necessary to concentrate the samples before further processing. This was performed by using Amicon Ultra centrifugal filter units (Milipore, USA) according to manufacturer's instructions. Protein concentration was measured using BioRad DC Protein Assay (see 3.2.8) and further used in Western blotting (see 3.2.10).

3.2.10 Western Blotting

3.2.10.1 SDS-polyacrylamide (SDS-PAGE) gel electrophoresis

After protein measurement protein concentration in each set of protein samples was equalized and equal amounts of protein were mixed with 5x sample buffer (SB):

5x SB component	**Final concentration**
Tris-HCl (**2M**, pH 6.8)	375 mM
SDS	10% (w/v)
Glycerol	50% (v/v)
β-Mercaptoethanol	12.5% (v/v)
Bromophenol blue	0.02% (w/v)

Next, samples were heat denatured at 100°C for 5 min. Samples were then loaded onto 10% polyacrylamide gels and run at 80-120 V until separated. Rainbow™ Molecular Weight Marker (GE Healthcare, USA) was included on each gel as molecular weight reference.

Running buffer component	**Final concentration**
Tris-HCl	20 mM
Glycine	186 mM
SDS 20% (w/v)	0.1% (w/v)

Separating gel component	**Final concentration**	**Volume**
Tris/Cl pH 8,9 [1.5M]	375 mM	1.5 ml
Acrylamid 30% (w/v)	10% (w/v)	2 ml
SDS 10% (w/v)	0.1% (w/v)	60 µl
APS 10% (w/v)	0.05% (w/v)	30 µl
TEMED	0.1% (v/v)	6 µl
dd H_2O	-	2.4 ml

Stacking gel component	Final concentration	Volume
Tris/Cl pH 6,8 [0.5M]	125 mM	625 µl
Acrylamid 30% (w/v)	6% (w/v)	500 µl
SDS 10% (w/v)	0.1% (w/v)	25µl
APS 10% (w/v)	0.05% (w/v)	12.5µl
TEMED	0.1% (v/v)	2.5 µl
dd H_2O	-	1.34 ml

3.2. 10.2 Immunoblotting

The proteins separated on polyacrylamide gels were transferred onto nitrocellulose membranes using Mini Trans-Blot Electrophoretic Transfer Cell unit (BioRad, USA) for 1h at 100V.

Blotting buffer component	Final concentration
Tris-HCl	38mM
Glycine	40mM
Methanol	20% (v/v)

Membranes were then blocked for 1h in 5% skim powder milk in 1x TBST and incubated overnight with indicated antibodies (see Appendix Table 2) solutions in 5% milk overnight at 4°C with shaking. After three 10 min. washing steps in TBST membranes were incubated with appropriate horseradish peroxidase (HRP)-conjugated secondary antibodies (see appendix Table 3) for 1h at room temperature (rt) on shaker. Three further TBST washing steps were then followed by developing with SuperSignal West Femto Chemiluminescent Substrate (Thermo Scientific, USA) and capturing the chemiluminescent signal in FujiFilm LAS 4000 analyzer (FijiFilm, Japan). Afterwards the antibodies were removed using Restore Western Blot Stripping Buffer (Thermo Scientific, USA) and membranes were reprobed with Glyceraldehyde 3-phosphate dehydrogenase (GAPDH) or ß-actin as loading controls. Each western blotting experiment was independently repeated.

3.2.11 Sircol Collagen Assay

For measuring salt-, acid-, and pepsin soluble collagen fractions in heart tissue, Sircol Collagen Assay was employed according to manufacturer's instructions. 100mg of tissue was homogenized in RIPA buffer (with proteases and phosphatases inhibitors; Thermo Scientific, USA) in Precellys homogenizer (Peqlab, Germany). Next, each lysate was divided into three fractions, supplemented with PBS, 0.5M acetic acid or 0.1mg/ml pepsin (in 0.5M acetic acid) and incubated overnight at 4°C. For all further steps blanks (PBS, acetic acid or pepsin solutions were included). Acid Neutralizing Reagent was added to all acetic acid containing samples and subsequently Isolation and Concentration Reagent was added to all samples followed by overnight incubation at 4°C. All tubes were then centrifuged and the supernatant was carefully removed. For further steps standard solutions (pure collagen I, 2-50 µg of collagen) were included. All samples were further incubated with 1ml Sircol Dye Reagent for 30 min. on shaker followed by centrifugation. Next, ice-cold Acid-Salt Wash reagent was applied and the samples were spun down. After removing of supernatant the pellet was resuspended in 400µl of Alkali Reagent, transferred as duplicates on multiwell plate and absorbance was measured at λ=555.

For rat cardiac fibroblast collagen synthesis assay the protocol was modified by omitting acetic acid and pepsin digestion as well as concentration steps. For measuring collagen concentration in cell media, 1ml of media was concentrated overnight and further processed according to standard protocol.

3.2.12 BrdU incorporation assay

For cell proliferation measurements BrdU incorporation assay (Roche, Switzerland) was performed according to manufacturer's instructions. Briefly, rat cardiac fibroblasts were grown on 96- or 48-well plates and incubated with given concentrations of Wnt3a, LiCl or β-catenin-targeting siRNA for 24-48h. For the two last hours of incubation BrdU labeling solution was added (final concentration 10 µM). This was followed by 30 min fixing and 90

min anti-BrdU antibody incubation steps. Next, antibody solution was removed, cells were washed with 1x PBS and incubated for 15-30 min with developing agent. Within this time frame colorimetric measurement was performed in Infinite 200 PRO multiplate reader at λ=450 nm (measurements at reference wavelength λ=690 nm were automatically subtracted for each well). For each study blank (- cells) and background (-medium, -BrdU) controls were included.

3.2.13 Immunofluorescence staining

3.2.13.1 Immunocytochemistry

For immunocytochemical analysis, rat cardiac fibroblasts were fixed in ice-cold acetone-methanol (1:1) solution for 10 min. at room temperature. The slides were then washed with 1x PBS buffer and blocked with 5% BSA (w/v in 1xPBS) solution for 1h at RT.

1x PBS component	**Final concentration**
NaCl	137mM
KCl	2.7mM
Na_2HPO_4	10mM
KH_2PO_4	2mM
pH adjusted to 7.4 with 1M NaOH	

Primary antibodies were diluted (see Appendix Table2) in 1-3% BSA in PBS and incubated overnight at 4°C. This was followed by 30 min. wash in 1xPBS buffer and 1h incubation with adequate fluorescent dye-labeled secondary antibody (1h, RT). After PBS wash step the nuclei was stained with Draq5 (Enzo Life Sciences, USA) for 10 min at RT, the slides were washed and mounted with Fluorescence Mounting Medium (Dako, Denmark). For immunofluorescence analysis Zeiss confocal microscope (Carl Zeiss, Germany) was used.

3.2.13.2 Immunofluorescent cryosections staining

For the analysis of protein localization in animal tissue appropriate organs were harvested and washed in cold HBSS (Gibco, USA) buffer. Prior to embedding the organs in Tissue-Tek (Sakura, USA) right ventricles were separated from left ventricles. Embedded samples were next snap-frozen in dry ice cooled 2-butanol and the cryoblocks were stored at -80°C. For

immunofluorescent staining 6-10 µm thick sections were used and the same protocol as for immunocytochemistry was followed.

If needed, counterstaining steps were included after secondary antibody and PBS wash steps were included as follows. For staining F-actin filaments the samples were incubated for 25 min. with Alexa488-labeled Phalloidin (1:40, Molecular Probes). Cell membranes were stained for 40 min. with Alexa488-labeled WGA (10ng/ml, Molecular Probes). Fibroblasts were visualized in the heart tissue by double staining with direct Cy^3-labeled vimentin antibodies (1h, 1:300, Sigma -Aldrich).

3.2.12.3 Immunofluorescent staining quantification

The quantification of BAT-Gal positive cells as well as siRNA (Cy3-labeled) transfected cells was performed using STEPanizer© stereology tool, ver, 1.0 applet.

3.2.13 Statistical analysis

All results are expressed as means +/- standard error (SEM). Statistical analysis was performed using Student's t-test for comparison of two groups and 1-way ANOVA with Newman-Keuls post hoc test for comparison of more than two groups. Differences between the groups was considered significant when $P<0.05$.

4. Results

4.1 Cardiac hypertrophy and fibrosis in PAB and MCT models of right ventricular remodeling

In the present study two animal models have been employed – pulmonary artery banding model of right ventricular hypertrophy and monocrotaline model of pulmonary hypertension with RV remodeling. Monocrotaline (MCT) is a pyrrolizidine alkaloid derived from the plant *Crotalaria spectabilis*. This phytotoxin is activated in the liver to the reactive monocrotaline pyrrole metabolite, which leads to vascular injury and subsequently to vascular remodeling and right ventricular hypertrophy. A single dose of MCT is sufficient to produce a progressive and sustained pulmonary hypertension in rats [108]. Pulmonary artery banding is based on the narrowing of internal diameter of the pulmonary artery and serves as a model of right ventricular hypertrophy and heart failure. This model does not exhibit any other direct effects on the heart apart from the increase in afterload. For this reason the changes observed PAB model result solely from the increased cardiac pressure overload (in contrast to other models of PAH, such as MCT model)[40].

Two weeks after PAB procedure and 4 to 6 weeks after monocrotaline injection hearts were harvested for further analysis (Fig. 8a). Preliminary examination of cardiac hypertrophy was conducted based on the RV to LV plus septum wet weight ratio. As shown in Fig. 8b, all treated animals developed significant RV hypertrophy. In the MCT model, 5 weeks' time point mostly resembled the results obtained for the PAB model and hence it was mainly subjected to further analysis.

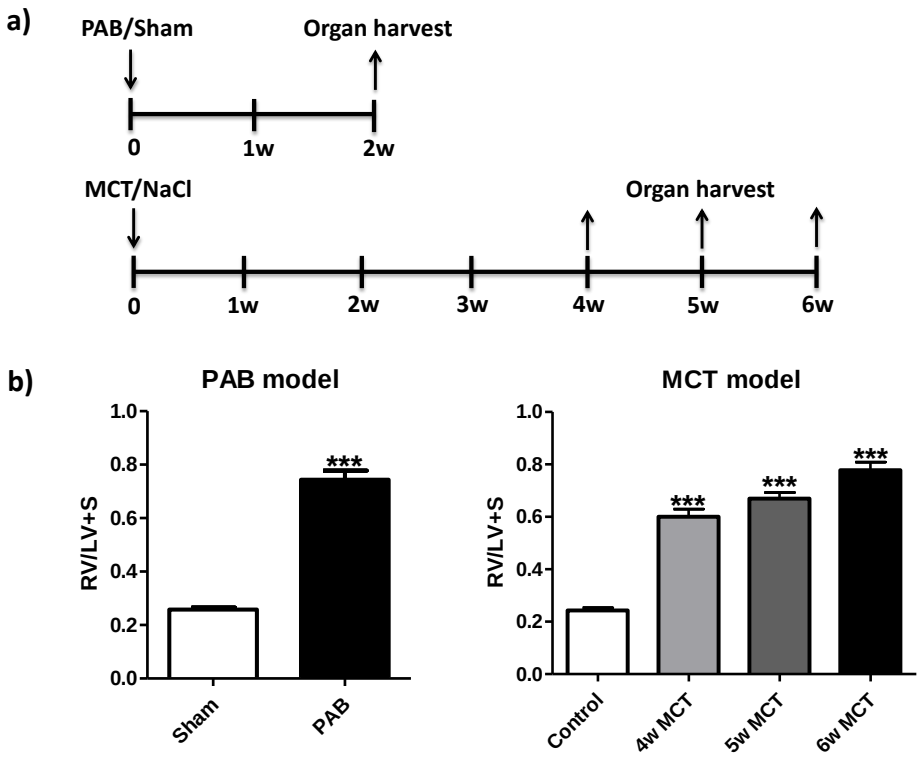

Figure 8. Experimental setup for PAB and MCT models of right ventricular remodeling: a) hearts were collected 2 weeks after PAB (or Sham) procedure and 4-6 weeks after MCT (or NaCl) s.c. injection; b) hypertrophy was assessed by right ventricle to left ventricle plus septum (RV/LV+S) wet weight ratio. PAB n=10, MCT n=5-10; *** P<0.001

Further, we investigated the expression of well-described hypertrophic markers by qRT-PCR technique in both models as well as cardiac fibrosis by changes in the total amount of collagen. We found upregulation of several hypertrophic markers in the right ventricles of PAB rats, including: αSKA, βMHC, BNP, ANP and TIMP (P<0.001). The level of αMHC was downregulated in agreement with the literature (P<0.01; see chapter 1.4). No significant changes in expression of genes associated with cardiac hypertrophy were observed in the left ventricles except the increased level of ANP. Additionally the expression of both, collagen type 1 and 3 was also significantly elevated in right ventricles of banded animals (P<0.001; Fig. 9a).

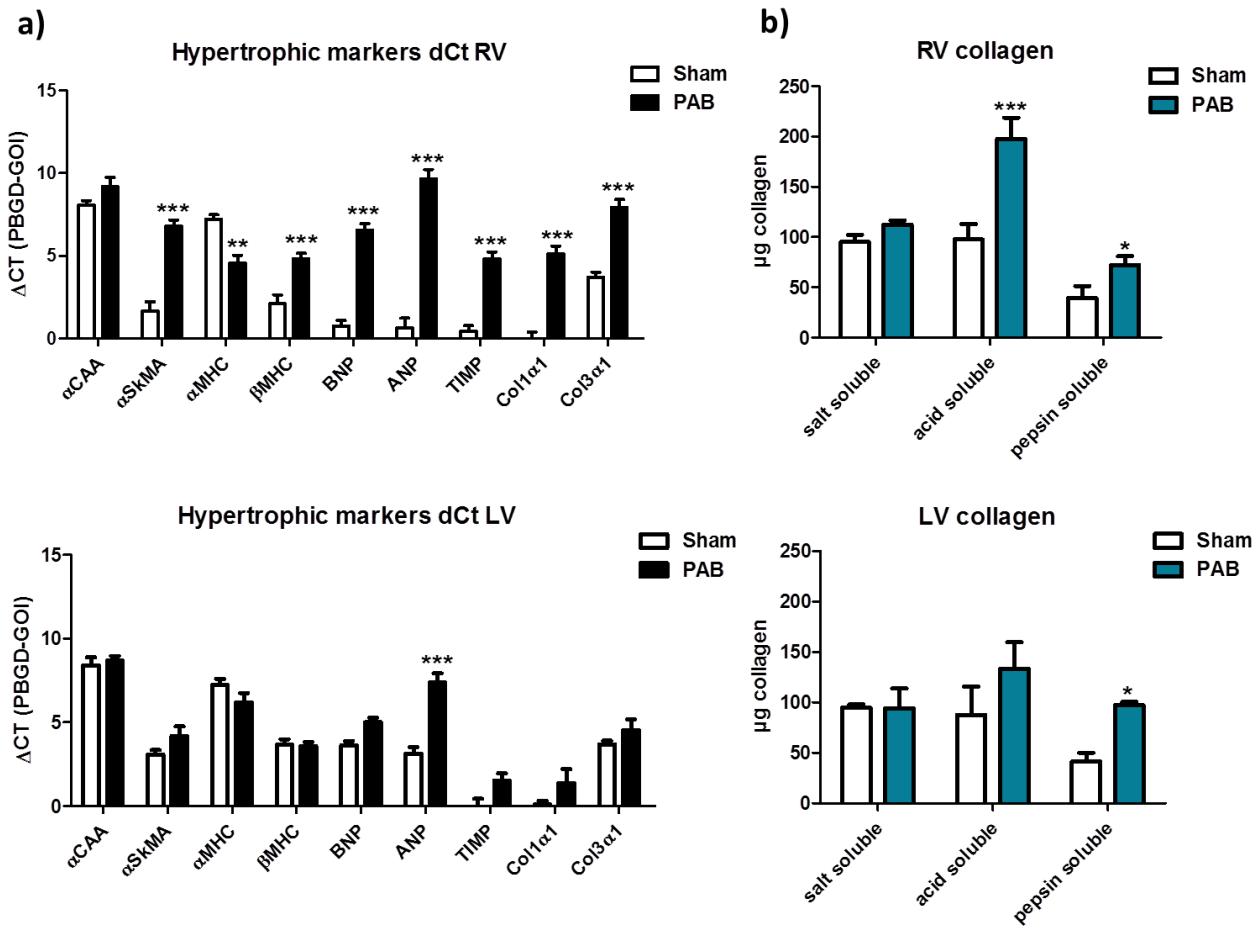

Figure 9. Assessment of right-ventricular hypertrophy after pulmonary artery banding by hypertrophic markers expression: a) qRT-PCR, and b) Sircol Assay. n=5 (a), n=10 (b), RV – right ventricle, LV - left ventricle; * (P<0,05); ** (P< 0,01); *** (P<0,001) vs. Sham

For total collagen content measurement we employed sircol assay for three collagen fractions: salt, acid and pepsin soluble fractions corresponding to collagen crosslinking levels. We found an immense increase in acid-soluble fraction as well as significant increase in pepsin soluble fraction of total collagen in PAB right ventricles (Fig. 9b). Surprisingly we observed also an increase in pepsin soluble fraction in the left ventricles of PAB animals (Fig. 9b).

Expression profile alteration in the right ventricles of MCT animals resembled those obtained in PAB animals, including αSKA, βMHC, BNP, ANP, TIMP, Colα1 and Colα3 upregulation (P<0.001-0.05) and αMHC downregulation (P<0.05; Fig. 10a). Also in this

model, no change was observed in most hypertrophic markers expression in left ventricles besides αMHC downregulation (P<0.001) and ANP upregulation (P<0.001).

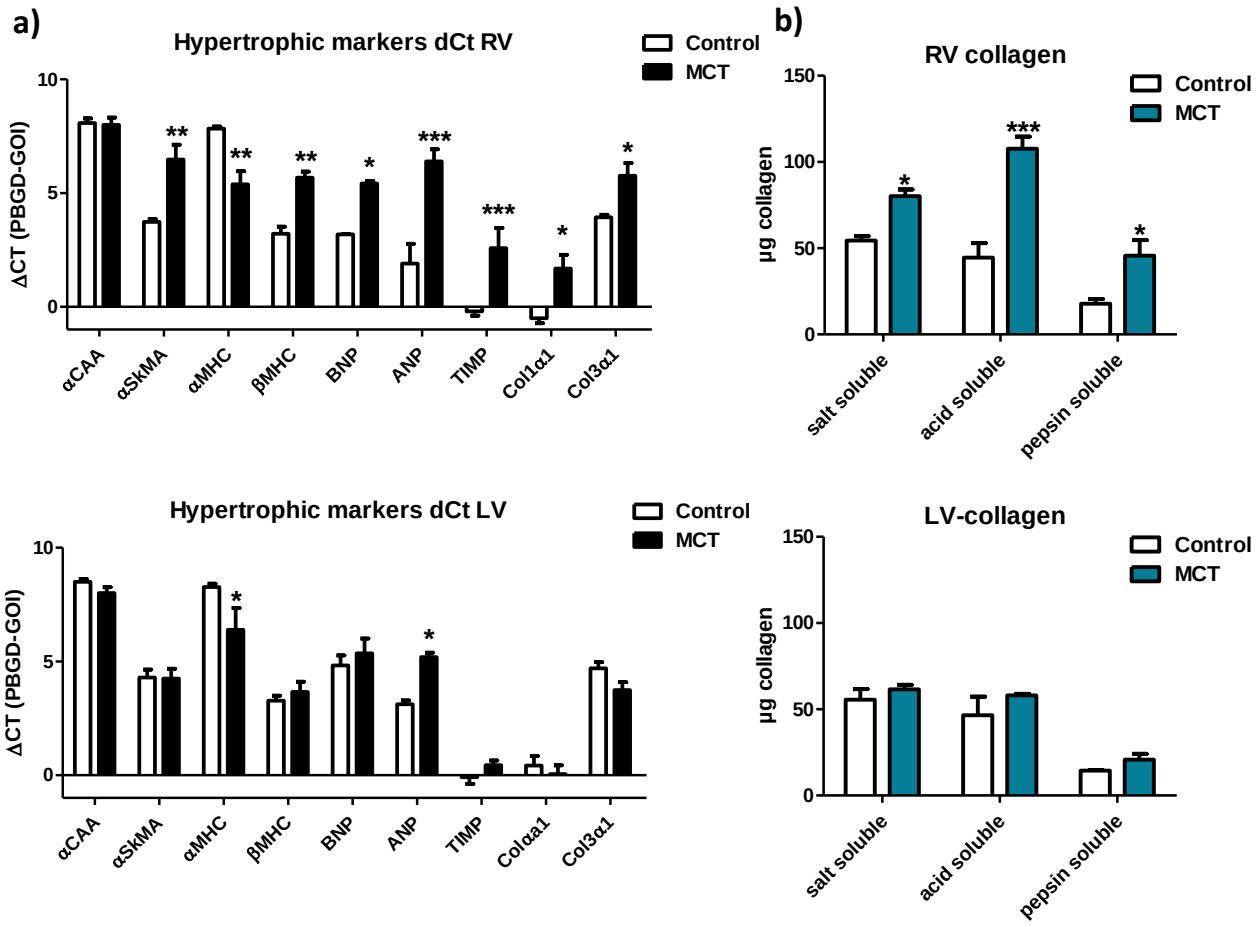

Fig. 10. Assesment of right-ventricular hypertrophy after MCT treatment by hypertrophic markers expression: a) qRT-PCR, and b) Sircol Assay. n=5 (a), n=10 (b); RV – right ventricle, LV - left ventricle; * (P<0.05); ** (P< 0.01); *** (P<0.001) vs. Control

The changes in total collagen in right ventricles of MCT rats were observed (P<0.5-0.001) within all fractions as compared to control. No significant differences in total collagen content were found in the left ventricles of MCT and control animals. Further, we assessed the cardiac fibrosis by immunofluorescence staining of vimentin, a reliable marker for identification of cardiac fibroblasts [32] and collagen type 1α.

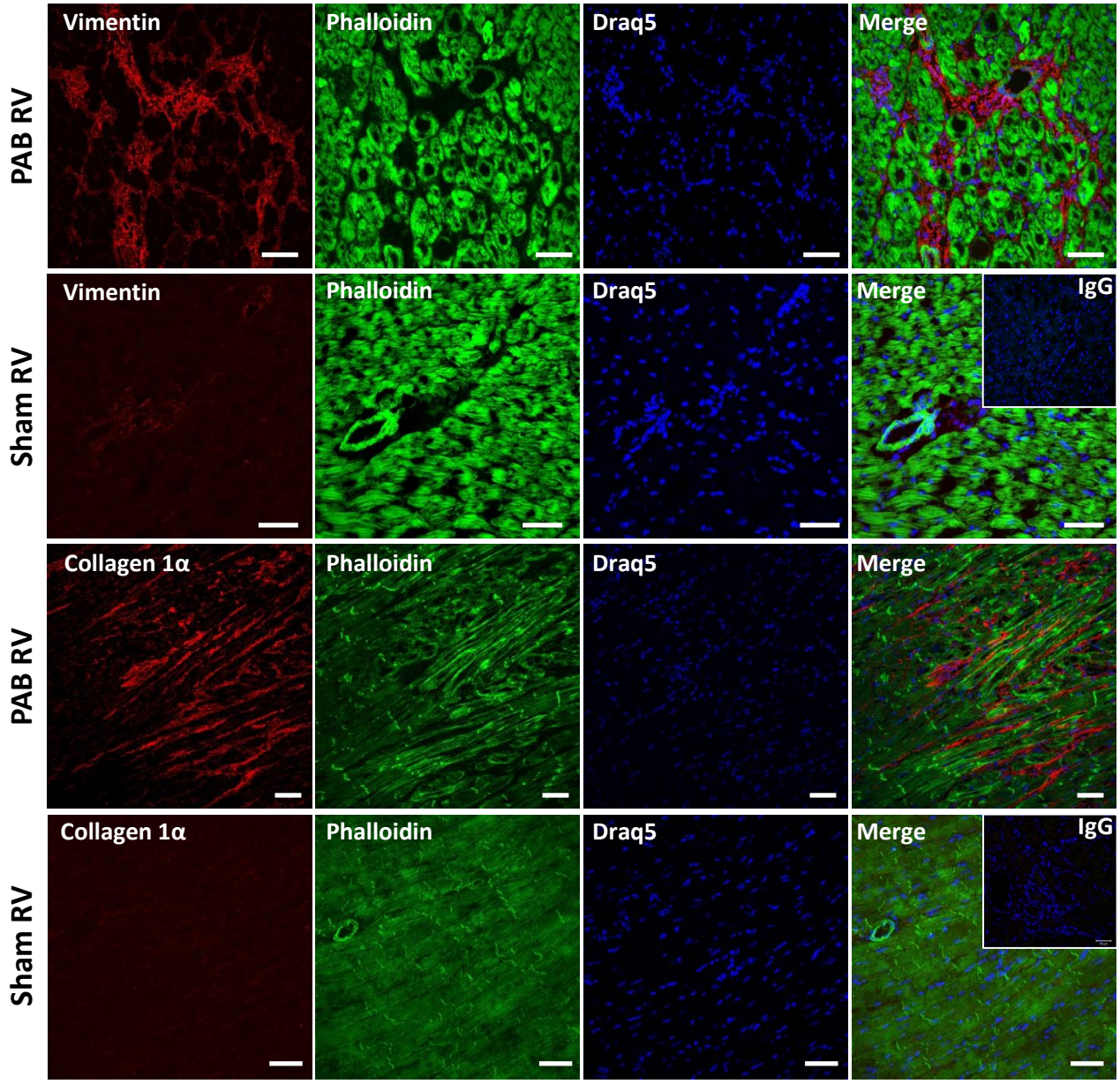

Fig. 10. Assessment of right ventricular fibrosis after PAB by IF staining: Cryosections derived from PAB/Sham ventricles were stained for the presence of fibroblast marker - vimentin and collagen 1α (red). The sections were counterstained with Phalloidin (green) and Draq5 (blue) for cardiomyocyte and nuclei detection, accordingly. n=2, RV – right ventricle, LV - left ventricle, IgG – isotype control; bars represent 50 µm

Right ventricles of PAB rats showed elevated levels of both, vimentin and collagen as compared to RVs of Sham animals (Fig. 10). In addition, no changes were observed in left ventricles within all groups (data not shown).

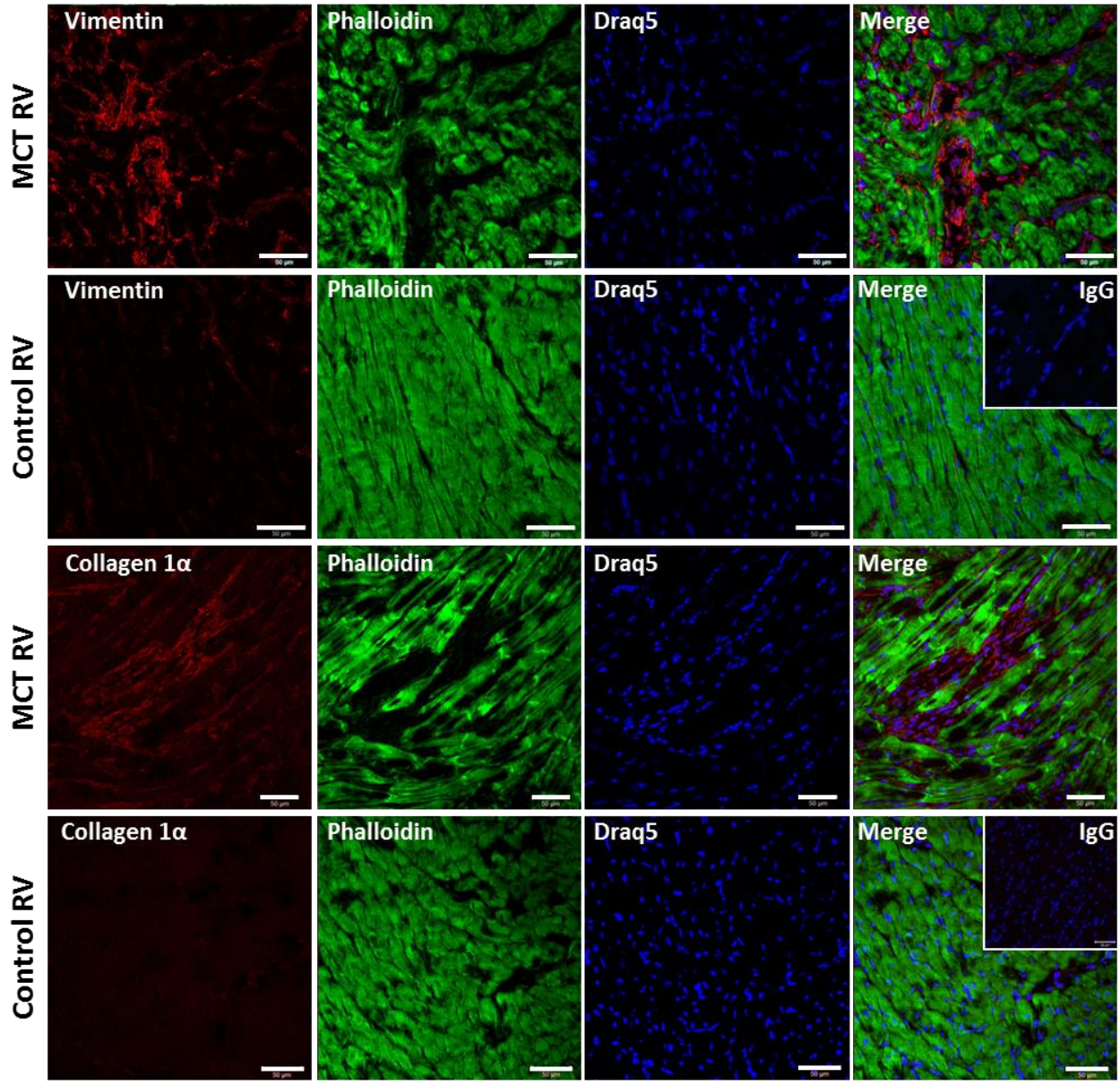

Fig. 11. Assessment of right ventricular fibrosis after MCT treatment by IF staining: Cryosections derived from MCT/Control ventricles were stained for the presence of fibroblast marker - vimentin and collagen 1α (red). The sections were counterstained with Phalloidin (green) and Draq5 (blue) for cardiomyocyte and nuclei detection, accordingly; n=2, RV – right ventricle, LV - left ventricle, IgG – isotype control; bars represent 50 μm

Similarly, right ventricles of MCT rats showed higher levels of vimentin and collagen staining as compared to controls (Fig. 11). However, we found also increased level of vimentin and collagen staining in the left ventricles of MCT animals (data not shown).

4.2 Wnt/β-catenin signaling molecules expression in PAB and MCT models

To elucidate Wnt/β-catenin signaling molecules expression in hypertrophied hearts we performed mRNA and protein screening experiments in PAB and MCT models. The qRT-PCR analysis revealed upregulation of β-catenin, GSK3β and both Fz1 and Fz2 in the right ventricles of PAB animals (P<0.01, Fig. 12). Those changes were limited only to RVs and no alterations were observed within the left ventricles.

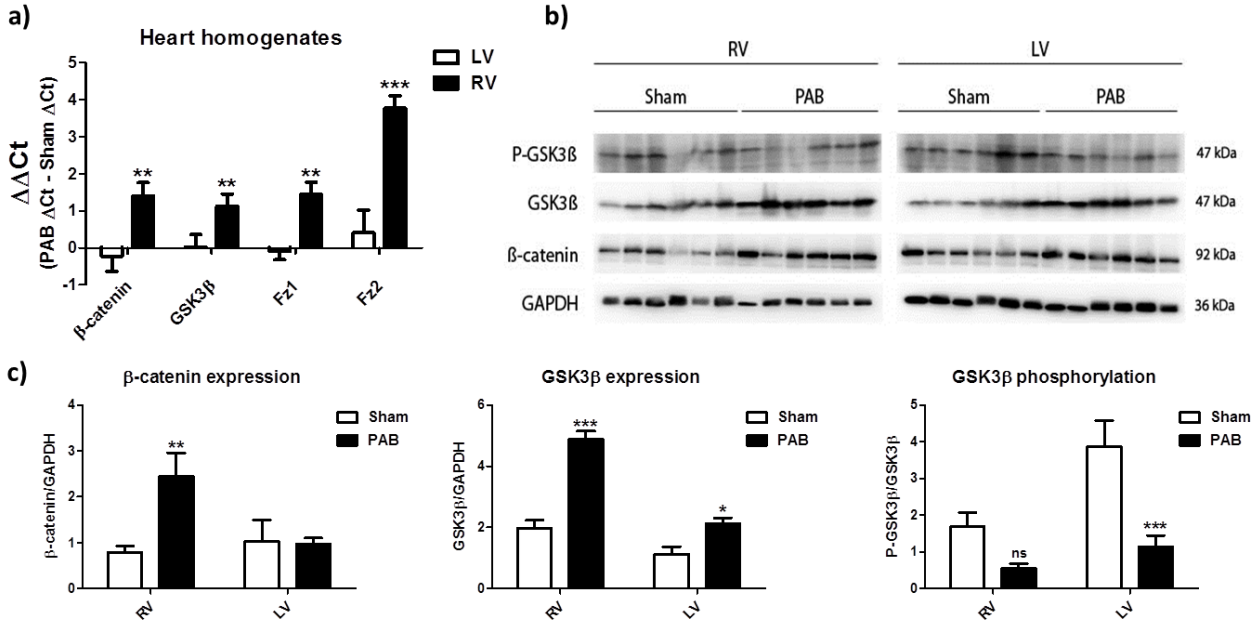

Fig. 12. Wnt signaling molecules expression in heart homogenates derived from PAB animals: a) qRT-PCR, n=10; b) Western blotting analysis, n=5; and c) quantification of Western blotting by densitometry. RV - right ventricle; LV - left ventricle; * (P<0.05); ** (P< 0.01); *** (P<0.005) vs. Sham

Similarly, upregulation of β-catenin and GSK3β was observed on the protein level in PAB RVs (P<0.01, Fig. 12b-c). GSK3β phosphorylation levels were lower in both ventricles, but this reduction was not significant for the RVs. In MCT hearts (5 weeks after treatment) we observed an upregulation of GSK3β and Fz2 mRNAs (P<0.05, Fig.13a). β-catenin and Fz1 receptor mRNAs showed the tendency to be upregulated but did not reach the statistical significance.

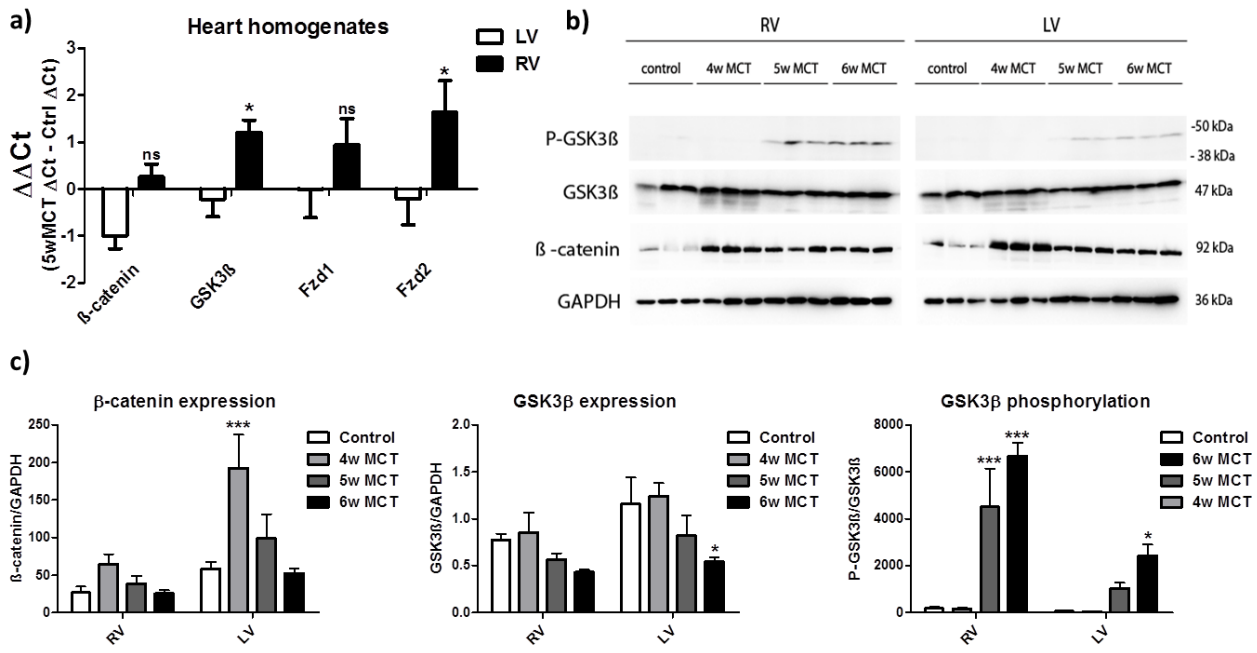

Fig. 13. Wnt signaling molecules expression in heart homogenates derived from MCT animals: a) qRT-PCR, n=10; b) Western blotting analysis, n=3; and (c) quantification of Western blotting by densitometry. RV - right ventricle, LV - left ventricle, 4w, 5w, 6w – 4, 5 and 6 weeks; * (P<0.05); ** (P< 0.01); *** (P<0.005) vs. Control

On the protein levels we also detected tendency to increase β-catenin and GSK3β in MCT model (especially in 4 week time points, Fig. 13b-c). Interestingly, although statistically not significant, those changes have been observed in both, the right and the left ventricle.

4.3 Isolation and characterization of cardiac fibroblasts

Since it was shown that Wnt/Fz signaling may influence the migration and the differentiation of cardiac fibroblasts [109], we decided to examine the role of this signaling pathway in the course of right ventricular hypertrophy. Primary cardiac fibroblast were isolated separately from right and left ventricles of PAB and Sham animals. The purity of isolation procedure was further confirmed by the expression of known fibroblast markers described in the literature [32]. All isolated cells were positive for fibronectin and collagen 1α as assessed by immunofluorescence staining (Fig. 14a, expression of markers in LV- RCFs are not shown).

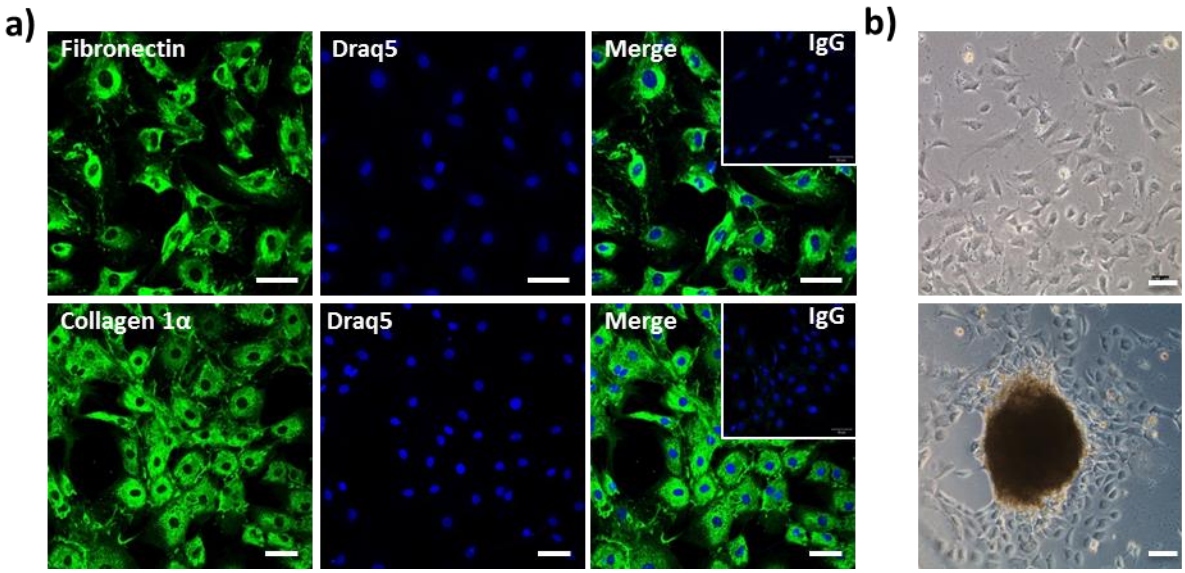

Fig. 14. Characterization of isolated primary cardiac fibroblasts I: a) representative pictures showing expression of fibroblast markers: fibronectin and collagen 1α in the right ventricular RCFs by IF, IgG – isotype control, bars represent 50 µm; b) bright filed pictures showing cardiac fibroblasts attaching to cell culture plate following isolation procedure (upper panel) and cells migrating out from the cardiac tissue particles (lower panel), bars represent 100 µm

In addition, expression of fibroblast markers was analyzed in several successive passages of isolated cells. From passages 2 to 5, no changes have been observed in the expression of collagen 1α (Col1α1), fibronectin (Fn) and prolyl 4-hydroxylase β-subunit (P4Hb) (Fig. 15a). Expression of DDR2, a collagen receptor was slightly decreased in P5 ($P<0.05$) and collagen 3α mRNA was decreased within passages 4 and 5 ($P<0.05$ and $P<0.01$, accordingly). In left ventricular RCFs only fibronectin was elevated in P4-P5 (data not shown). Based on these results all further experiments were performed on cells in passage 2 to 4.

Further, proliferation of cardiac fibroblasts was determined by BrdU incorporation. We found increased proliferation of cardiac fibroblasts derived from right ventricles of PAB animals ($P<0.005$), whereas proliferation rates in other groups did not vary (Fig. 15b).

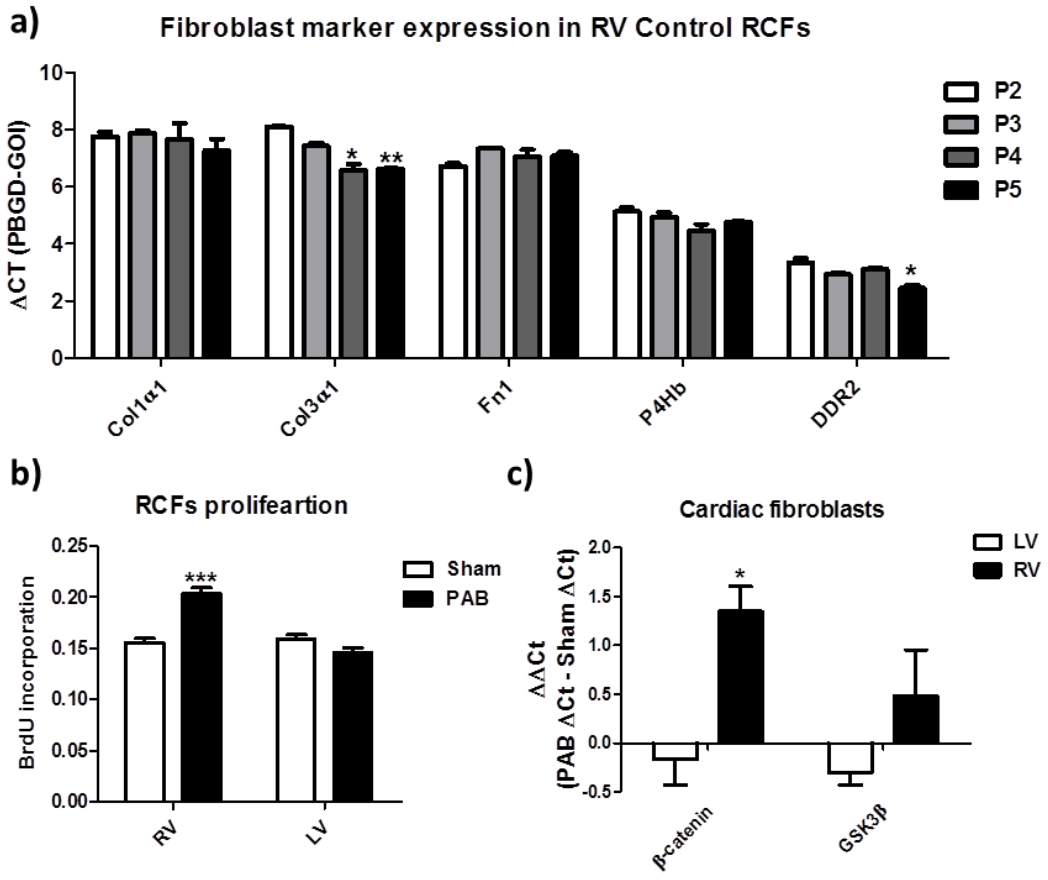

Fig. 15 Characterization of isolated primary cardiac fibroblasts II: a) Expression of fibroblast markers in right ventricular RCFs through passages (P2-P5) by qRT-PCR, n=3; b) assessment of RCFs proliferation by BrdU incorporation, n=10; and c) Expression of β-catenin and GSK3β in RCFs by qRT-PCR. n=3; RV - right ventricle; LV - left ventricle * (P<0.05); ** (P< 0.01) *** (P<0.005) vs. Control

Given that the right ventricle PAB rats show an increased expression of Wnt signaling components, further screening analysis of Wnt signaling molecules was assessed in cardiac fibroblasts to check whether cardiac fibroblasts may be, at least in part, responsible for observed changes. Indeed, β-catenin mRNA levels were significantly increased in PAB right ventricular fibroblasts (Fig. 15c, P<0.05). GSK3β levels were also increased in PAB RV-RCFs but this has not reached statistical significance.

4.4 Effects of Wnt3a stimulation on primary rat cardiac fibroblasts

In order to examine how the Wnt pathway may act on cardiac fibroblasts we have designed series of experiments involving Wnt3a stimulation. In these fundamental experiments, we used the whole heart fibroblasts purchased from Cell Applications (USA). First, cardiac fibroblasts were treated with Wnt3a (2.5ng/ml) for 12 and 24 h followed by qRT-PCR analysis of changes in gene expression pattern. We found elevated mRNA levels of β-catenin and Dvl as well as GSK3β (Fig. 16a, $P<0.01$ and $P<0.05$, accordingly) 12h after Wnt3a stimulation. Apart from that we observed elevated levels of Axin2 - a negative regulator of the Wnt pathway, and Cyclin B1, responsible for G2/M transition, 12 and 24 h after stimulation with Wnt3a ($P<0.01$ in 12h and $P<0.005$ in 24h).

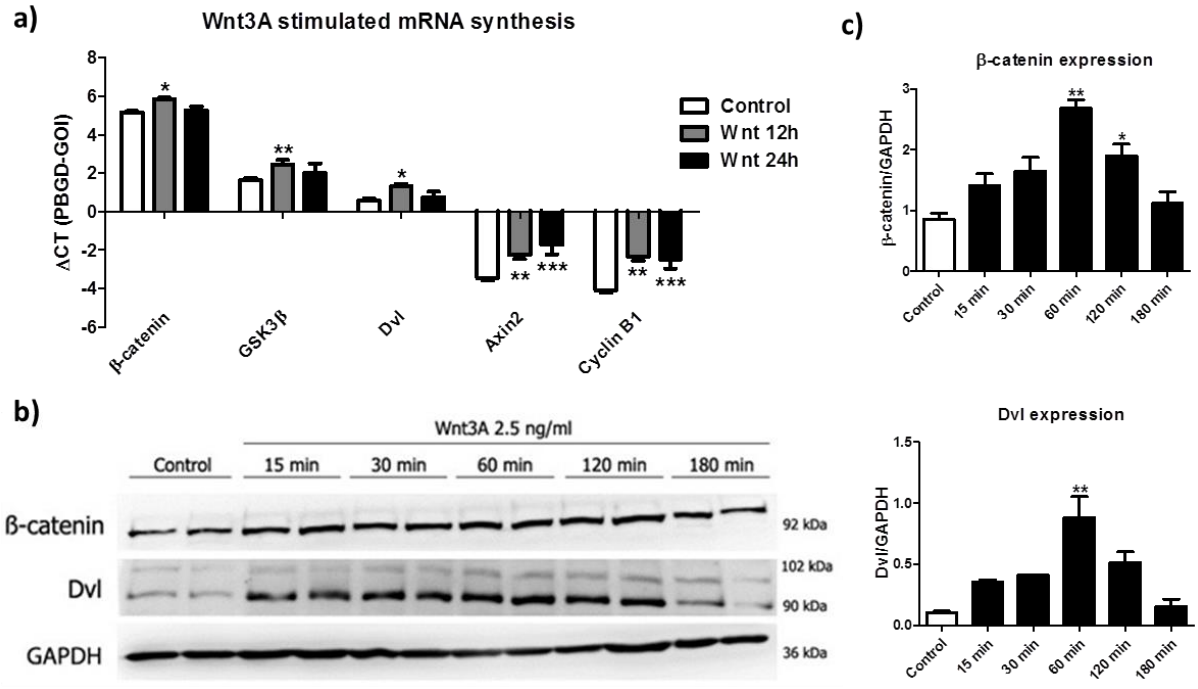

Fig. 16. Wnt3a primary cardiac fibroblasts stimulation: a) 12-24h Wnt3a [2.5ng/ml] cardiac fibroblasts stimulation followed by qRT-PCR, n=4; b) 15-180 min Wnt3a [2.5ng/ml] stimulation followed by WB. n=2; (c) quantification of Western blotting by densitometry; * ($P<0.05$); ** ($P< 0.01$) *** ($P<0.005$) vs. Control

Since the accumulation and nuclear translocation of β-catenin is the hallmark of activated canonical Wnt signaling, we decided to address this issue in cardiac fibroblasts treated with Wnt3a. Preliminary analysis of whole cell lysates has demonstrated accumulation of β-catenin in response to Wnt3a stimulation, which reached peak 1 hour after treatment (Fig. 16b-c; $P<0.01$). To further evaluate the nuclear translocation of β-catenin, cardiac fibroblasts stimulated for 1 to 6 h with Wnt3a were then submitted to protein fractionation procedure. We found increased levels of β-catenin in the nuclear fraction at 3 and 6 hours after Wnt3a treatment (Fig. 17a, 17b $P<0.05$ at 3h). Accumulation of β-catenin in cytosolic fraction was observed at 1 and 3 h ($P<0.05$), which roughly resembled the results obtained for whole cell lysates (Fig. 16b and 17a-b). The membrane fraction remained unchanged except a slight reduction in the level of β-catenin at 3 h post stimulation (Fig. 17a-b; $P<0.05$). All membranes were tested for the presence of contaminating proteins from other factions and have been proven to be pure (Fig 17c).

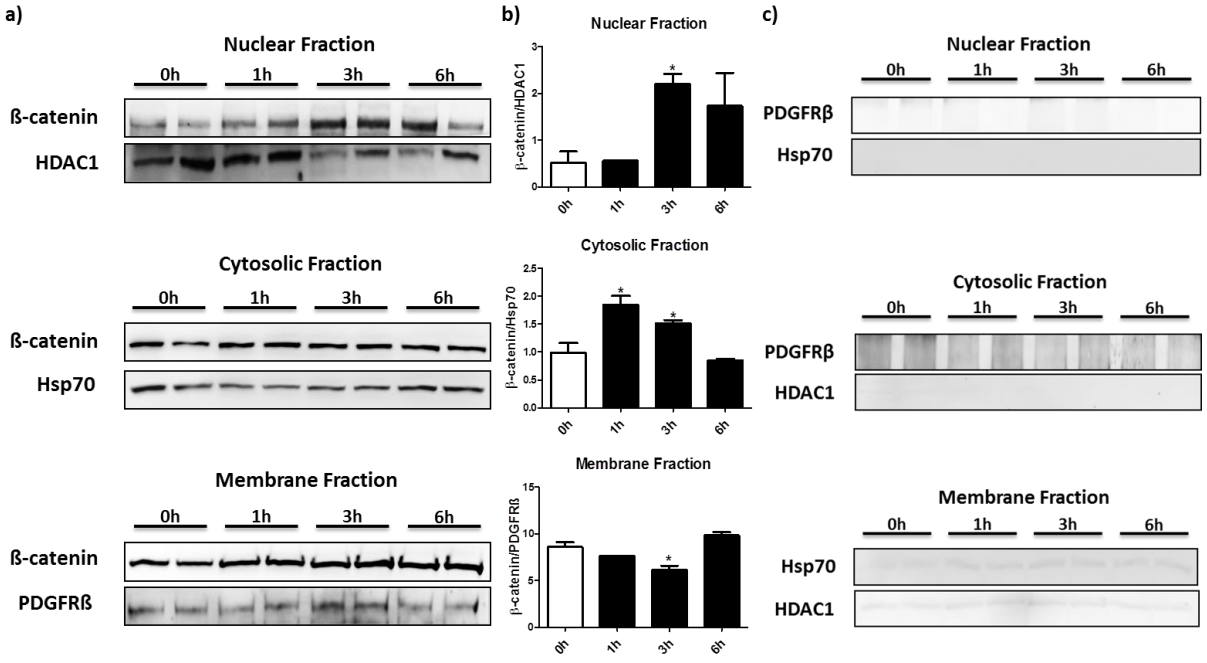

Fig. 17. Subcellular localization of β-catenin assessed by protein fractionation: a) cardiac fibroblasts were stimulated with Wnt3a for 1-6h followed by protein fractionation and WB, n=2; b) quantification of Western blotting by densitometry; and (c) fractionation purity control. n=2; * ($P<0.05$) vs. Control

4.5 siRNA-mediated β-catenin knockdown

In order to further explore the functional role of β-catenin in cardiac fibroblasts, we have established siRNA-mediated β-catenin knockdown experiments. To determine the transfection efficiency, whole heart cardiac fibroblasts were transfected with 1-2µg of Cy3-labeled scrambled siRNA (Fig. 18a). Transfection efficiency was determined on the basis of siRNA-positive cells percentage. As illustrated in Figure 18a, cardiac fibroblasts transfection was observed at both concentrations of siRNA.

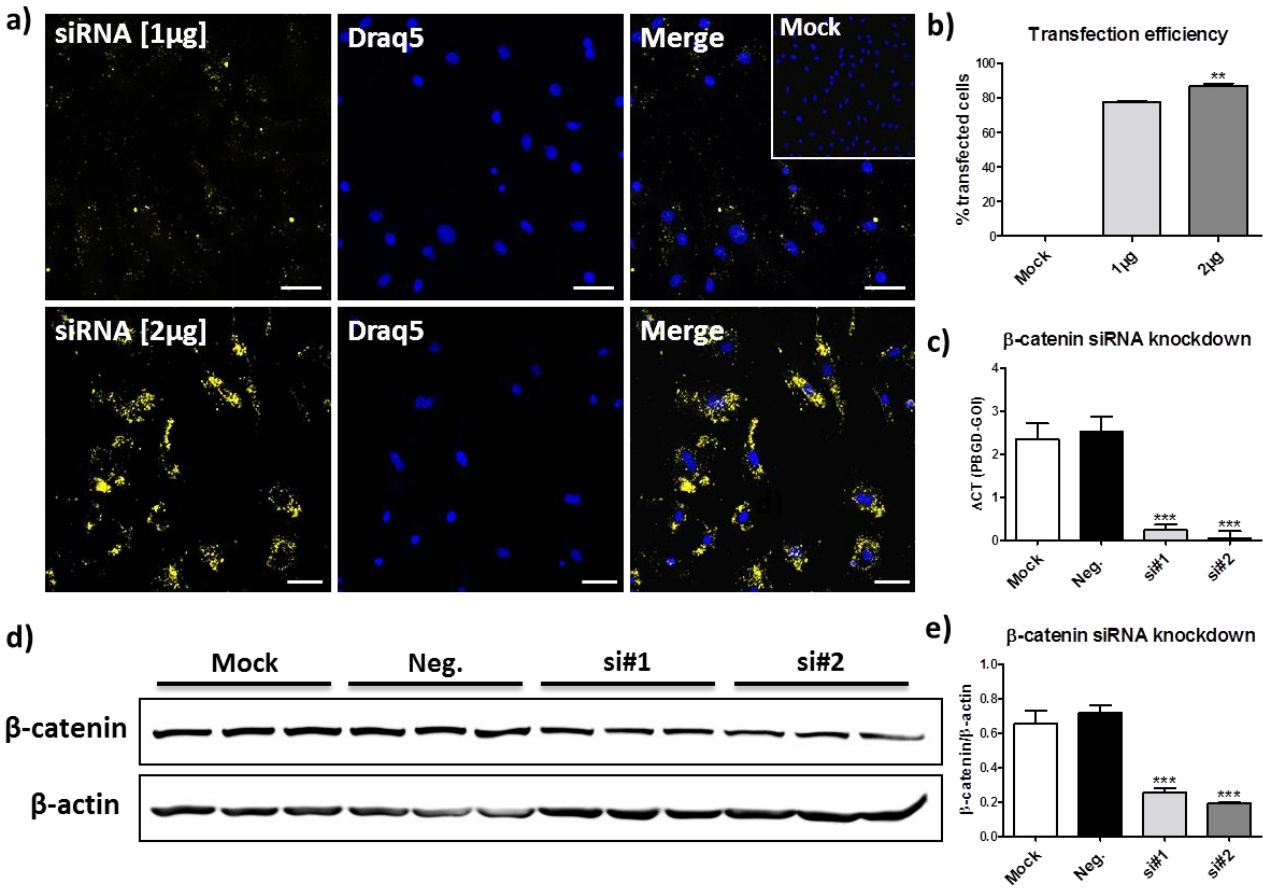

Fig. 18. siRNA mediated ß-catenin knockdown: a) transfection efficiency evaluation; 1-2 µg of Cy-3 labeled scrambled siRNA (yellow) was used and visualized by immunofluorescence microscopy, counterstained with Draq5 (blue) and b) transfection efficiency quantification based on siRNA-positive cells counting. n=2, ** (P<0.01 vs. 1µg). (c-e) β-catenin knockdown with two different siRNAs (#1-2, 2µg, Qiagen) followed by c) qRT-PCR analysis; d) immunoblotting; and (e) quantification of Western blotting by densitometry. n=3, ** (P<0.01); *** (P<0.005) vs. negative control

However, 2µg of siRNA showed better transfection efficiency as assessed by the amount of siRNA in cells (Fig. 18a) as well as the percentage of transfected cells (Fig. 18b, $P<0.01$). For that reason 2µg of siRNA was used in all further experiments.

β-catenin knockdown was accomplished by using two different siRNAs (Qiagen, Germany) and was monitored using qRT-PCR technique. Both siRNAs significantly reduced β-catenin mRNA levels (Fig. 18c, $P<0.001$). To further confirm the knockdown, β-catenin protein levels were determined by Western blotting. On the protein level both siRNAs were able to significantly decrease the level of β-catenin (Fig. 18d-e, $P<0.001$). Transfection agent (mock control) as well as scrambled siRNA (negative control) had no effect on the levels of β-catenin (Fig. 18c-e). Hence, we can conclude we have established efficient β-catenin knockdown.

4.6 The impact of Wnt/β-catenin signaling on collagen production

As it has been previously described that Wnt signaling may affect the synthesis of collagen in immortalized cardiac fibroblast cell line [109], we decided to investigate this phenomenon in primary rat cardiac fibroblasts. Wnt3a stimulation of RCFs resulted in upregulation of Collagens 1α, 3α ($P<0.001$) and Collagen 4α ($P<0.01$) at 12 and 24 h post treatment (Fig. 19a). Increased Collagen synthesis was also observed on the protein level 48 hours after Wnt3a treatment as assessed by sircoll assay (Fig. 19b, $P<0.001$). Additionally, we also found increased collagen secretion as increased total collagen amounts were also detected in the culture medium from RCFs stimulated Wnt3a ($P<0.01$). These results were further confirmed using β-catenin knockdown approach. β-catenin depleted cells showed decreased collagen synthesis in basal (10% FCS) conditions as compared to scrambled siRNA negative control ($P<0.01$ and $P<0.001$ for siRNA #1 and #2, accordingly). Thus, these results indicate the functional role of Wnt/β-catenin signaling in the synthesis and secretion of Collagen by RCFs.

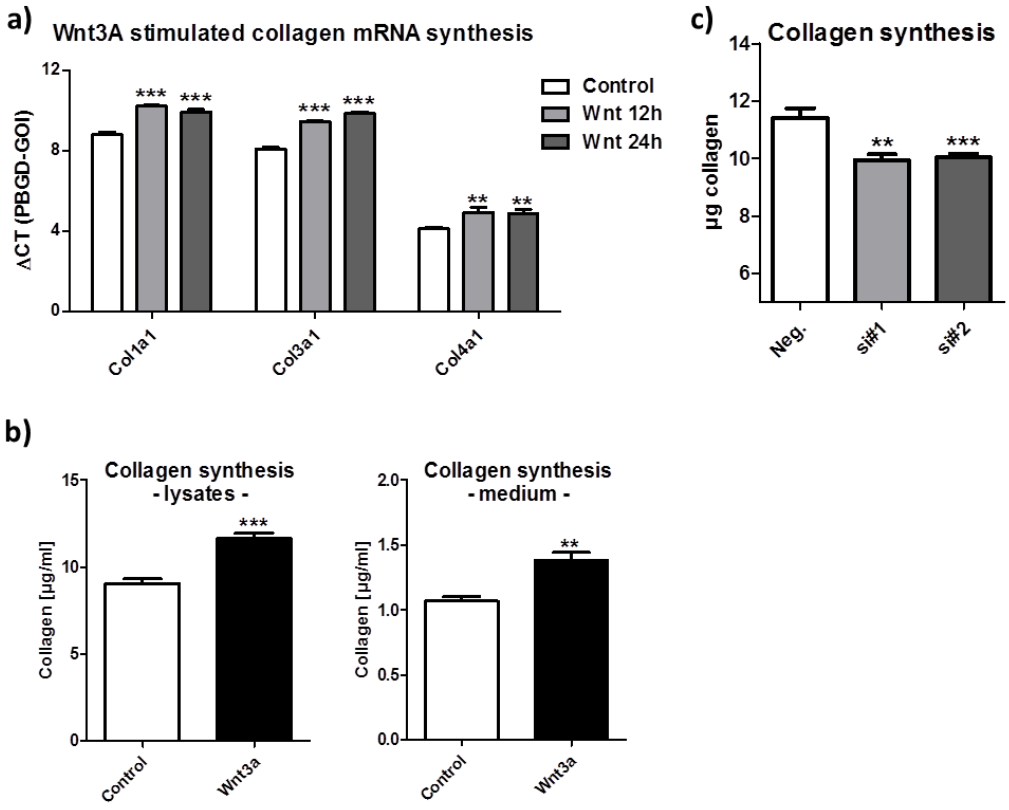

Fig. 19. The impact of Wnt/β-catenin signaling on collagen production: a) Collagen mRNA expression 12-24h after Wnt3a stimulation [2,5ng/ml] by qRT-PCR, n=4; b) Collagen synthesis and secretion 48h after Wnt3a treatment by sircoll assay, lysates n=10, medium n=5; and c) Collagen synthesis 48h after β-catenin siRNA-mediated knockdown in basal (10% FCS) conditions by sircoll assay. n=6; ** (P< 0.01); *** (P<0.005) vs. Control (a,b - serum starved cells, c - scrambled siRNA)

4.7 The impact of Wnt/β-catenin signaling on RCFs proliferation

Given that Wnt signaling pathway may contribute to increased production of collagen by cardiac fibroblasts, and thus can influence the development of cardiac fibrosis, we sought to test whether this effect can be further exerted by enhanced proliferation of these cells. For this purpose we examined the expression of pro-proliferative proteins and incorporation of BrdU in RCFs after stimulation with Wnt3a and knockdown of β-catenin.

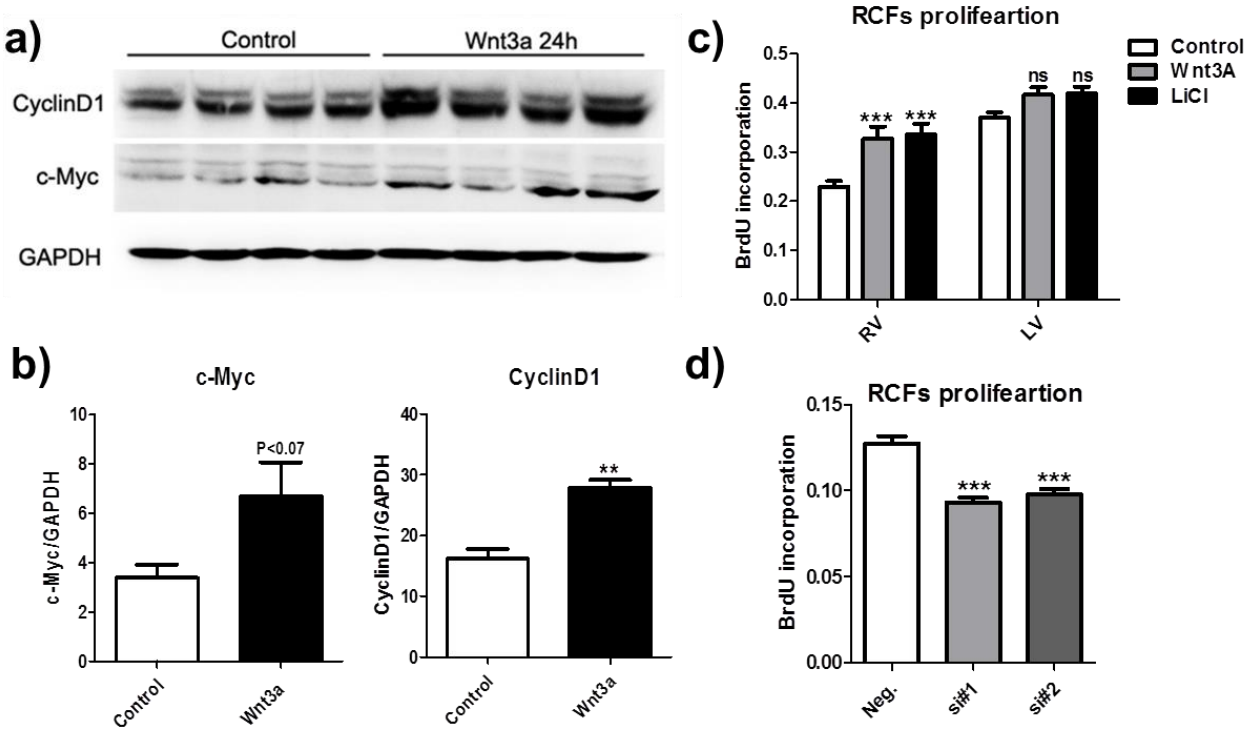

Fig. 20. The impact of Wnt/β-catenin signaling on RCFs proliferation: RCFs proliferation was determined by (a, b) the expression of pro-proliferative proteins and (c, d) BrdU incorporation. a) Wnt3a RCFs stimulation [2.5ng/ml, 24h] followed by WB, n=4; b) quantification of Western blotting by densitometry; c) Wnt3a RCFs stimulation [2.5ng/ml, 24h] followed by BrdU incorporation assay, n=8; and d) β-catenin siRNA-mediated knockdown [2µg, 48h] followed by BrdU incorporation assay. n=6; ** (P< 0,01); *** (P<0,005) vs. Control (serum starved cells in a-c, scrambled siRNA in d)

It was found that 24 h of Wnt3a stimulation was sufficient to increase the levels of expression of two Wnt/β-catenin downstream genes - cyclin D1 (P<0.01) and c-Myc (P<0.07), both of which positively regulate cell proliferation (Fig. 20a-b). Next, we defined proliferation of RCFs derived from the right and left ventricles of healthy rats in response to Wnt3a. In this experiment, lithium chloride treatment was included as a positive control. Lithium chloride is a GSK3β inhibitor and if Wnt3a activates the canonical Wnt signaling, it should resemble the results obtained for Wnt3a stimulation. Both, treatment with Wnt3a and LiCl resulted in a significant increase in BrdU incorporation of right ventricular fibroblasts (Fig. 20c, P<0.001). Surprisingly, in the left ventricular fibroblasts increased rates

of DNA synthesis that did not reach statistical significance were observed. Similarly, β-catenin knockdown resulted in reduction in BrdU incorporation rates as compared to scrambled siRNA control (Fig. 20d, $P<0.001$). Collectively, this data shows that Wnt/β-catenin signaling may also affect the proliferation of cardiac fibroblasts.

4.8 Activation of Wnt signaling pathway *in vivo*

The *in vitro* experiments strongly suggested the functional role of canonical Wnt signaling in right heart remodeling, or more specifically in cardiac fibrosis. To elucidate the role of this signaling pathway *in vivo* we recruited BAT-Gal reporter mice and subjected them to pulmonary artery banding procedure. BAT-gal mice carry a reporter gene - *LacZ* under a minimal TATA box promoter of the *siamosis* gene [107]. Upstream of the promoter, seven LEF/TCF-binding sites are inserted (Fig. 21a). After Wnt signaling activation, β-catenin together with LEF and TCF transcription factors binds to these sites, leading to the *LacZ* gene expression of the nuclear β-Galactosidase.

We found β-Galactosidase-positive cells in both, PAB and Sham animals. Nevertheless, a significant increase of β-Galactosidase positive cells after PAB procedure when compared to other groups could be observed (Fig. 21b-c, $P<0.05$). Thus, activation of Wnt/β-catenin signaling pathway occurs in vivo and we can conclude that this signaling is important for the development of right ventricular remodeling and could eventually offer new treatment strategies.

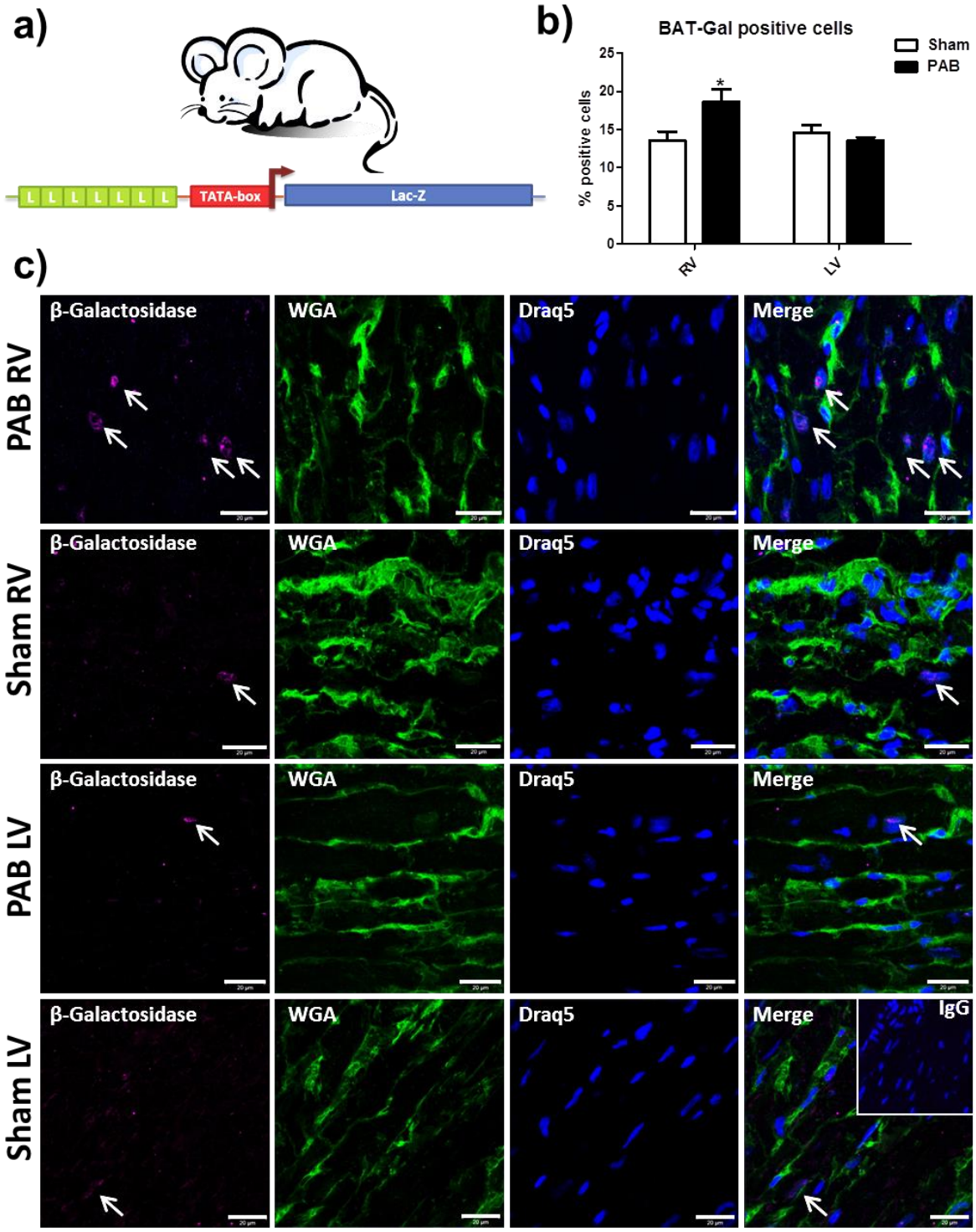

Fig. 21. Pulmonary artery banding induced Wnt/β-catenin pathway activation: a) BAT-Gal mice carry 7 LEF/TCF binding sites (L) upstream of minimal promoter (TATA box) from *siamosis* gene and *LacZ* reporter gene; b) quantification of β-Galactosidase positive cells based on cell counting, n=4 ; * ($P< 0.05$); and c) representative images of β-Galactosidase (magenta) staining, counterstained with WGA (green) and Draq5 (blue). Scale bars represent 20µm

5. Discussion

The main focus of this project was to elucidate the pathological processes underlying right ventricular remodeling. Pulmonary hypertension is one of the essential causes of this condition. In fact, right ventricular function is one of the major determinants of PAH patients' survival [5]. In this project, we found elevated levels of several Wnt signaling pathway molecules in the hypertrophied right ventricles. Importantly, based on the results obtained from reporter mice we were able to associate activated Wnt pathway with the process of right ventricular remodeling. Further, our *in vitro* studies revealed cardiac fibroblasts as one of the possible targets of Wnt signaling contributing to myocardial hypertrophy.

5.1 Cardiac hypertrophy in PAB and MCT models of right ventricular remodeling

In the present study right ventricular hypertrophy was mimicked by two animal models: monocrotaline and pulmonary artery banding. The MCT model is characterized by vascular injury, which leads subsequently to vascular remodeling and right ventricular hypertrophy. The PAB model, on the other hand, does not exhibit any other direct effects on the heart apart from the increase in the afterload. The use of both aforementioned models allows the determination whether the observed changes are directly pressure-dependent or if they can be influenced by factors not attributable to pressure overload. Sprague-Dawley rats used in this project were subjected to PAB or MCT treatment followed by organ harvest 2 and 4-6 weeks after procedure, accordingly. At the given time of the organ harvest both models were characterized by substantial right ventricular hypertrophy as assessed by RV/LV+S ratios. Further evaluation of RV hypertrophy in both models based on their expression of known genes related to RVH, we observed an upregulation of several hypertrophic markers in the right ventricles of PAB and MCT rats, including: αSKA, βMHC, BNP, ANP and TIMP and downregulation of αMHC, in line with the literature [31, 73, 76-78].

No significant changes in the expression of genes associated with cardiac hypertrophy were observed in the left ventricles except the increased level of ANP. This could be associated with advanced cardiac hypertrophy and ventricular interdependence, since elevated levels of ANP expression in the left ventricles have been already reported in the MCT model [110]. Importantly, collagen type 1 and 3 were significantly elevated in right ventricles of banded and MCT treated animals, suggesting myocardial fibrosis. Furthermore, a significant increase in acid-soluble as well as in pepsin soluble fraction of total collagen in PAB RVs whereas right ventricles of MCT rats showed elevated levels of all collagen (salt-, acid-, and pepsin- soluble) fractions. Surprisingly, we observed also an increase in pepsin soluble fraction in the left ventricles of PAB animals, which could be explained only through the indirect effects of right ventricular pressure overload on the left ventricle. Cardiac fibrosis in both models was further confirmed by immunofluorescence staining of vimentin and collagen type 1α. Right ventricles of PAB and MCT rats showed elevated levels of both, vimentin and collagen 1α as compared to RVs of appropriate control animals. No changes were observed in left ventricles of PAB animals but the left ventricles of MCT rats demonstrated elevated levels of vimentin and collagen 1α staining, pointing to the early fibrosis of the left ventricle of these animals (data not shown). This indicated a possible direct effect of monocrotaline on the heart. Monocrotaline model is often used in studies on PAH, because of its technical simplicity, reproducibility and low cost in comparison with other models. It has been previously speculated that RVH in this model is a direct consequence of the pressure overload. Recent reports indicate, however, that monocrotaline may have additional indirect effects on the heart. One of the major criticisms of MCT model is its ability to induce liver damage and hepatic veno-occlusive disease. It is also possible that the pro-inflammatory responses provoked by MCT-induced pulmonary vaculitis may contribute to the development of heart failure [108]. In fact, Akhavein *et al.* observed an impairment of the left ventricular function associated with diffuse myocarditis in rats treated with MCT [111]. In contrast, Chen *et al.* have not observed any fibrotic changes or inflammatory infiltrations in the left hearts of MCT rats [112]. These results indicate that the use of MCT model in studies on right ventricular hypertrophy may need to

be complimented or verified in exclusive models right ventricular hypertrophy. For this reason further experiments, except for the screening of Wnt signaling molecules, have been carried out only on samples from the PAB model.

5.2 Wnt/β-catenin signaling molecules expression in PAB and MCT models

As Wnt/β-catenin signaling has been previously implicated to maladaptive growth of the left ventricle we sought to elucidate expression of its molecules in hypertrophied hearts. The qRT-PCR analysis revealed upregulation of β-catenin, and two Frizzled receptors: Fz1 and Fz2 in the right ventricles of PAB animals. Interestingly, also mRNA levels of GSK3β were elevated in RVs followed PA banding. Those changes were limited only to RVs and no alterations were observed within the left ventricles. Similarly, upregulation of β-catenin and GSK3β was observed on the protein level in PAB RVs. GSK3β phosphorylation levels were lower in both ventricles, but this reduction was not significant for the RVs. In MCT hearts (5 weeks after treatment) we found upregulation of GSK3β and Fz2 mRNAs. β-catenin and Fz1 receptor mRNA levels showed the tendency to be upregulated but did not reach the significance level. On the protein levels we also detected tendency in higher levels of β-catenin and GSK3β in the MCT model (especially in 4 week time points). Interestingly, although statistically not significant, those changes have been observed in both, the right and the left ventricles. This again indicated that observed changes in monocrotaline model might not be specific to cardiac hypertrophy but induced directly by MCT. Additionally, the MCT model revealed distinct GSK3β phosphorylation at 5 and 6 weeks post treatment.

β-catenin was shown to be stabilized upon hypertrophic stimuli in left ventricle, which involves the inhibition of GSK3β kinase activity [104]. Our results showing upregulation of β-catenin levels on mRNA and protein levels in PAB model are in line with this study. Unfortunately monocrotaline animals presented only a tendency in β-catenin upregulation. GSK3β levels in both models showed some discrepancies, which to some extent are also seen in studies on the left ventricle. Our observations indicate that the level of GSK3β

increases in response to pressure-overload, at least in the pulmonary artery banding induced right heart hypertrophy. This was also shown in transverse aortic constriction (TAC) induced left ventricular remodeling [113]. This and other studies addressed also phosphorylation status of GSK3β under stress conditions, showing GSK3β S9 phosphorylation-dependent inactivation in hypertrophied hearts, at least at one week after TAC [104, 113]. Our study revealed rather contradictory results concerning the phosphorylation of GSK3β namely, in the PAB model a decrease in phosphorylation of this protein was observed, while a significant increase in phosphorylation of GSK3β was observed in MCT model. Since cardiac hypertrophy in the MCT model in secondary to pulmonary vascular remodeling it is possible that other humoral factors can contribute to GSK3β inactivation in this model. On the other hand, since GSK3β phosphorylation is present in both ventricles, one can't exclude that MCT can trigger those changes directly acting on the heart. Interestingly, in human hearts, inhibition of GSK3β was seen in the end-stage heart failure, but was not observed in compensated hypertrophy [103]. Thus, observed discrepancies might also account to differences in hypertrophic stage despite similar hypertrophic ratios. Further experiments measuring actual GSK3β kinase activity in those samples should be undertaken to confirm these findings. Nevertheless, we can conclude that several Wnt signaling molecules are upregulated during hypertrophic response of the right ventricle pointing to possible involvement of this pathway in the cardiac remodeling.

5.3 Cardiac fibroblasts characterization and Wnt3a stimulation

To determine whether the observed changes in expression of Wnt signaling molecules in the pressure-overloaded right ventricles arise at least in part due to altered expression patterns of cardiac fibroblast, we have established a protocol for isolation of these cells from the right and left ventricle separately. To our knowledge this is a first study comparing right and left ventricular fibroblasts under pressure-overload conditions. Fibroblast phenotype of isolated cells was confirmed based on specific fibroblasts marker expression

by immonocytochemical and qRT-PCR analysis. Importantly, most of fibroblast markers expression remained unchanged through passages 2 to 5, including Col1α1, Fn and P4Hb, except DDR2 and Col3α1.

In order to assess differences between individual populations of cardiac fibroblasts (RV vs. LV, PAB vs. Sham) we have measured proliferation rates of these cells based on BrdU incorporation. We observed increased proliferation rates of cardiac fibroblasts derived from right ventricles of PAB animals ($P<0.005$) in basal (10% FCS) conditions whereas proliferation rates in other groups did not vary. Increased proliferation of RV-PAB fibroblasts may be explained by mechanical stress as well as humoral stimulation associated with pressure overload. Along this line, we found significantly increased β-catenin mRNA levels in right ventricular fibroblasts derived from PAB rats. GSK3β levels were also increased in PAB RV-RCFs but this has not reached significance level. This pointed to the possible effects of Wnt/β-catenin signaling on cardiac fibroblasts during myocardial remodeling and its involvement in hyperproliferation status of RV-PAB fibroblasts. In order to examine how the Wnt signaling could influence cardiac fibroblasts we stimulated RCFs with Wnt3a, traditionally considered to activate Wnt canonical pathway [86]. Cardiac fibroblasts treated with Wnt3a displayed elevated mRNA levels of β-catenin and Dvl as well as GSK3β 12h after Wnt3a stimulation. Additionally expression of Axin2 - a negative regulator of the Wnt pathway, and Cyclin B1, responsible for G2/M transition, was significantly increased 12 and 24 h after Wnt3a treatment.

As β-catenin expression is largely regulated at the protein level we wanted to determine its accumulation in whole cell lysates after treatment with Wnt3a. Stimulation of cardiac fibroblasts with Wnt3a produced a distinct accumulation of β-catenin, which reached peak level 1 h after treatment. Additionally, corresponding accumulation of Dvl has been observed. Activation of Wnt signaling typically involves Dvl protein phosphorylation that can be observed as a mobility shift when blotted with total-Dvl antibody. Interestingly, in our experiment, Wnt3a RCFs stimulation resulted mainly with an increase in the overall level of Dvl, whereas its phosphorylation was only slightly increased in response to Wnt3a. Thus,

it is possible that Wnt signaling, at least in cardiac fibroblasts, can also influence Dishevelled stability. Nevertheless, additional experiments using specific p-Dvl antibodies should be performed to confirm Dvl activation in response to Wnt3a stimuli.

Since the nuclear translocation of β-catenin is the hallmark of activated Wnt canonical signaling, we sought to address this issue by protein fractionation of cell lysates derived from Wnt3a stimulated cardiac fibroblasts. We found β-catenin accumulation in cytosolic fraction 1 and 3 hours after Wnt3a treatment, which resembled the results obtained for whole cell lysates. Subsequently β-catenin translocated to the nucleus (at 3-6 hours post stimulation, $P<0.05$ at 3h). The membrane fraction remained unchanged except a weak reduction in the level of β-catenin at 3 h post stimulation.

Thus, we can confirm that cardiac fibroblasts derived from pressure-overloaded right hearts exhibit different characteristics in comparison to fibroblasts derived from Sham animals. Those differences may be associated with Wnt signaling, since the mRNA levels of β-catenin in PAB-RV cardiac fibroblasts were significantly increased.

5.4 The impact of Wnt/β-catenin signaling on collagen production

Cardiac fibrosis is an important component of the remodeling of the heart and can eventually lead to myocardial stiffening and failure. Collagen deposition and turnover play a primary role in this pathological process [32, 49]. Since our previous experiments pointed the possible impact of canonical Wnt pathway on right ventricular RCFs, we tested if this signaling could influence the synthesis and secretion of collagen by cardiac fibroblasts. Wnt3a stimulation of RCFs resulted in upregulation of collagens 1α, 3α and collagen 4α mRNA levels at 12 and 24 h post treatment. Increased collagen synthesis was also observed on the protein level 48 h after Wnt3a treatment. Additionally, Wnt3a stimulation induced collagen secretion as increased total collagen amounts were also detected in the culture medium from RCFs stimulated with Wnt3a. These results were further confirmed using β-catenin knockdown approach. β-catenin depleted cells showed decreased collagen

synthesis in basal (10% FCS) conditions as compared to scrambled siRNA negative control. Similar effect of Wnt signaling on collagen synthesis has been previously described in immortalized cardiac fibroblast cell line [109]. However to date, genes encoding collagens have not been revealed as direct downstream genes of β-catenin. It is therefore intriguing to speculate that the participation of other proteins may mediate the activation of collagen synthesis. Wnt1-induced secreted protein-1 (WISP1) is a promising candidate gene, which may be involved in this process. WISP-1 is a member of connective tissue growth factor and nephroblastoma overexpressed family of growth factors shown to play a role in cellular growth and survival. It has been shown that the Wnt1 and β-catenin signaling leads to elevated expression of WISP-1 [114]. Recently, Colston et al. [115] showed WISP-1 upregulation in the heart post myocardial infarction, resulting in myocardial hypertrophy, fibroblast proliferation, and increased collagen synthesis. Therefore, the exact molecular mechanism by which Wnt signaling can generate excessive collagen synthesis need to be addressed in future. Nevertheless, our results clearly indicate the functional role of Wnt/β-catenin signaling in the synthesis and secretion of Collagen by RCFs.

5.5 The impact of Wnt/β-catenin signaling on RCFs proliferation

Both, enhanced ECM protein synthesis of individual fibroblasts and fibroblast proliferation can contribute to the development and progression of myocardial fibrosis [32]. Our primary results using immunodetection of fibroblast marker – vimentin in rat hearts showed increased fibroblast density in PAB RVs suggesting that cardiac fibroblast proliferation can also take place in the pressure induced cardiac remodeling. Additionally we observed an increased BrdU incorporation of cardiac fibroblasts derived from right ventricles of banded animals ($P<0.005$) *in vitro,* whereas DNA synthesis rates in other groups did not vary. This was in line with other report showing higher H^3-thymidine incorporation by non-myocyte cells in isoproterenol-induced cardiac hypertrophy [116]. It has been also suggested that

pericytes and bone marrow-derived cells can contribute to the myocardial fibroblast population [117].

In order to elucidate if Wnt signaling could also influence cell growth we examined the expression of pro-proliferative proteins and incorporation of BrdU in cardiac fibroblasts after stimulation with Wnt3a and siRNA-mediated knockdown of β-catenin. Two Wnt/β-catenin downstream genes - Cyclin D1 and c-Myc (positively regulating cell proliferation) were elevated 24 h after Wnt3a stimulation. Similarly, Wnt3a increased BrdU incorporation rates of cardiac fibroblasts. Lithium chloride treatment exerted the same effect suggesting that observed proliferation of RCFs is triggered by activation of Wnt canonical pathway. DNA synthesis rates of the left ventricular fibroblasts were only slightly elevated after Wnt3a or LiCl treatment. Interestingly the LV-RCFs BrdU incorporation rates were significantly greater than that observed for RV-RCFs in basal conditions and after treatment. The observed differences could be due to different properties of the two populations of fibroblasts. As the pulmonary circulation is of low pressure, right ventricular fibroblasts are normally exposed to less stress as compared to fibroblasts in the left ventricles. This could explain the greater rate of incorporation of BrdU in the LV-RCFs in basic conditions and their lower reactivity to Wnt3a stimulation. Indeed, distinct growth characteristics and proliferative responsiveness was already described in atrial versus ventricular fibroblasts [118]. In agreement with our previous results, β-catenin knockdown resulted in reduction in BrdU incorporation rates as compared to scrambled siRNA control ($P<0.001$). Interestingly, Ueda *et al.* [119] showed that Wnt signaling does not directly affect proliferation of rodent fibroblasts, but inhibits apoptosis of these cells in low serum conditions. In this study, the authors used fibroblast cell lines, which have completely different growth characteristics in comparison to primary cardiac fibroblasts, which may explain the differences in results obtained in both studies. In addition, knockdown of β-catenin exerting an inhibitory effect on fibroblast proliferation was carried out in medium containing 10% FCS. Collectively, this data indicates that Wnt/β-catenin signaling affects the

proliferation of cardiac fibroblasts *in vitro*. Still, future studies should clarify the role of Wnt/β-catenin signaling in apoptosis of cardiac fibroblasts.

5.6 Activation of Wnt signaling pathway *in vivo*

Since *in vitro* experiments strongly suggested the functional role of canonical Wnt signaling in right heart remodeling we sought to elucidate the role of this signaling pathway *in vivo*. For this purpose BAT-Gal reporter mice were recruited and subjected to pulmonary artery banding procedure. Wnt signaling activation can be easily visualized in those mice by nuclear

β-Galactosidase staining. We found β-Galactosidase-positive cells in both, PAB and Sham animals. Nevertheless, a significant increase of β-Galactosidase positive cells after PAB procedure when compared to other groups could be observed. Thus, activation of Wnt/β-catenin signaling pathway occurs *in vivo* and we can conclude that this signaling is important for the development of right ventricular remodeling and could eventually offer new treatment strategies.

5.7 Conclusions

In the present study, the components of Wnt canonical signaling, including its key mediator β-catenin, have been shown to be increased in pressure-overloaded hearts as well as in cardiac fibroblasts derived from those hearts. *In vitro,* we have been able to show that canonical Wnt signaling can trigger both, cardiac fibroblast proliferation and collagen synthesis and that those effects are dependent on β-catenin, as its knockdown exerts opposite effects. We have demonstrated that pressure overload is sufficient to induce Wnt signaling *in vivo*, ultimately confirming the role of this signaling pathway in cardiac remodeling. The main findings of this study are summarized in Figure 22. However, the precise molecular mechanism underlying those processes needs extensive

investigations. Taken all together we can conclude that Wnt signaling is important for the development of right ventricular remodeling and may eventually offer innovative treatment strategies.

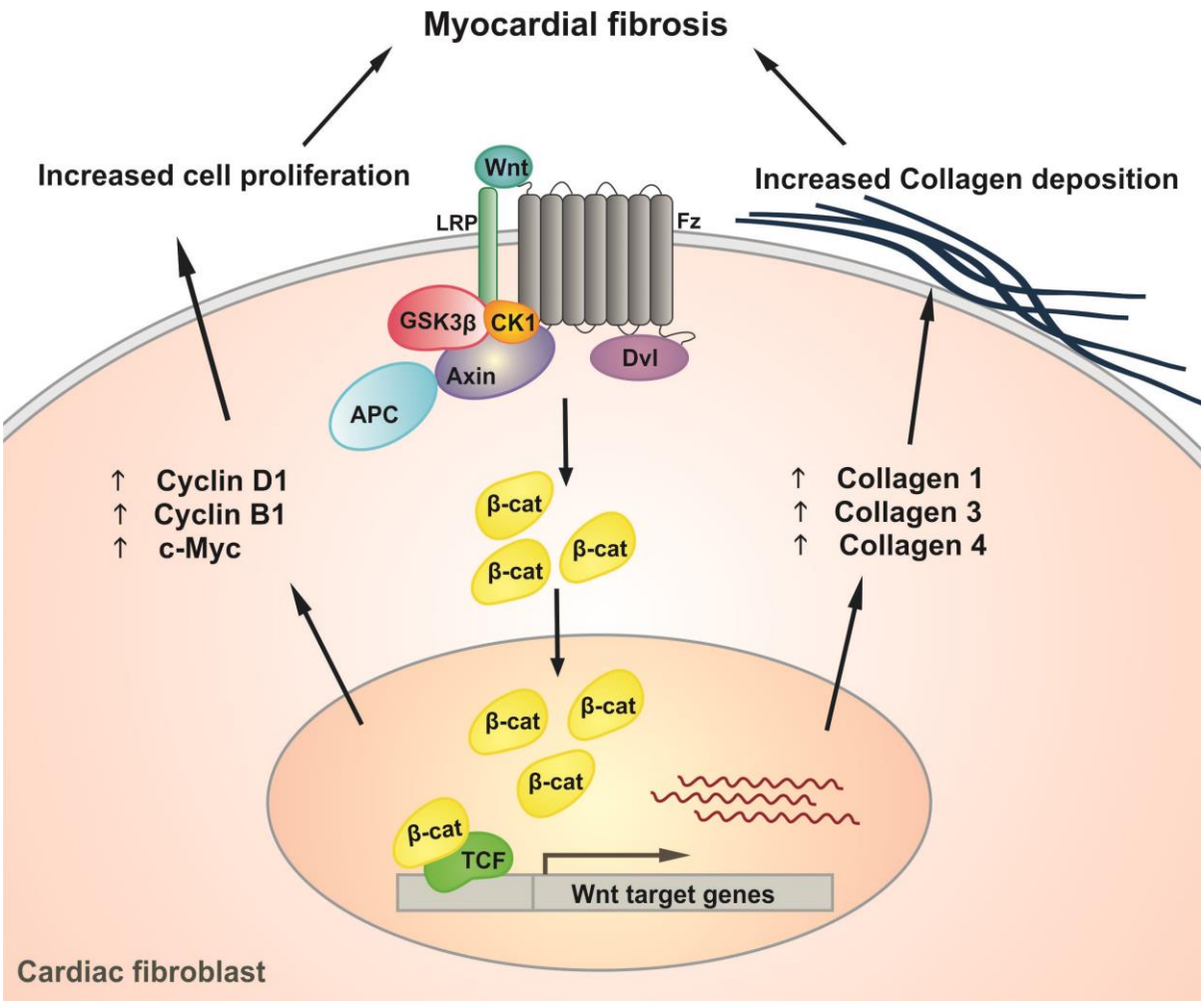

Fig. 22 Schematic summary of changes seen in cardiac fibroblasts derived from pressure-overloaded hearts. Pulmonary artery banding resulted in activation of Wnt pathway *in vivo*. In cardiac fibroblasts activated Wnt signaling leads to increased levels of collagen synthesis and elevated proliferation rates of those cells. This in turn may lead to the development of myocardial fibrosis influencing mechanical properties of the hypertrophied hearts.

6. Outlook

The current study shows that Wnt signaling plays a significant role in right ventricular remodeling. However, more research on this topic needs to be undertaken before the precise molecular mechanism underlying this process becomes clearly understood.

Some discrepancies were observed in the basic screening studies between the PAB and MCT models. The main difference was observed in the level of phosphorylation of GSK3β. As the MCT model turned out to be little suitable in studies on right ventricular hypertrophy, it would be advisable to include another animal model of pulmonary hypertension with RVH (e.g. Sugen5416/Hypoxia model) might be included in the study. In addition, since the GSK3β phosphorylation affects its activity, an additional experiment on its kinase activity would also add some information.

In our study, we showed that Wnt/β-catenin signaling can regulate collagen expression in cardiac fibroblasts. However to date, genes encoding collagens have not been revealed as direct downstream genes of β-catenin. To elucidate, if this phenomenon depends on β-catenin co-transcriptional activity, one could use RCFs stably transduced with dominant negative LEF-1. Additionally, it would be of interest to evaluate WISP-1 levels in the right ventricles of PAB animals, since this molecule was previously shown to influence cardiac fibrosis and hypertrophy post infarction.

As for the studies on the cardiac fibroblasts proliferation, two additional experiments should be carried out. First, a confirmation of cardiac fibroblast proliferation on heart sections (e.g. PCNA or Ki-67 staining) would clarify if proliferating RCFs are distributed equally throughout the myocardium or do the cluster (e.g. in the perivascular areas pointing to possible involvement of circulating cells in cardiac fibrosis). Furthermore, subjecting RCFs (Wnt stimulated versus β-catenin-siRNA treated) to apoptosis assay could finally confirm that observed changes in the cell count are due to increased proliferation and not survival.

Finally, more extensive in vivo studies should ultimately confirm the role of Wnt signaling in cardiac remodeling and present new therapeutic possibilities. As the reporter mice experiments were conducted on a limited number of animals, the number of mice used in trials should be significantly increased. As we have observed some basal activation of Wnt signaling in Sham operated mice, one can't exclude a "leaky" expression in those animals. Therefore reporter mice experiments should be further confirmed on transgenic animals. Of particular interest would be mice expressing non-degradable (removed exon 3) or non-functional (removed exon3-6) version of β-catenin in fibroblasts. According to our hypothesis performing pulmonary artery banding on those mice should lead to deterioration or improvement of cardiac function, accordingly. Lastly, performing animal studies with the use of Wnt signaling inhibitors (e.g. Tankyrase) could finally lead to the development of novel therapeutic strategies against right ventricular hypertrophy and fibrosis.

7. Summary

Right ventricular remodeling refers to changes in size, shape and function of the right heart after cardiac injury. It is a progressive disorder connected to several conditions, including pulmonary hypertension. It is also a leading predictor for the development of right heart failure and death. Nonetheless, until recently the importance of right ventricular function in health and disease has been often underestimated. Previous studies showed that Wnt signaling pathway plays an important role in left ventricular remodeling in response to hypertrophic stimuli. While all of the available literature describes the impact of this signaling cascade in maladaptive growth of the left ventricle, its role in the right heart hypertrophy is unknown. Given that, we hypothesized that canonical Wnt signaling could also play a role in the development of right heart hypertrophy. As the Wnt pathway is crucial for the development of right ventricle we speculated its contribution to RVH could be more prominent.

In this study, we employed and characterized the PAB and MCT animal models of right ventricular hypertrophy. Both models presented with substantial right heart hypertrophy as judged by RV/LV+S ratios as well as mRNA expression of known hypertrophic markers. Additionally, the right ventricles of PAB and MCT animals showed advanced fibrotic changes.

We were able to show an upregulation of several Wnt signaling molecules, including β-catenin, GSK3β and Frizzled receptors on mRNA level in hypertrophied right ventricles of PAB animals. Most importantly, β-catenin and GSK3β protein levels were also elevated in those animals. Similarly, we found increased mRNA levels of GSK3β and Fz2 receptor in the right ventricles of MCT rats. β-catenin and GSK3β protein levels showed a tendency to be elevated in those animals but did not reach significance level. Furthermore we found a significant upregulation in β-catenin expression in cardiac fibroblasts derived from right ventricles of PAB animals as compared to Sham-RVs implying that CFs could be at least in part responsible for observed changes. Based on BrdU incorporation experiments, we also

found that right ventricular fibroblasts exhibit increased proliferation rates. To further elucidate if this increased proliferation could be dependent on activated canonical Wnt signaling we performed several experiments employing Wnt3a stimulation and siRNA mediated β-catenin knockdown.

The hallmark of Wnt canonical pathway is the accumulation and nuclear translocation of β-catenin. We could show both, accumulation of β-catenin in the cytoplasm as well as increased β-catenin nuclear levels in RCFs stimulated with Wnt3a. Wnta3a-mediated activation of Wnt signaling resulted further in the upregulated expression of several genes, most prominently Axin2 and Cyclin B1. We could further link Wnt/β-catenin signaling with elevated collagen synthesis as well as increased cardiac fibroblast proliferation, two fundamental processes of myocardial fibrosis. We showed that Wnt3a stimulation leads to elevated mRNA levels of Collagens 1, 3 and 4 as well as total collagen synthesis in RCFs. Additionally we could observe increased collagen secretion. In accordance, siRNA-mediated β-catenin knockdown resulted in decreased collagen expression. We further showed that Wnt3a stimulation was sufficient to increase the levels of expression of two Wnt/β-catenin downstream genes - Cyclin D1 and c-Myc, both of which positively regulate cell proliferation. Likewise, Wnt3a stimulation and LiCl treatment resulted in significantly elevated rates of BrdU incorporation as compared to control. Finally, β-catenin knockdown resulted in reduction in DNA synthesis rates as compared to scrambled siRNA control.

In order to confirm our findings *in vivo* we recruited BAT-Gal reporter mice and subjected them to pulmonary artery banding procedure. Activation of Wnt-canonical pathway was assessed by β-Galactosidase nuclear staining of cryosections derived from those animals. Although β-Galactosidase positive cells were present in all included groups, we observed a substantially greater amount of those cells in the right ventricles of rats subjected to PAB. Thus, activation of Wnt/β-catenin signaling pathway occurs *in vivo* and we can conclude that this signaling is important for the development of right ventricular remodeling and could eventually offer new treatment strategies.

8. Zusammenfassung

Rechtsventrikuläres Remodeling bezeichnet die Veränderungen von Größe, Form und Funktion des rechten Herzens nach Herzschädigung oder veränderten hämodynamischen Verhältnissen. Es ist eine fortschreitende Erkrankung, die mit mehreren Krankheiten, einschließlich pulmonaler Hypertonie (PH), verbunden ist. Es ist auch ein führender Indikator für die Entwicklung des rechten Herzversagens und Tod. Dennoch wurde bis vor kurzem die Bedeutung der rechtsventrikulären Funktion in Gesundheit und Krankheit oft unterschätzt. Frühere Studien zeigten, dass der Wnt-Signalweg eine wichtige Rolle bei dem linksventrikulären Remodeling spielt. Während die gesamte vorhandene Literatur die Auswirkungen dieser Signalkaskade in maladaptivem Wachstum des linken Ventrikels beschreibt, ist seine Rolle in der Hypertrophie des rechten Herzens bislang unbekannt. Daher stellten wir die Hypothese auf, dass der kanonische Wnt-Signalweg auch eine Rolle bei der Entwicklung der rechtsventrikulären Hypertrophie spielt.

In dieser Studie haben wir Tiermodelle der rechtsventrikulären Hypertrophie verwendet und charakterisiert (PAB, pulmonalarterielles Banding; MCT, Monocrotalin induzierte PH). Beide Modelle zeigen eine erhebliche Hypertrophie des rechten Herzens, was durch Erhöhung des RV/LV+S Verhältnisses sowie durch mRNA-Expression von bekannten hypertrophen Markern charakterisiert ist. Zusätzlich zeigen rechte Ventrikel aus beiden Tiermodellen fortgeschrittene fibrotische Veränderungen.

Wir konnten eine Hochregulation von mehreren Wnt-Signalmolekülen, darunter β-Catenin, GSK3β und Frizzled-Rezeptoren, auf mRNA-Ebene in hypertrophierten rechten Ventrikeln der PAB Tieren zeigen. Auf Proteinebene konnten wir erhöhte Mengen an β-Catenin und GSK3β nachweisen. Ebenso fanden wir erhöhte mRNA-Spiegel von GSK3β und Fz2 Rezeptoren in den rechten Ventrikeln von MCT-Ratten. β-Catenin und GSK3β Proteinmengen zeigten in diesem Modell allerdings nur eine Tendenz der Erhöhung. Darüber hinaus fanden wir eine signifikant erhöhte Expression von β-Catenin in kardialen Fibroblasten aus der rechten Herzkammer der PAB Tieren im Vergleich zu Sham-RVs, was

bedeutet, dass diese Zellen, zumindest zum Teil, verantwortlich für die beobachteten Veränderungen sein könnten. Basierend auf BrdU-Inkorporation Experimenten, haben wir herausgefunden, dass die rechte Herzkammer eine erhöhte Proliferation von Fibroblasten aufwies.

Das Kennzeichen des kanonischen Wnt-Signalwegs ist eine Akkumulation und Kerntranslokation von β-Catenin. Wir zeigten sowohl die Akkumulation von β-Catenin im Zytoplasma als auch erhöhte β-Catenin Lokalisation im Kern nach Stimulation mit Wnt3a. Wnta3a-vermittelte Aktivierung der Wnt-Signalweg führte weiter in die hochregulierten Expression verschiedener Gene, besonders Axin2 und Cyclin B1. Wir konnten weiterhin den Wnt/β-Catenin-Signalweg mit erhöhter Kollagen-Synthese sowie mit erhöhter kardialer Fibroblasten-Proliferation (zwei grundlegender Prozesse der myokardialen Fibrose) verknüpfen. Die Wnt3a Stimulation führt zu erhöhter Expression der Kollagene 1, 3 und 4 sowie der gesamten Kollagensynthese in kardialen Fibroblasten Ebenfalls führte der siRNA-vermittelte β-catenin-Knockdown zu einer verminderten Kollagen Expression. Weiterhin zeigten wir, dass eine Wnt3a Stimulierung ausreichend war, um das Niveau der Expression von zwei Wnt/β-catenin regulierten Genen, nämlich Cyclin-D1 und c-Myc, die beide positive Regulatoren der Zellproliferation sind, zu erhöhen. Ebenso ergab Wnt3a Stimulierung und LiCl Behandlung signifikant erhöhte Raten des BrdU- Inkorporation im Vergleich zur Kontrolle. Schließlich führte der β-Catenin-Knockdown zu einer Verringerung der DNA-Synthese im Vergleich zur Kontrolle.

Um unsere Befunde *in vivo* zu bestätigen, wurden BAT-Gal Reporter-Mäuse einer Pulmonalarterien-Stenose (PAB) unterzogen. Die Aktivierung des kanonischen Wnt- Wegs wurde durch β-Galactosidase Kernfärbung von Kryoschnitten von diesen Tieren beurteilt. Obwohl β-Galactosidase-positive Zellen in allen Gruppen anwesend waren, stellten wir eine wesentlich größere Menge dieser Zellen in den rechten Ventrikeln von PAB Ratten fest. Somit erfolgt die Aktivierung der Wnt/β-Catenin-Signalweg *in vivo* und wir können feststellen, dass dieses Signal wichtig für das Remodeling des rechten Ventrikels- ist, was therapeutisch genutzt werden kann.

9. Appendix

Table 1. List of real-time primers

Gene	Primer sequence	Annealing T [˚C]	Product size
αCAA	F: GCC AGC CCA GCT GAA CCC AG	59	200 bp
	R: ATG ACA CCC TGG TGG CGT GG		
αMHC	F: CGG ACA CTG GAG GAC CAG GC	60	121 bp
	R: GCC TAG CCA GCT CGC CGT TC		
αSkMA	F: GGC ACC CAG GGC CAG AGT CA	60	177 bp
	R: TGACACCCTGGTGACGGGGC		
ANP	F: GAT GGA GGT GCT CTC GGG CG	59	181 bp
	R: TTC GGT ACC GGA AGC TGT TGC AG		
Axin2	F: GAC GCG CTG ACC GAC GAT TCC	60	192 bp
	R: AGC AGG TTC CAC GGG CGT CA		
ß-catenin	F: TCA GAT CTT AGC TTA CGG CAA	60	134 bp
	R: TTG TTG CTA GAG CAG ACA GAC		
βMHC	F: ACCGGAGAATCCGGAGCTGGT	60	120 bp
	R: CAA GGT GCC CTT GCC TGG GG		
BNP	F: CAG CTG CCT GGC CCA TCA CT	59	167 bp
	R: GCT CCA GCA GCT TCT GCA TCG T		
Col1α1	F: AGA TGG TCG CCC TGG ACC CG	60	120 bp
	R: GGG ACA CCT CGT TCT CCA GCC T		
Col3α1	F: CCC TGC TCG GAA TTG CAG AGA CC	59	166 bp
	R: CCG CGG GAC AGT CAT GGG AC		
Col4α1	F: ATG GAA TCC CGG GGT CGG CA	60	184 bp
	R: GGG CCG GGA GGA CCC ATG AA		
Col8α1	F: TTC CAC GGT CCT CTC CGT GGG	59	114 bp
	R: CAA TGG GGC TGG GTC CCG TC		
Cyclin B1	F: TGC GAA CCA GAG GTG GAA CTG GA	60	132 bp
	R: TTC GGC AGG TGC ACA TCC AGA TGT		
DDR2	F: AAC CAG CCT GTC CTG GTG GC	59	157 bp
	R: TGC AGA GCG GGT CCT CAG TG		
Dvl1	F: TGA TGA GGC TGC CCG GAC CA	60	154 bp
	R: GCT CAG CCG GCT CGT GTT GT		
Fn1	F: TGG AGC CAG GAA CCG AGT ACA CC	60	191 bp
	R: AGG GTT GGT GAC GAA GGG GGT		

Frizzled1	F: CGT ACT GAG TGG AGT GTG TTT TG	60	188 bp
	R: TGA GCT TTT CCA GTT TCT CTG TC		
Frizzled2	F: TAC CTG TTC ATC GGC ACA TC	60	143 bp
	R: GTG TAG AGC ACG GAG AAG ACG		
GSK3ß	F: ACT TTG TGA CTC AGG AGA ACT	60	141 bp
	R: TCG CCA CTC GAG TAG AAG AAA		
P4H3α	F: CTA CTG CTC CAG CCC GCA CG	59	152 bp
	R: TGC TTT TCC CCT GAA GCC ACC A		
P4Hß	F: ACA AAC CGG AGT CAG ACG AGC TG	59	102 bp
	R: GCA GTT CCT GGC TCA TCA GGT GG		
PBGD	F: ATG TCC GGT AAC GGC GGC	58	135 bp
	R: CAA GGT TTT CAG CAT CGC TAC		
TIMP	F: AGT TTC TCA TCG CGG GCC GT	59	144 bp
	R: ACA CTG TGC ACA CCC CAC AGC		

Table 2. List of primary antibodies

Primary antibody	**Source**	**Dilution WB**	**Dilution IF/IHC**	**Company**
αSMA	Mouse		1:200	Sigma Aldrich
ß-actin	Mouse	1:5000		Sigma Aldrich
ß -catenin	Rabbit	1:1000	1:100	Cell Signaling
ß -Galactosidase	Rabbit		1:100	Abcam
c-Myc	Rabbit	1:1000		Cell Signaling
Collagen 1α1	Mouse		1:70	Meridian Life Sciences
CyclinD1	Rabbit	1:200		Santa Cruz
Dvl-2	Rabbit	1:200		Santa Cruz
Fibronectin	Rabbit		1:200	Abcam
GAPDH	Mouse	1:5000		Novus Biologicals
GSK3ß - p(S9)	Rabbit	1:1000		Cell Signaling
GSK3ß total	Rabbit	1:200		Santa Cruz
HDAC1	Rabbit	1:500		Cell Signaling
Hsp90	Rabbit	1:500		Epitomics
PDGFRß	Rabbit	1:200		Santa Cruz
PLCß	Rabbit	1:1000		Cell Signaling
PLCß(p)	Rabbit	1:1000		Cell Signaling

Vimentin-Cy3	Mouse	1:300	Sigma Aldrich

Table 3. List of secondary antibodies

Secondary antibody	Dilution	Company
Alexa 555-conjugated anti-mouse Ab	1:1000	Molecular Probes
Alexa 488-conjugated anti-rabbit Ab	1:1000	Molecular Probes
Alexa 488-conjugated anti-mouse Ab	1:1000	Molecular Probes
Alexa 555-conjugated anti-rabbit Ab	1:1000	Molecular Probes
HRP-conjugated anti rabbit Ab	1:1000	Dako cytomation
HRP-conjugated anti-mouse Ab	1:30000	Sigma Aldrich

Table 4. List of cellular dyes

Dye	Dilution	Company
Alexa 488-conjugated Phalloidin	1:40	Molecular Probes
Alexa 488-conjugated WGA	10ng/ml	Molecular Probes
DAPI	1:1000	Molecular Probes
Draq5 nuclear stain	1:500	Enzo Life Sciences

10. References

1. Voelkel, N.F., et al., *Right ventricular function and failure: report of a National Heart, Lung, and Blood Institute working group on cellular and molecular mechanisms of right heart failure.* Circulation, 2006. **114**(17): p. 1883-91.
2. Buckingham, M., S. Meilhac, and S. Zaffran, *Building the mammalian heart from two sources of myocardial cells.* Nat Rev Genet, 2005. **6**(11): p. 826-35.
3. Haddad, F., et al., *Right ventricular function in cardiovascular disease, part I: Anatomy, physiology, aging, and functional assessment of the right ventricle.* Circulation, 2008. **117**(11): p. 1436-48.
4. Sheehan, F. and A. Redington, *The right ventricle: anatomy, physiology and clinical imaging.* Heart, 2008. **94**(11): p. 1510-5.
5. Sandoval, J., et al., *Survival in primary pulmonary hypertension. Validation of a prognostic equation.* Circulation, 1994. **89**(4): p. 1733-44.
6. Gaine, S.P. and L.J. Rubin, *Primary pulmonary hypertension.* Lancet, 1998. **352**(9129): p. 719-25.
7. Kovacs, G., et al., *Pulmonary arterial pressure during rest and exercise in healthy subjects: a systematic review.* Eur Respir J, 2009. **34**(4): p. 888-94.
8. Simonneau, G., et al., *Updated clinical classification of pulmonary hypertension.* J Am Coll Cardiol, 2009. **54**(1 Suppl): p. S43-54.
9. Humbert, M., et al., *Pulmonary arterial hypertension in France: results from a national registry.* Am J Respir Crit Care Med, 2006. **173**(9): p. 1023-30.
10. McGoon, M., et al., *Screening, early detection, and diagnosis of pulmonary arterial hypertension: ACCP evidence-based clinical practice guidelines.* Chest, 2004. **126**(1 Suppl): p. 14S-34S.
11. D'Alonzo, G.E., et al., *Survival in patients with primary pulmonary hypertension. Results from a national prospective registry.* Ann Intern Med, 1991. **115**(5): p. 343-9.
12. Rabinovitch, M., *Molecular pathogenesis of pulmonary arterial hypertension.* J Clin Invest, 2008. **118**(7): p. 2372-9.
13. Stenmark, K.R., et al., *Role of the adventitia in pulmonary vascular remodeling.* Physiology (Bethesda), 2006. **21**: p. 134-45.
14. Stenmark, K.R., K.A. Fagan, and M.G. Frid, *Hypoxia-induced pulmonary vascular remodeling: cellular and molecular mechanisms.* Circ Res, 2006. **99**(7): p. 675-91.
15. Yi, E.S., et al., *Distribution of obstructive intimal lesions and their cellular phenotypes in chronic pulmonary hypertension. A morphometric and immunohistochemical study.* Am J Respir Crit Care Med, 2000. **162**(4 Pt 1): p. 1577-86.
16. Cool, C.D., et al., *Three-dimensional reconstruction of pulmonary arteries in plexiform pulmonary hypertension using cell-specific markers. Evidence for a dynamic and heterogeneous process of pulmonary endothelial cell growth.* Am J Pathol, 1999. **155**(2): p. 411-9.
17. Tuder, R.M., et al., *Exuberant endothelial cell growth and elements of inflammation are present in plexiform lesions of pulmonary hypertension.* Am J Pathol, 1994. **144**(2): p. 275-85.
18. Palevsky, H.I., et al., *Primary pulmonary hypertension. Vascular structure, morphometry, and responsiveness to vasodilator agents.* Circulation, 1989. **80**(5): p. 1207-21.

19. Frid, M.G., E.P. Moiseeva, and K.R. Stenmark, *Multiple phenotypically distinct smooth muscle cell populations exist in the adult and developing bovine pulmonary arterial media in vivo.* Circ Res, 1994. **75**(4): p. 669-81.
20. Stenmark, K.R. and M.G. Frid, *Smooth muscle cell heterogeneity: role of specific smooth muscle cell subpopulations in pulmonary vascular disease.* Chest, 1998. **114**(1 Suppl): p. 82S-90S.
21. Stiebellehner, L., et al., *Bovine distal pulmonary arterial media is composed of a uniform population of well-differentiated smooth muscle cells with low proliferative capabilities.* Am J Physiol Lung Cell Mol Physiol, 2003. **285**(4): p. L819-28.
22. Sobin, S.S. and P.C. Chen, *Ultrastructural changes in the pulmonary arterioles in acute hypoxic pulmonary hypertension in the rat.* High Alt Med Biol, 2000. **1**(4): p. 311-22.
23. Short, M., et al., *Hypoxia induces differentiation of pulmonary artery adventitial fibroblasts into myofibroblasts.* Am J Physiol Cell Physiol, 2004. **286**(2): p. C416-25.
24. Frid, M.G., et al., *Hypoxia-induced pulmonary vascular remodeling requires recruitment of circulating mesenchymal precursors of a monocyte/macrophage lineage.* Am J Pathol, 2006. **168**(2): p. 659-69.
25. Barst, R.J., *PDGF signaling in pulmonary arterial hypertension.* J Clin Invest, 2005. **115**(10): p. 2691-4.
26. Penaloza, D. and J. Arias-Stella, *The heart and pulmonary circulation at high altitudes: healthy highlanders and chronic mountain sickness.* Circulation, 2007. **115**(9): p. 1132-46.
27. Cahill, E., et al., *The pathophysiological basis of chronic hypoxic pulmonary hypertension in the mouse: vasoconstrictor and structural mechanisms contribute equally.* Exp Physiol, 2012.
28. Moudgil, R., E.D. Michelakis, and S.L. Archer, *The role of k+ channels in determining pulmonary vascular tone, oxygen sensing, cell proliferation, and apoptosis: implications in hypoxic pulmonary vasoconstriction and pulmonary arterial hypertension.* Microcirculation, 2006. **13**(8): p. 615-32.
29. Cohn, J.N., R. Ferrari, and N. Sharpe, *Cardiac remodeling--concepts and clinical implications: a consensus paper from an international forum on cardiac remodeling. Behalf of an International Forum on Cardiac Remodeling.* J Am Coll Cardiol, 2000. **35**(3): p. 569-82.
30. Bishop, J.E., et al., *Increased collagen synthesis and decreased collagen degradation in right ventricular hypertrophy induced by pressure overload.* Cardiovasc Res, 1994. **28**(10): p. 1581-5.
31. Adachi, S., et al., *Distribution of mRNAs for natriuretic peptides in RV hypertrophy after pulmonary arterial banding.* Am J Physiol, 1995. **268**(1 Pt 2): p. H162-9.
32. Camelliti, P., T.K. Borg, and P. Kohl, *Structural and functional characterisation of cardiac fibroblasts.* Cardiovasc Res, 2005. **65**(1): p. 40-51.
33. Ikeda, S., M. Hamada, and K. Hiwada, *Cardiomyocyte apoptosis with enhanced expression of P53 and Bax in right ventricle after pulmonary arterial banding.* Life Sci, 1999. **65**(9): p. 925-33.
34. Levy, D., et al., *Prognostic implications of echocardiographically determined left ventricular mass in the Framingham Heart Study.* N Engl J Med, 1990. **322**(22): p. 1561-6.
35. Meerson, F.Z., *Compensatory hyperfunction of the heart and cardiac insufficiency.* Circ Res, 1962. **10**: p. 250-8.
36. Pluim, B.M., et al., *The athlete's heart. A meta-analysis of cardiac structure and function.* Circulation, 2000. **101**(3): p. 336-44.
37. McMullen, J.R. and G.L. Jennings, *Differences between pathological and physiological cardiac hypertrophy: novel therapeutic strategies to treat heart failure.* Clin Exp Pharmacol Physiol, 2007. **34**(4): p. 255-62.

38. Gaynor, S.L., et al., *Right atrial and ventricular adaptation to chronic right ventricular pressure overload.* Circulation, 2005. **112**(9 Suppl): p. I212-8.
39. Hessel, M.H., et al., *Characterization of right ventricular function after monocrotaline-induced pulmonary hypertension in the intact rat.* Am J Physiol Heart Circ Physiol, 2006. **291**(5): p. H2424-30.
40. Bogaard, H.J., et al., *The right ventricle under pressure: cellular and molecular mechanisms of right-heart failure in pulmonary hypertension.* Chest, 2009. **135**(3): p. 794-804.
41. Dias, C.A., et al., *Reversible pulmonary trunk banding. II. An experimental model for rapid pulmonary ventricular hypertrophy.* J Thorac Cardiovasc Surg, 2002. **124**(5): p. 999-1006.
42. Hamrell, B.B., et al., *Myocyte morphology of free wall trabeculae in right ventricular pressure overload hypertrophy in rabbits.* J Mol Cell Cardiol, 1986. **18**(2): p. 127-38.
43. Hannan, R.D., et al., *Cardiac hypertrophy: a matter of translation.* Clin Exp Pharmacol Physiol, 2003. **30**(8): p. 517-27.
44. Bogaard, H.J., et al., *Chronic pulmonary artery pressure elevation is insufficient to explain right heart failure.* Circulation, 2009. **120**(20): p. 1951-60.
45. Vonk Noordegraaf, A. and N. Galie, *The role of the right ventricle in pulmonary arterial hypertension.* Eur Respir Rev, 2011. **20**(122): p. 243-53.
46. Gan, C.T., et al., *Impaired left ventricular filling due to right-to-left ventricular interaction in patients with pulmonary arterial hypertension.* Am J Physiol Heart Circ Physiol, 2006. **290**(4): p. H1528-33.
47. Haddad, F., et al., *Right ventricular function in cardiovascular disease, part II: pathophysiology, clinical importance, and management of right ventricular failure.* Circulation, 2008. **117**(13): p. 1717-31.
48. Vliegen, H.W., et al., *Myocardial changes in pressure overload-induced left ventricular hypertrophy. A study on tissue composition, polyploidization and multinucleation.* Eur Heart J, 1991. **12**(4): p. 488-94.
49. Weber, K.T., et al., *Patterns of myocardial fibrosis.* J Mol Cell Cardiol, 1989. **21 Suppl 5**: p. 121-31.
50. Goldsmith, E.C., et al., *Organization of fibroblasts in the heart.* Dev Dyn, 2004. **230**(4): p. 787-94.
51. Berk, B.C., K. Fujiwara, and S. Lehoux, *ECM remodeling in hypertensive heart disease.* J Clin Invest, 2007. **117**(3): p. 568-75.
52. Bishop, J.E. and G.J. Laurent, *Collagen turnover and its regulation in the normal and hypertrophying heart.* Eur Heart J, 1995. **16 Suppl C**: p. 38-44.
53. Iwanaga, Y., et al., *Excessive activation of matrix metalloproteinases coincides with left ventricular remodeling during transition from hypertrophy to heart failure in hypertensive rats.* J Am Coll Cardiol, 2002. **39**(8): p. 1384-91.
54. Woodiwiss, A.J., et al., *Reduction in myocardial collagen cross-linking parallels left ventricular dilatation in rat models of systolic chamber dysfunction.* Circulation, 2001. **103**(1): p. 155-60.
55. Ross, R.S. and T.K. Borg, *Integrins and the myocardium.* Circ Res, 2001. **88**(11): p. 1112-9.
56. Goldsmith, E.C., et al., *Integrin shedding as a mechanism of cellular adaptation during cardiac growth.* Am J Physiol Heart Circ Physiol, 2003. **284**(6): p. H2227-34.
57. Franchini, K.G., et al., *Early activation of the multicomponent signaling complex associated with focal adhesion kinase induced by pressure overload in the rat heart.* Circ Res, 2000. **87**(7): p. 558-65.
58. Laser, M., et al., *Integrin activation and focal complex formation in cardiac hypertrophy.* J Biol Chem, 2000. **275**(45): p. 35624-30.

59. Mehta, P.K. and K.K. Griendling, *Angiotensin II cell signaling: physiological and pathological effects in the cardiovascular system.* Am J Physiol Cell Physiol, 2007. **292**(1): p. C82-97.
60. Baker, K.M., et al., *Renin-angiotensin system involvement in pressure-overload cardiac hypertrophy in rats.* Am J Physiol, 1990. **259**(2 Pt 2): p. H324-32.
61. Kim, S., et al., *Angiotensin II induces cardiac phenotypic modulation and remodeling in vivo in rats.* Hypertension, 1995. **25**(6): p. 1252-9.
62. Rouleau, J.L., et al., *Cardioprotective effects of ramipril and losartan in right ventricular pressure overload in the rabbit: importance of kinins and influence on angiotensin II type 1 receptor signaling pathway.* Circulation, 2001. **104**(8): p. 939-44.
63. Agapitov, A.V. and W.G. Haynes, *Role of endothelin in cardiovascular disease.* J Renin Angiotensin Aldosterone Syst, 2002. **3**(1): p. 1-15.
64. Molenaar, P., et al., *Characterization and localization of endothelin receptor subtypes in the human atrioventricular conducting system and myocardium.* Circ Res, 1993. **72**(3): p. 526-38.
65. Davenport, A.P., et al., *Human endothelin receptors characterized using reverse transcriptase-polymerase chain reaction, in situ hybridization, and subtype-selective ligands BQ123 and BQ3020: evidence for expression of ETB receptors in human vascular smooth muscle.* J Cardiovasc Pharmacol, 1993. **22 Suppl 8**: p. S22-5.
66. Giannessi, D., S. Del Ry, and R.L. Vitale, *The role of endothelins and their receptors in heart failure.* Pharmacol Res, 2001. **43**(2): p. 111-26.
67. Ito, H., et al., *Endothelin-1 is an autocrine/paracrine factor in the mechanism of angiotensin II-induced hypertrophy in cultured rat cardiomyocytes.* J Clin Invest, 1993. **92**(1): p. 398-403.
68. Shubeita, H.E., et al., *Endothelin induction of inositol phospholipid hydrolysis, sarcomere assembly, and cardiac gene expression in ventricular myocytes. A paracrine mechanism for myocardial cell hypertrophy.* J Biol Chem, 1990. **265**(33): p. 20555-62.
69. Fujisaki, H., et al., *Natriuretic peptides inhibit angiotensin II-induced proliferation of rat cardiac fibroblasts by blocking endothelin-1 gene expression.* J Clin Invest, 1995. **96**(2): p. 1059-65.
70. Del Ry, S., et al., *Endothelin-1, endothelin-1 receptors and cardiac natriuretic peptides in failing human heart.* Life Sci, 2001. **68**(24): p. 2715-30.
71. Molkentin, J.D., et al., *A calcineurin-dependent transcriptional pathway for cardiac hypertrophy.* Cell, 1998. **93**(2): p. 215-28.
72. Heineke, J. and J.D. Molkentin, *Regulation of cardiac hypertrophy by intracellular signalling pathways.* Nat Rev Mol Cell Biol, 2006. **7**(8): p. 589-600.
73. Boheler, K.R. and K. Schwartz, *Gene expression in cardiac hypertrophy.* Trends Cardiovasc Med, 1992. **2**(5): p. 176-82.
74. Palmer, B.M., *Thick filament proteins and performance in human heart failure.* Heart Fail Rev, 2005. **10**(3): p. 187-97.
75. Lowes, B.D., et al., *Changes in gene expression in the intact human heart. Downregulation of alpha-myosin heavy chain in hypertrophied, failing ventricular myocardium.* J Clin Invest, 1997. **100**(9): p. 2315-24.
76. Bakerman, P.R., K.R. Stenmark, and J.H. Fisher, *Alpha-skeletal actin messenger RNA increases in acute right ventricular hypertrophy.* Am J Physiol, 1990. **258**(4 Pt 1): p. L173-8.
77. Black, F.M., et al., *The vascular smooth muscle alpha-actin gene is reactivated during cardiac hypertrophy provoked by load.* J Clin Invest, 1991. **88**(5): p. 1581-8.
78. Suurmeijer, A.J., et al., *Alpha-actin isoform distribution in normal and failing human heart: a morphological, morphometric, and biochemical study.* J Pathol, 2003. **199**(3): p. 387-97.
79. Yap, L.B., et al., *The natriuretic peptides and their role in disorders of right heart dysfunction and pulmonary hypertension.* Clin Biochem, 2004. **37**(10): p. 847-56.

80. Nagaya, N., et al., *Plasma brain natriuretic peptide as a prognostic indicator in patients with primary pulmonary hypertension.* Circulation, 2000. **102**(8): p. 865-70.
81. Galie, N., et al., *Guidelines for the diagnosis and treatment of pulmonary hypertension: the Task Force for the Diagnosis and Treatment of Pulmonary Hypertension of the European Society of Cardiology (ESC) and the European Respiratory Society (ERS), endorsed by the International Society of Heart and Lung Transplantation (ISHLT).* Eur Heart J, 2009. **30**(20): p. 2493-537.
82. Haddad, F., E. Ashley, and E.D. Michelakis, *New insights for the diagnosis and management of right ventricular failure, from molecular imaging to targeted right ventricular therapy.* Curr Opin Cardiol, 2010. **25**(2): p. 131-40.
83. Moon, R.T., et al., *WNT and beta-catenin signalling: diseases and therapies.* Nat Rev Genet, 2004. **5**(9): p. 691-701.
84. Miller, J.R., *The Wnts.* Genome Biol, 2002. **3**(1): p. REVIEWS3001.
85. Hausmann, G., C. Banziger, and K. Basler, *Helping Wingless take flight: how WNT proteins are secreted.* Nat Rev Mol Cell Biol, 2007. **8**(4): p. 331-6.
86. van Amerongen, R., A. Mikels, and R. Nusse, *Alternative wnt signaling is initiated by distinct receptors.* Sci Signal, 2008. **1**(35): p. re9.
87. Angers, S. and R.T. Moon, *Proximal events in Wnt signal transduction.* Nat Rev Mol Cell Biol, 2009. **10**(7): p. 468-77.
88. Kawano, Y. and R. Kypta, *Secreted antagonists of the Wnt signalling pathway.* J Cell Sci, 2003. **116**(Pt 13): p. 2627-34.
89. Komiya, Y. and R. Habas, *Wnt signal transduction pathways.* Organogenesis, 2008. **4**(2): p. 68-75.
90. Bienz, M. and H. Clevers, *Armadillo/beta-catenin signals in the nucleus--proof beyond a reasonable doubt?* Nat Cell Biol, 2003. **5**(3): p. 179-82.
91. Clevers, H., *Wnt/beta-catenin signaling in development and disease.* Cell, 2006. **127**(3): p. 469-80.
92. Roberts, D.M., K.C. Slep, and M. Peifer, *It takes more than two to tango: Dishevelled polymerization and Wnt signaling.* Nat Struct Mol Biol, 2007. **14**(6): p. 463-5.
93. Hurlstone, A. and H. Clevers, *T-cell factors: turn-ons and turn-offs.* EMBO J, 2002. **21**(10): p. 2303-11.
94. Daniels, D.L. and W.I. Weis, *Beta-catenin directly displaces Groucho/TLE repressors from Tcf/Lef in Wnt-mediated transcription activation.* Nat Struct Mol Biol, 2005. **12**(4): p. 364-71.
95. Veeman, M.T., J.D. Axelrod, and R.T. Moon, *A second canon. Functions and mechanisms of beta-catenin-independent Wnt signaling.* Dev Cell, 2003. **5**(3): p. 367-77.
96. Haegel, H., et al., *Lack of beta-catenin affects mouse development at gastrulation.* Development, 1995. **121**(11): p. 3529-37.
97. Kerkela, R., et al., *Deletion of GSK-3beta in mice leads to hypertrophic cardiomyopathy secondary to cardiomyoblast hyperproliferation.* J Clin Invest, 2008. **118**(11): p. 3609-18.
98. Ai, D., et al., *Canonical Wnt signaling functions in second heart field to promote right ventricular growth.* Proc Natl Acad Sci U S A, 2007. **104**(22): p. 9319-24.
99. Malekar, P., et al., *Wnt signaling is critical for maladaptive cardiac hypertrophy and accelerates myocardial remodeling.* Hypertension, 2010. **55**(4): p. 939-45.
100. van de Schans, V.A., et al., *Interruption of Wnt signaling attenuates the onset of pressure overload-induced cardiac hypertrophy.* Hypertension, 2007. **49**(3): p. 473-80.
101. Haq, S., et al., *Glycogen synthase kinase-3beta is a negative regulator of cardiomyocyte hypertrophy.* J Cell Biol, 2000. **151**(1): p. 117-30.

102. Michael, A., et al., *Glycogen synthase kinase-3beta regulates growth, calcium homeostasis, and diastolic function in the heart.* J Biol Chem, 2004. **279**(20): p. 21383-93.
103. Haq, S., et al., *Differential activation of signal transduction pathways in human hearts with hypertrophy versus advanced heart failure.* Circulation, 2001. **103**(5): p. 670-7.
104. Haq, S., et al., *Stabilization of beta-catenin by a Wnt-independent mechanism regulates cardiomyocyte growth.* Proc Natl Acad Sci U S A, 2003. **100**(8): p. 4610-5.
105. Chen, X., et al., *The beta-catenin/T-cell factor/lymphocyte enhancer factor signaling pathway is required for normal and stress-induced cardiac hypertrophy.* Mol Cell Biol, 2006. **26**(12): p. 4462-73.
106. Baurand, A., et al., *Beta-catenin downregulation is required for adaptive cardiac remodeling.* Circ Res, 2007. **100**(9): p. 1353-62.
107. DasGupta, R. and E. Fuchs, *Multiple roles for activated LEF/TCF transcription complexes during hair follicle development and differentiation.* Development, 1999. **126**(20): p. 4557-68.
108. Gomez-Arroyo, J.G., et al., *The monocrotaline model of pulmonary hypertension in perspective.* Am J Physiol Lung Cell Mol Physiol, 2012. **302**(4): p. L363-9.
109. Laeremans, H., et al., *Wnt/frizzled signalling modulates the migration and differentiation of immortalized cardiac fibroblasts.* Cardiovasc Res, 2010. **87**(3): p. 514-23.
110. Hardziyenka, M., et al., *Right ventricular failure following chronic pressure overload is associated with reduction in left ventricular mass evidence for atrophic remodeling.* J Am Coll Cardiol, 2011. **57**(8): p. 921-8.
111. Akhavein, F., et al., *Decreased left ventricular function, myocarditis, and coronary arteriolar medial thickening following monocrotaline administration in adult rats.* J Appl Physiol, 2007. **103**(1): p. 287-95.
112. Chen, L., et al., *Attenuation of compensatory right ventricular hypertrophy and heart failure following monocrotaline-induced pulmonary vascular injury by the Na+-H+ exchange inhibitor cariporide.* J Pharmacol Exp Ther, 2001. **298**(2): p. 469-76.
113. Matsuda, T., et al., *Distinct roles of GSK-3alpha and GSK-3beta phosphorylation in the heart under pressure overload.* Proc Natl Acad Sci U S A, 2008. **105**(52): p. 20900-5.
114. Xu, L., et al., *WISP-1 is a Wnt-1- and beta-catenin-responsive oncogene.* Genes Dev, 2000. **14**(5): p. 585-95.
115. Colston, J.T., et al., *Wnt-induced secreted protein-1 is a prohypertrophic and profibrotic growth factor.* Am J Physiol Heart Circ Physiol, 2007. **293**(3): p. H1839-46.
116. Benjamin, I.J., et al., *Isoproterenol-induced myocardial fibrosis in relation to myocyte necrosis.* Circ Res, 1989. **65**(3): p. 657-70.
117. Baudino, T.A., et al., *Cardiac fibroblasts: friend or foe?* Am J Physiol Heart Circ Physiol, 2006. **291**(3): p. H1015-26.
118. Burstein, B., et al., *Differential behaviors of atrial versus ventricular fibroblasts: a potential role for platelet-derived growth factor in atrial-ventricular remodeling differences.* Circulation, 2008. **117**(13): p. 1630-41.
119. Ueda, Y., et al., *Wnt/beta-catenin signaling suppresses apoptosis in low serum medium and induces morphologic change in rodent fibroblasts.* Int J Cancer, 2002. **99**(5): p. 681-8.

11. Declaration

I declare that I have completed this dissertation single-handedly without the unauthorized help of a second party and only with the assistance acknowledged therein. I have appropriately acknowledged and referenced all text passages that are derived literally from or are based on the content of published or unpublished work of others, and all information that relates to verbal communications. I have abided by the principles of good scientific conduct laid down in the charter of the Justus Liebig University of Giessen in carrying out the investigations described in the dissertation.

12. Acknowledgments

I would like to express my great gratitude to all who have contributed to this thesis.

I am honored to thank Prof. Dr. Werner Seeger for his commitment and valuable advices concerning this project.

I owe my deepest gratitude to my supervisor, Prof. Dr. Ralph Schermuly. Thank you for the opportunity to work on this project, for your dedication and professional guidance.

I wish to express my sincere thanks to Prof. Dr. Dr. habil. Hans-Christian Siebert for his kind supervision.

I would like to express particular gratitude to my co-supervisor Dr. Soni Pullamsetti. Thank you for all your input in designing the experiments of this project, solving the problems, your patience and understanding.

I sincerely thank to Molecular Biology and Medicine of the Lung (MBML) and International Giessen Graduate Centre for the Life Sciences (GGL) graduate programs for their excellent training.

Further, I would like to thank all my colleagues from Schermuly Lab, Pullamsetti Lab, Voswinkel Lab and Savai Lab for all the help and creating a great working atmosphere every day. In particular I would like to thank Swati Dabral for the four years of fruitful discussions and her friendship. Special thanks to Dr. Wiebke Janssen, Julia Neuman and Uta Eule for performing all the animal experiments and to Dr. Ying-Yu Lai for her help in establishing cardiac fibroblast isolation.

Last, but not least, I would like to thank my family and my boyfriend for their support throughout my doctoral studies.